Pharmacological Research 144 (2019) 19–50

Contents lists available at ScienceDirect

Pharmacological Research

journal homepage: www.elsevier.com/locate/yphrs

Invited Review

Properties of FDA-approved small molecule protein kinase inhibitors

Robert Roskoski Jr.

Blue Ridge Institute for Medical Research, 3754 Brevard Road, Suite 116, Box 19, Horse Shoe, NC 28742-8814, United States

ARTICLE INFO

Chemical compounds studied in this article:
Afatinib (PubMED CID: 10184653)
Binimetinib (PubMED CID: 10288191)
Crizotinib (PubMED CID: 11626560)
Dabrafenib (PubMED CID: 44462760)
Encorafenib (PubMED CID: 50922675)
Imatinib (PubMED CID: 5291)
Ribociclib (PubMED CID: 44631912)
Sorafenib (PubMED CID: 216239)
Tofacitinib (PubMED CID: 9926791)
Trametinib (PubMED CID: 11707110)

Keywords:
Catalytic spine
Hydrophobic interaction
Protein kinase inhibitor classification
Protein kinase structure
Regulatory spine
Shell residues

ABSTRACT

Because mutations, overexpression, and dysregulation of protein kinases play essential roles in the pathogenesis of many illnesses, this enzyme family has become one of the most important drug targets in the past 20 years. The US FDA has approved 48 small molecule protein kinase inhibitors, nearly all of which are orally effective with the exceptions of netarsudil (which is given as an eye drop) and temsirolimus (which is given intravenously). Of the 48 approved drugs, the majority (25) target receptor protein-tyrosine kinases, ten target non-receptor protein-tyrosine kinases, and 13 target protein-serine/threonine protein kinases. The data indicate that 43 of these drugs are used in the treatment of malignancies (36 against solid tumors including lymphomas and seven against non-solid tumors, e.g., leukemias). Seven drugs are used in the treatment of non-malignancies: baricitinib, rheumatoid arthritis; fostamatinib, chronic immune thrombocytopenia; ruxolitinib, myelofibrosis and polycythemia vera; nintedanib, idiopathic pulmonary fibrosis; sirolimus, renal graft vs. host disease; netarsudil, glaucoma; tofacitinib, rheumatoid arthritis, Crohn disease, and ulcerative colitis. Moreover, ibrutinib and sirolimus are used for the treatment of both malignant and non-malignant diseases. The most common drug targets include ALK, B-Raf, BCR-Abl, epidermal growth factor receptor (EGFR), and vascular endothelial growth factor receptor (VEGFR). Most of the small molecule inhibitors (45) interact directly with the protein kinase domain. In contrast, sirolimus, temsirolimus, and everolimus are larger molecules (MW ≈ 1000) that bind to FKBP-12 to generate a complex that inhibits mTOR (mammalian target of rapamycin). This review presents the available drug-enzyme X-ray crystal structures for 27 of the approved drugs as well as the chemical structures and physicochemical properties of all of the FDA-approved small molecule protein kinase antagonists. Six of the drugs bind covalently and irreversibly to their target. Twenty of the 48 drugs have molecular weights greater than 500, exceeding a Lipinski rule of five criterion. Excluding the macrolides (everolimus, sirolimus, temsirolimus), the average molecular weight of drugs is 480 with a range of 306 (ruxolitinib) to 615 (trametinib). Nearly half of the antagonists (23) have a lipophilic efficiency with values of less than five while the recommended optima range from 5–10. One of the vexing problems is the near universal development of resistance that is associated with the use of small molecule protein kinase inhibitors for the treatment of cancer.

1. The importance of therapeutic protein kinase inhibitors

Because mutations, overexpression, and dysregulation of protein kinases play essential roles in the pathogenesis of many illnesses including asthma, autoimmune, cardiovascular, inflammatory, and nervous diseases as well as cancer, this enzyme family has become one of the most important drug targets during the past 20 years [1,2]. Perhaps 20–33% of drug discovery efforts worldwide are directed at the prote in kinase superfamily. The interest in protein kinase inhibitors was fueled by the approval of imatinib in 2001 for the treatment of Philadelphia-chromosome-positive chronic myelogenous leukemias. This disorder is caused by the formation of the activated chimeric BCR-Abl protein-tyrosine kinase, which is inhibited by the drug.

Structure-based drug development is aided by the more than six thousand protein kinase X-ray crystal structures in the public domain. There may be a greater number of three-dimensional proprietary structures that are used by the pharmaceutical industry during the drug discovery process. There are about 175 different orally effective protein

Abbreviations: ALL, acute lymphoblastic leukemia; AS, activation segment; BP, back pocket; C-spine, catalytic spine; CDK, cyclin-dependent kinase; CML, chronic myelogenous leukemia; CS1, catalytic spine residue 1; CL, catalytic loop; EGFR, epidermal growth factor receptor; F, front pocket; FGFR, fibroblast growth factor receptor; FKBP12/mTOR, FK Binding Protein-12/mammalian target of rapamycin; GK, gatekeeper; GRL, glycine-rich loop; KLIFS-3, kinase-ligand interaction fingerprint and structure residue-3; LAM, lymphangioleiomyomatosis; LE, ligand efficiency; LipE, lipophilic efficiency; NSCLC, non-small cell lung cancer; PDGFR, platelet-derived growth factor receptor; PKA, protein kinase A; R-spine, regulatory spine; RS1, regulatory spine residue 1; SEGA, subependymal giant cell astrocytomas; Sh2, shell residue 2; VEGFR, vascular endothelial growth factor receptor

E-mail address: rrj@brimr.org.

https://doi.org/10.1016/j.phrs.2019.03.006
Received 6 March 2019; Accepted 7 March 2019
Available online 13 March 2019

kinase inhibitors in clinical trials worldwide [3]; a complete listing that is regularly updated can be found at www.icoa.fr/pkidb/. There are four dozen FDA-approved medicines (see Supplementary material) that are directed against about 20 different protein kinases. Drugs targeting an additional 15–20 protein kinases are in clinical trials worldwide [3,4]. However, this represents only a small fraction of the protein kinase superfamily.

Manning et al. discovered that the human protein kinase super family consists of 518 members that include 478 typical and 40 atypical enzymes [5]. Protein kinases catalyze the following reaction;

$$MgATP^{1-} + protein - O{:}\ H \rightarrow protein - O{:}\ PO_3^{2-} + MgADP + H^+$$

Based upon the nature of the phosphorylated –OH groups, these enzymes are classified as protein-serine/threonine kinases (385 members), protein-tyrosine kinases (90), and protein-tyrosine kinase-like enzymes (43). The protein-tyrosine kinases include both receptor (58) and non-receptor (32) proteins. A small group of enzymes including MEK1/2, which catalyze the phosphorylation of both threonine and tyrosine residues within the activation segment of target proteins, are classified as dual specificity kinases. Assuming that the human genome consists of 20,000 genes and the human kinome consists of about 500 genes, then protein kinases make up about 2.5% of all genes. Accordingly, about 1 in 40 human genes encodes a protein kinase. Manning et al. reported that chromosomal mapping revealed that 244 protein kinases map to disease loci or cancer amplicons [5] so that one can anticipate a substantial increase in the number of protein kinases that will be targeted for the treatment of additional illnesses.

The US FDA has approved 48 small molecule protein kinase inhibitors as of 1 March 2019 (see Supplementary material), nearly all of which are orally effective with the exception of netarsudil (which is given as an eye drop) and temsirolimus (which is given intravenously). Of the 48 approved drugs, the majority (25) inhibit receptor protein-tyrosine kinases, 10 inhibit non-receptor protein-tyrosine kinases, and 13 are directed at protein-serine/threonine protein kinases (Table 1). The data indicate that 43 kinase inhibitors are directed toward malignancies (37 against solid tumors including lymphomas and eight against non-solid tumors, e.g., leukemias). Ibrutinib and imatinib are used in the treatment of solid and non-solid tumors are were counted twice. At least 18 of these drugs are multikinase inhibitors. This has potential advantages and disadvantages. It may be that the therapeutic efficacy of these drugs may be related to the inhibition of more than one enzyme. For example, sunitinib and cabozantinib have potent Axl off-target activity, which may add to their clinical effectiveness [6]. Contrariwise, the inhibition of non-target enzymes may promote various toxicities and adverse events. Accordingly, we have the question of whether magic shotguns are to be favored over magic bullets [7].

Seven of the FDA-approved protein kinase inhibitors are directed toward non-malignancies. For example, baricitinib is used in the treatment of rheumatoid arthritis, fostamatinib is used for the treatment of chronic immune thrombocytopenia, ruxolitinib is used for the treatment of myelofibrosis and polycythemia vera, nintedanib is used in the treatment of idiopathic pulmonary fibrosis, sirolimus is used to prevent rejections following renal transplantation, tofacitinib is used for the treatment of rheumatoid arthritis, psoriatic arthritis, and ulcerative colitis (www.brimr.org/PKI/PKIs.htm), and netarsudil is used to treat glaucoma [8]. Six drugs form covalent bonds with their target enzymes including acalabrutinib (targeting BTK in mantle cell lymphomas), afatinib (targeting EGFR in NSCLC), dacomitinib (targeting mutant *EGFR* in lung cancers), ibrutinib (targeting BTK in mantle cell lymphomas, chronic lymphocytic leukemias, marginal zone lymphomas, chronic graft vs. host disease, and Waldenström macroglobulinemia), neratinib (targeting ErbB2 in HER2-positive lung cancers), and osimertinib (targeting *EGFR* T970M mutants in NSCLC).

2. Protein kinase structure and mechanism

2.1. Primary, secondary, and tertiary structures

Protein kinases have a small amino-terminal lobe and large carboxyterminal lobe that contain several conserved α-helices and β-strands as first described by Knighton et al. for protein kinase A (PKA) [9,10]. The small lobe is dominated by a five-stranded antiparallel β-sheet (β1–β5) [11,12]. It also contains a regulatory αC-helix that occurs in active or inactive orientations. This lobe contains a conserved glycine-rich (GxGxΦG) ATP-phosphate-binding loop, sometimes called the P-loop, which occurs between the β1- and β2-strands, where Φ refers to a hydrophobic residue. The glycine-rich loop is followed by a conserved valine (GxGxΦGxV) that interacts hydrophobically with the adenine base of ATP and many small molecule inhibitors. The β3-strand contains a conserved AxK signature sequence while a conserved glutamate occurs near the middle of the αC-helix. The presence of salt bridge between the β3-strand lysine and the αC-helix glutamate is a prerequisite for the formation of the activated state and corresponds to the "αC_{in}" conformation. For example, K745 forms an electrostatic bond with E762 of active EGFR (Fig. 1A). The αC_{in} conformation is necessary, but it is not sufficient for the expression of full kinase activity. However, the absence of this electrostatic bond indicates that the kinase is inactive and it is called the "αC_{out}" conformation (Fig. 1C). States between the αC_{in} and αC_{out} conformation are called αC-dilated [13,14]. The C-terminus of the αC-helix is anchored to the αC-β4 back loop. Specific back loop residues of the small lobe are anchored to the carboxyterminal lobe αE-helix residues; this portion of the back loop dynamically functions as part of the carboxyterminal lobe [12].

The large lobe is mostly α-helical (Fig. 1A) with eight conserved helices (αD–αI, αEF1, αEF2) [15]. The large lobe of active protein kinases also contains four short conserved β-strands (β6–β9). The inactive conformations of many enzymes lack the β6- and β9-strands (Fig. 1E). The second residue in the β7-strand, which is found on the bottom of the adenine binding pocket, interacts hydrophobically with virtually all ATP-competitive protein kinase inhibitors. The primary structure of the β6–β9 strands occurs between the αE- and αF-helices. The large lobe contains the catalytic loop residues that participate in the phosphoryl transfer from ATP to the protein substrates.

Hanks and Hunter identified 12 subdomains (I–VIa, VIb–XI) that constitute the functional core of protein kinases [16]. The K/E/D/D (Lys/Glu/Asp/Asp) motif plays an important role in the catalytic function of essentially all active protein kinases. The *K* of *K*/E/D/D is a conserved β3-strand lysine that forms electrostatic bonds with the α- and β-phosphates of ATP as illustrated for active EGFR (Fig. 2A). The *E* of the K/*E*/D/D signature is the glutamate within the αC-helix that forms a salt bridge with the conserved β3-strand lysine. The aspartate residue within the catalytic loop (the first *D* of K/E/*D*/D), which is a Lowry-Brönsted base (proton acceptor), plays a central role in catalysis. Madhusudan et al. hypothesized that this aspartate abstracts the proton from the –OH group of the protein substrate, which facilitates the nucleophilic attack of oxygen on the γ-phosphorus atom of ATP (Fig. 2A/B) [17]. Moreover, Zhou and Adams proposed that this catalytic loop aspartate places the substrate hydroxyl group in a position that enables an in-line nucleophilic attack [18]. See Ref. [19] for a broad overview of the enzymology of protein kinases.

The second *D* of the K/E/D/*D* signature is the first residue of the activation segment. The activation segment of nearly all protein kinases begins with DFG and ends with APE. This segment, which is generally 35–40 residues long, is a key regulatory element in protein kinases [20]. The activation segment controls both protein substrate binding and overall catalytic efficiency. The primary structure of the catalytic loop of protein kinases, which is proximal to the β7- and β8-strands, consists of $HRD(x)_4N$. The primary structure of the activation segment occurs after the catalytic loop. Two Mg^{2+} ions, $Mg^{2+}(1)$ and $Mg^{2+}(2)$, are required for the catalytic activity of most protein kinases. The EGFR

Table 1
FDA-approved small molecule protein kinase inhibitors, their protein kinase targets, and therapeutic indications.

Drug[a] (Code) Trade name	Year approved	Primary targets[a]	Therapeutic indications[b]
Abemaciclib (LY2835219) Verzenio	2017	CDK4/6	Combination therapy and monotherapy for breast cancers
Acalabrutinib (ACP-196) Calquence	2017	BTK	Mantle cell lymphomas
Afatinib (BIBW 2992) Tovok	2013	EGFR	NSCLC
Alectinib (CH5424802) Alecensa	2015	ALK	ALK-positive NSCLC
Axitinib (AG-013736) Inlyta	2012	VEGFR	Advance renal cell carcinomas
Baricitinib (LY 3009104) Olumiant	2018	JAK1/2/3 & Tyk	Rheumatoid arthritis
Binimetinib (MEK162) Mektovi	2018	MEK1/2	Melanomas
Bosutinib (SKI-606) Bosulif	2012	BCR-Abl	Chronic myelogenous leukemias
Brigatinib (AP 26113) Alunbrig	2017	ALK	ALK-positive NSCLC
Cabozantinib (BMS-907351) Cometriq	2012	RET	Advanced medullary thyroid cancers
Ceritinib (LDK378) Zykadia	2014	ALK	ALK-positive NSCLC resistant to crizotinib
Cobimetinib (GDC-0973) Cotellic	2015	MEK1/2	*BRAF* mutation-positive melanomas in combination with vemurafenib
Crizotinib (PF 2341066) Xalkori	2011	ALK	ALK or ROS1-postive NSCLC
Dabrafenib (GSK2118436) Tafinlar	2013	B-Raf	*BRAF* mutation-positive melanomas and NSCLC
Dacomitinib (PF-00299804) Visimpro	2018	EGFR	*EGFR*-mutant NSCLC
Dasatinib (BMS-354825) Sprycell	2006	BCR-Abl	Chronic myelogenous leukemias
Encorafenib (LGX818) Braftovi	2018	B-Raf	Combination therapy for $BRAF^{V600E/K}$ melanomas
Erlotinib (OSI-774) Tarceva	2004	EGFR	NSCLC, pancreatic cancers
Everolimus (RAD001) Afinitor	2009	FKBP12/mTOR	HER2-negative breast cancers, pancreatic neuroendocrine tumors, renal cell carcinomas, angiomyolipomas, subependymal giant cell astrocytomas
Fostamatinib (R788) Tavalisse	2018	Syk	Chronic immune thrombocytopenia
Gefitinib (ZD1839) Iressa	2003	EGFR	NSCLC
Gilteritinib (ASP2215) Xospata	2018	Flt3	Acute myelogenous leukemias
Ibrutinib (PCI-32765) Imbruvica	2013	BTK	Chronic lymphocytic leukemias, mantle cell lymphomas, marginal zone lymphomas, graft vs. host disease
Imatinib (STI571) Gleevec	2001	BCR-Abl	Philadelphia chromosome-positive CML or ALL, aggressive systemic mastocytosis, chronic eosinophilic leukemias, dermatofibrosarcoma protuberans, hypereosinophilic syndrome, gastrointestinal stromal tumors, myelodysplastic/myeloproliferative disease
Lapatinib (GW572016) Tykerb	2007	EGFR	HER2-positive breast cancers
Larotrectinib (LOXO-101) Vitrakvi	2018	TRK	Solid tumors with NTRK fusion proteins
Lenvatinib (AK175809) Lenvima	2015	VEGFR, RET	Differentiated thyroid cancers
Lorlatinib (PF-06463922) Lorbrena	2018	ALK	ALK-positive NSCLC
Midostaurin (CPG 41251) Rydapt	2017	Flt3	Acute myelogenous leukemias, mastocytosis, mast cell leukemias
Neratinib (HKI-272) Nerlynx	2017	ErbB2	HER2-positive breast cancers
Netarsudil (AR11324) Rhopressa	2018	ROCK1/2	Glaucoma
Nilotinib (AMN107) Tasigna	2007	BCR-Abl	Philadelphia chromosome-positive CML
Nintedanib (BIBF-1120) Vargatef	2014	FGFR	Idiopathic pulmonary fibrosis
Osimertinib (AZD-9292) Tagrisso	2015	EGFR	NSCLC
Palbociclib (PD-0332991) Ibrance	2015	CDK4/6	Estrogen receptor- and HER2-positive breast cancers
Pazopanib (GW786034) Votrient	2009	VEGFR	Renal cell carcinomas, soft tissue sarcomas
Ponatinib (AP 24534) Iclusig	2012	BCR-Abl	Philadelphia chromosome-positive CML or ALL
Regorafenib (GSK2118436) Tafinlar	2012	VEGFR	Colorectal cancers
R406	2018	Syk	Chronic immune thrombocytopenia
Ribociclib (LEE011) Kisqali	2017	CDK4/6	Combination therapy for breast cancers
Ruxolitinib (INCB-018424) Jakafi	2011	JAK1/2/3 & Tyk2	Myelofibrosis, polycythemia vera
Sirolimus (AY 22989) Rapamycin	1999	FKBP12/mTOR	Kidney transplant, lymphangioleiomyomatosis
Sorafenib (BAY 43-9006) Nexavar	2005	VEGFR	Hepatocellular carcinomas, renal cell carcinomas, thyroid cancers (differentiated)
Sunitinib (SU11248) Sutent	2006	VEGFR	Gastrointestinal stromal tumors, pancreatic neuroendocrine tumors, renal cell carcinomas
Temsirolimus (CCI-779) Torisel	2007	FKBP12/mTOR	Advanced renal cell carcinomas
Tofacitinib (CP-690550) Tasocitinib	2012	JAK1/2/3 & Tyk2	Rheumatoid arthritis
Trametinib (GSK1120212) Mekinist	2013	MEK1/2	Melanomas
Vandetanib (ZD6474) Zactima	2011	VEGFR	Medullary thyroid cancers
Vemurafenib (PLX-4032) Zelboraf	2011	B-Raf	$BRAF^{V600E}$ mutant melanomas

[a] Although many of these drugs are multikinase inhibitors, only the primary therapeutic targets are given here.
[b] ALL, acute lymphoblastic leukemia; CML, chronic myelogenous leukemia; ErbB2/HER2, human epidermal growth factor receptor-2; NSCLC, non-small cell lung cancer.

activation segment DFG-D855 binds to one magnesium ion ($Mg^{2+}(1)$) and the catalytic loop HRD(x)$_4$N-N842 binds to the second magnesium ion ($Mg^{2+}(2)$) as depicted in Fig. 2A.

The center of the activation segment, which is its most diverse part in various protein kinases in terms of length and sequence, is known as the activation loop. This segment in many protein kinases contains one or more phosphorylatable residues. In most protein kinases, but not all, activation segment phosphorylation is required for full enzyme activity. The beginning of the activation segment is spatially near the conserved HRD component of the catalytic loop and the N-terminus of the αC-helix. Although the αC-helix is found within the amino-terminal lobe, it occupies a strategically important position between the two lobes.

The activation segment exhibits an open or extended conformation in all active enzymes and closed conformation in many dormant enzymes. The first two residues of the activation segment of protein kinases exist in two different conformations. The DFG-D side chain of active protein kinases points toward the ATP-binding site as it coordinates $Mg^{2+}(1)$. This configuration is called the "DFG-D_{in}" conformation (Fig. 1A). In the dormant activation segment conformation of many protein kinases, DFG-D extends in the opposite direction away from the active site. This corresponds to the "DFG-D_{out}" conformation (Fig. 1E). It is the ability of the DFG-D aspartate to bind (DFG-D_{in}) or

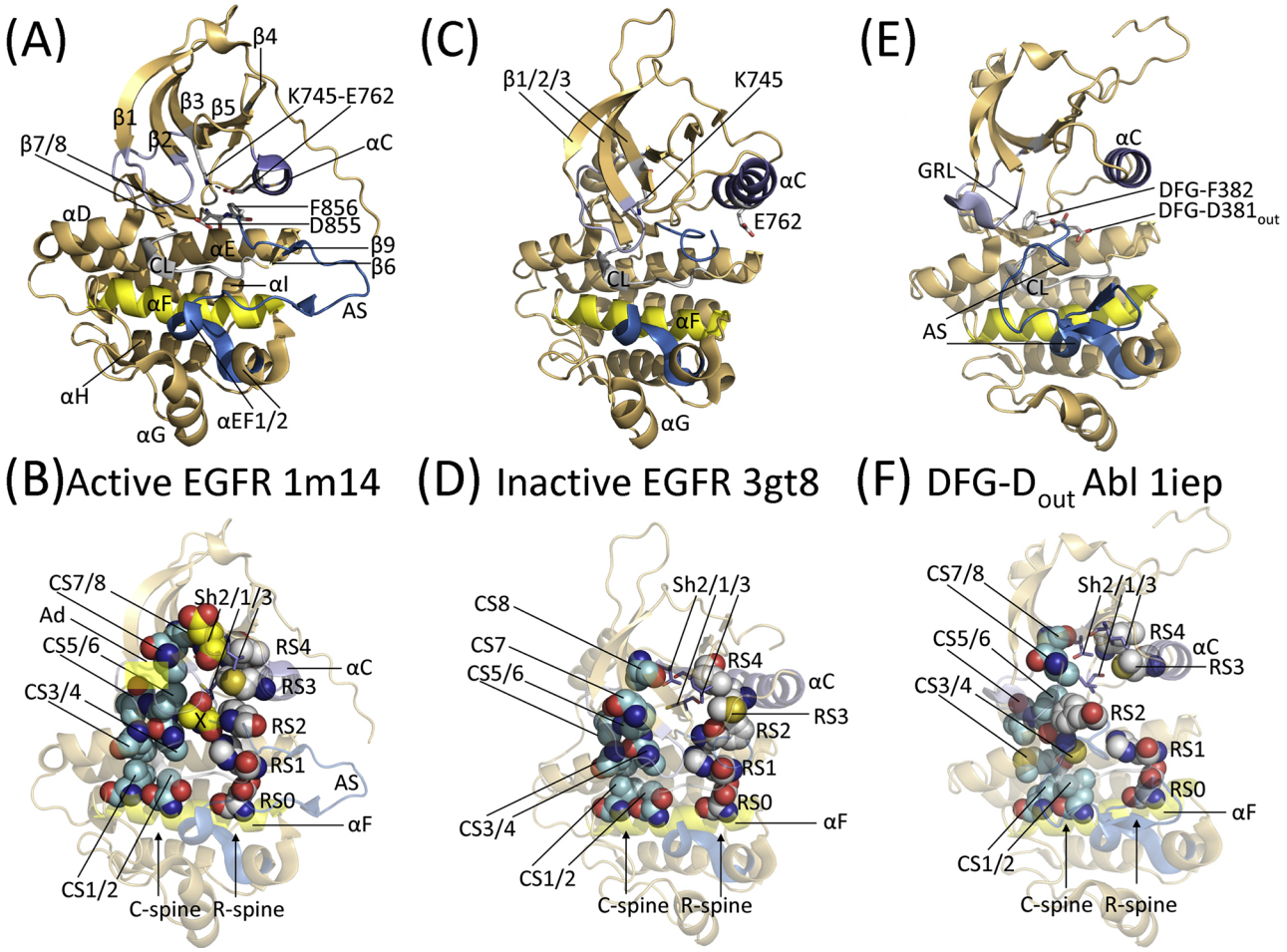

Fig. 1. Structure of active EGFR (A) and its spine and shell residues (B). Structure of inactive αC_{out} EGFR (C) and its spine and shell residues (D). Structure of inactive DGF-D_{out} Abl (E) and its spine and shell residues (F). Ad, adenine; CL, catalytic loop; CS1, catalytic spine residue 1; GRL, glycine-rich loop; RS2, regulatory spine residue 2; Sh3, shell residue 3. The x residue in (B) corresponds to the xDFG signature. The PDB ID (protein data bank identification no.) is given in the titles. Figures 1,2,4–9 were prepared using the PyMOL Molecular Graphics System Version 1.5.0.4 Schrödinger, LLC.

not bind (DFG-D_{out}) to Mg^{2+}(1) within the deep cleft that is essential. The DFG-D_{out} conformation is more commonly observed in the X-ray crystal structures of protein-tyrosine kinases than protein-serine/threonine kinases [21]. See Ref. [1] for more information regarding the details of these two activation segment structures. Functionally important EGFR and Abl protein kinase residues are listed in Table 2.

2.2. Protein kinase hydrophobic skeletons

Kornev et al. investigated the structures of active and dormant conformations of two dozen protein kinases using a local spatial alignment algorithm to determine functionally important residues [22,23]. Their investigation revealed a composite of eight hydrophobic amino acid residues that form a catalytic spine and four hydrophobic amino acid residues that form a regulatory spine. Residues from both the small and large lobes occur in both the C-spine and R-spine. Both spines make up a stable, but flexible, assembly involving the two lobes. The C-spine participates in the positioning of ATP and the R-spine interacts with the protein substrate to enable catalysis. The R-spine contains residues from both the activation segment and the αC-helix, whose structures are important in determining active and inactive enzyme states. The proper positioning and alignment of both spines are necessary, but not sufficient, for the generation of a catalytically active protein kinase.

The R-spine is made up of the initial residue of the β4-strand and a residue near the carboxyterminal end of the αC-helix (both in the small lobe). The R-spine also contains the catalytic loop HRD-histidine (HRD-H) along with the activation segment DFG-phenylalanine (DFG-F) (both in the large lobe). The αC-helix R-spine residue is four residues C-terminal to the conserved αC-helix glutamate. The backbone of HRD-H forms a hydrogen bond with a conserved aspartate residue in the αF-helix. Meharena et al. labeled the R-spine residues going from the base to the apex as RS0, RS1, RS2, RS3, and RS4 [24]. We later labeled the catalytic spine residues going from the base to the apex as CS1–8 [25].

Table 3 lists the residues that make up the catalytic and regulatory spines of human EGFR and Abl and Fig. 1B, D, and F depict their location in active human EGFR, αC_{out} EGFR, and DFG-D_{out} Abl. For a listing of the properties of the spine and shell residues of the ALK receptor protein-tyrosine kinase see Refs. [27,28], for those of the CDK (cyclin-dependent kinase) family of protein/serine kinases see [15,29], for those of the EGFR family of protein-tyrosine kinases see [30–32], for those of the ERK1/2 protein-serine/threonine kinases see [33,34], for those of the Janus kinase non-receptor protein-tyrosine kinases see [35], for those of the Kit receptor protein-tyrosine kinase see [36], for those of the MEK1/2 dual-specificity protein kinases see [37], for those of the PDGFRα/β protein-tyrosine kinases see [38], for those of the Raf protein-serine/threonine kinases see [39], for those of the RET receptor protein-tyrosine kinase see [40], for those of the ROS1 orphan receptor protein-tyrosine kinase see [41], for those of the Src non-receptor protein-tyrosine kinase see [42], and for those of the VEGFR1/2/3 protein-tyrosine kinases see [43]. The importance of the interaction of therapeutic protein kinase inhibitors with the C-spine, the R-spine, and

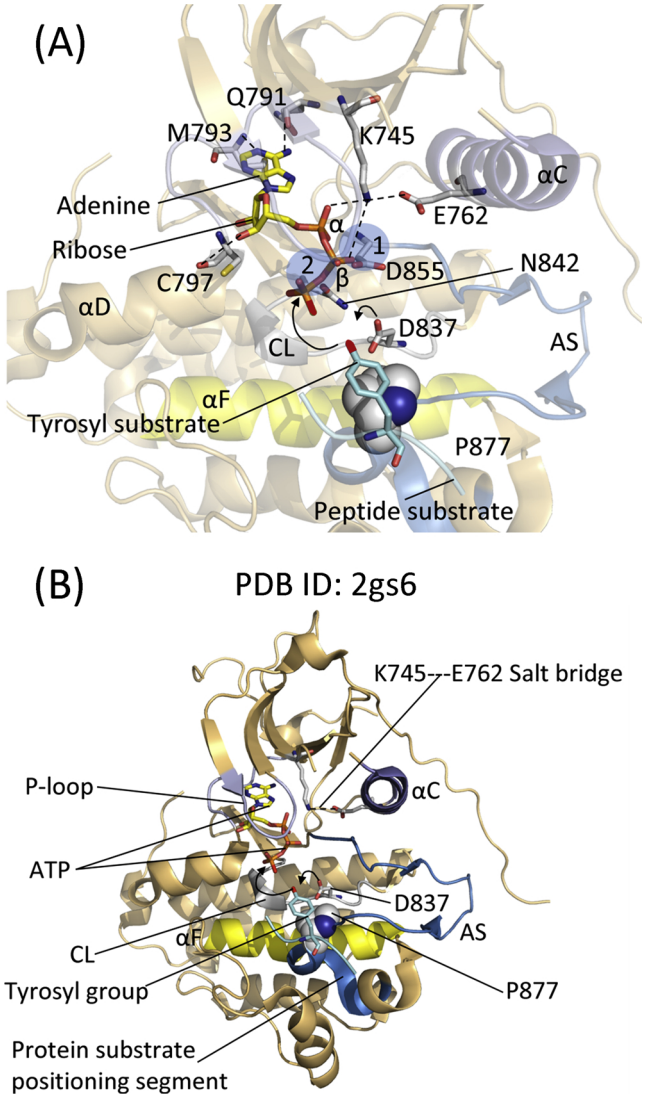

Fig. 2. (A) ATP-binding site and inferred mechanism of EGFR. The circles labeled 1 and 2 represent the approximate locations of Mg^{2+}(1) and Mg^{2+}(2). (B) Overall structure and mechanism of the EGFR-catalyzed reaction. AS activation segment. Prepared from PDB ID: 2gs6; however, the residue numbers correspond to those in the UniProtKD: P00523.

the shell residues is widespread and cannot be overstated.

The protein kinase catalytic spine consists of six residues from the large lobe and two residues from the small lobe (Fig. 1B/D/F). The binding of the adenine moiety of ATP in its pocket couples the two parts of the catalytic spine together, which facilitates the closure of the two lobes of the enzyme [23]. This fabrication of the catalytic spine prepares the enzyme for catalysis. The two residues of the small lobe that bind to the adenine component of the nucleotide substrate include the conserved alanine (CS8) from the AxK motif of the β3-strand and the conserved valine within GxGxΦGxV (CS7) of the β2-strand. Furthermore, CS6 from the middle of the β7-strand of the large lobe interacts hydrophobically with the adenine base of ATP. CS4 and CS5, which are the two hydrophobic residues that flank CS6, interact with CS3 at the beginning of the αD-helix. The CS3 residue interacts hydrophobically with CS1 of the αF-helix below it as well as the neighboring CS4. Both the regulatory and catalytic spines are supported by the hydrophobic αF-helix, which serves as a central foundation for the assembly of the complete protein kinase molecule. The exocyclic 6-amino nitrogen of ATP typically forms a hydrogen bond with the carbonyl backbone of the first hinge residue (Q791) as depicted for active EGFR (Fig. 2A); the hinge is a segment of protein kinases that connects the small and large lobes. Moreover, the adenine *N*1 of ATP characteristically forms a hydrogen bond with the backbone amide of the third hinge residue (M793) as depicted for EGFR. Most small-molecule protein kinase antagonists that are steady-state competitive inhibitors with respect to ATP also make hydrogen bonds with the backbone residues of the hinge [25].

Based upon site-directed mutagenesis studies, Meharena et al. discovered three residues in murine protein kinase A that strengthen the R-spine; they named these residues Sh1, Sh2, and Sh3 (Sh refers to shell) [24]. Their Sh1 V104G mutant had only 5% of the phosphotransferase activity of wild type PKA and the M118G/M120G Sh3/Sh2 double mutant had no activity. These findings indicate that the shell residues are important in stabilizing the PKA structure. We infer that the shell residues play a similar role in all protein kinases. The protein kinase Sh1 residue is found in the αC-β4 back loop. The Sh2 or gatekeeper residue occurs at the end of the β5-strand immediately before the hinge connecting the two lobes while Sh3 is found within the β5-strand two residues upstream of the Sh2 gatekeeper.

The term gatekeeper refers to the role that this amino acid plays in controlling access to the hydrophobic pocket next to the adenine binding site [44,45] that is occupied by fragments of numerous small molecule protein kinase inhibitors. Based upon the spatial pattern alignment algorithm [24], only three of the 14 amino acids nearby RS3 and RS4 in protein kinase A are conserved. These shell residues strengthen and stabilize the regulatory spine of protein kinase A and presumably most, if not all, protein kinases. To reiterate, many therapeutic steady-state ATP-competitive small molecule protein kinase antagonists interact with the catalytic spine (CS6/7/8), regulatory spine (RS1/2/3), and shell (Sh1 and Sh2) residues. Ung et al. reported that about 77% of protein kinases have a relatively large (e.g., Phe, Leu, Met) gatekeeper residue while the others have smaller gatekeeper residues (e.g., Val, Thr) [46].

3. Inhibitor classification and binding pockets

Dar and Shokat divided protein kinase antagonists into three groups, which they named types I, II, and III [45]. According to these investigators, type I inhibitors bind within and around the adenine-binding pocket of an active protein kinase. In contrast type, II inhibitors bind to an inactive DFG-D_{out} protein kinase while type III antagonists bind to an allosteric site that does not overlap the adenine-binding pocket. Zuccotto defined type I½ inhibitors as those drugs that bind to an inactive protein kinase with DFG-D_{in} [47]. Such an inactive protein kinase may display an αC_{out} conformation, a nonlinear or broken regulatory spine, a closed activation segment, an abnormal glycine-rich loop, or various combinations of these structural parameters. Subsequently, Gavrin and Saiah classified allosteric inhibitors as types III and IV [48]. According to them, type III inhibitors bind within the deep cleft between the small and large lobes and next to, but independent of, the ATP binding site. In contrast, type IV inhibitors do not bind within the cleft between the two lobes. Additionally, Lamba and Gosh proposed that agents that span two distinct regions of the protein kinase domain should be classified as bivalent or type V inhibitors [49]. For example, an antagonist that binds to the SH2 domain and adenine-binding pocket of Src would be classified as a type V inhibitor [50]. To complete this classification, we named type VI inhibitors as those agents that form covalent bonds with their target enzyme [25]. For example, afatinib is a covalent type VI inhibitor of mutant EGFR that is used for the treatment of NSCLC. Mechanistically, this medicinal initially binds like a type I inhibitor to an active EGFR conformation and then the C797–SH group of the enzyme attacks the drug to form an irreversible covalent Michael adduct (PDB ID: 4G5J) [25].

Because inactive protein kinase conformations exhibit greater structural variation than the conserved active conformation to which type I inhibitors bind, it was hypothesized that type II inhibitors would

Table 2
Important residues in human EGFR and Abl.[a]

	EGFR	Abl	Inferred function	Hanks no.
Protein kinase domain	712-979	242–493	Catalyzes substrate phosphorylation	I–XI
N-lobe				
Glycine-rich loop; GxGxΦG	^{719}GSGAFG^{724}	^{249}GGGQYG^{254}	Anchors ATP β- and γ-phosphates	I
β3-Lys (*K* of *K*/E/D/D)	K745	K271	Anchors ATP α- and β-phosphates	II
αC-Glu (*E* of K/*E*/D/D)	E762	E286	Forms ion pair with β3-Lys	III
αC-β5-strand HΦ interaction	I759-V786	F283-I313	Stabilizes N-lobe	III–V
αC-β4 loop and αE helix HΦ contact	H773-Q820	H295-A350	Stabilizes N-lobe C-lobe interaction	IV–VI
Gatekeeper residue	T790	T315	Limits access to back pocket	V
Hinge residues	^{792}LMPFG^{796}	^{316}EFMTY^{320}	Connect N- and C-lobes	V
C-lobe				
αE-AS loop and AS HΦ-interaction	L833-L861	F359-L387	Stabilizes AS	VIb–VII
Catalytic loop HRD (first *D* of K/E/*D*/D)	837	363	Catalytic base (abstracts proton)	VIb
Catalytic loop-AS H-bond	R537-L858, H835-D855	R362-L384	Stabilizes AS	VIb–VII
Intracatalytic loop H-bonds	None	H361-D363 D363-N369	Stabilizes catalytic loop	VIb
Catalytic loop asparagine (N)	842	368	Chelates Mg^{2+}(2)	VIb
Activation segment	853–884	381–409	Regulates enzyme activity	VII–VIII
AS *D*FG (second *D* of K/E/D/*D*)	853	381	Chelates Mg^{2+}(1)	VII
Mg^{2+}-positioning loop	^{855}DFGLA^{859}	^{381}DFGLS^{385}	Positions Mg^{2+}(1)	VII
AS phosphorylation site	Y869	Y393	Stabilizes AS after phosphorylation	VIII
Protein substrate-positioning loop	^{873}GKVP^{876}	^{400}KFPI^{403}	Constrains protein substrate	VIII
AP/LE; end of the AS	^{882}ALE^{884}	^{407}APE^{409}		VIII
APE and αH-αI loop salt bridge	E873-R958	E409-R483	Stabilizes AS	VIII–XI
MW (kDa)	134.3	122.8		
No. of residues	1210	1130		
UniProt KB ID	P00533	P00519		

[a] AS, activation segment.

Table 3
Human EGFR and Abl regulatory spine, shell, and catalytic spine residues.

	Symbol	KLIFS No. Ref. [26]	EGFR	Abl
Regulatory spine				
β4-strand (N-lobe)	RS4	38	L777	L301
αC-helix (N-lobe)	RS3	28	M766	M290
Activation loop DFG-F (C-lobe)	RS2	82	F856	F382
Catalytic loop HRD-H (C-lobe)	RS1	68	H835	H361
αF-helix (C-lobe)	RS0	None	D896	D421
Shell residues				
Two residues upstream from the gatekeeper	Sh3	43	L788	I313
Gatekeeper, end of the β5-strand	Sh2	45	T790	T315
αC-β4 back loop	Sh1	36	C775	V299
Catalytic Spine				
β3-strand AxK-A (N-lobe)	CS8	15	A743	A269
β2-strand V (N-lobe)	CS7	11	V726	V256
β7-strand (C-lobe)	CS6	77	L844	L370
β7-strand (C-lobe)	CS5	76	V845	V371
β7-strand (C-lobe)	CS4	78	V843	C369
αD-helix (C-lobe)	CS3	53	L798	L323
αF-helix (C-lobe)	CS2	None	L907	L428
αF-helix (C-lobe)	CS1	None	T903	I432

be more selective than type I inhibitors. The studies of Vijayan et al. lend support to this notion [13] while the studies by Kwarcinski et al. and Zhao et al. do not [51,52]. Thus, the relative selectivity of type I and type II inhibitors remains unclear. By definition, Type III allosteric inhibitors bind next to the adenine binding pocket [48]. Owing to the greater variation of this location when compared with the adenine-binding pocket, type III inhibitors have the potential to exhibit greater selectivity than type I, I½, or II inhibitors. Moreover, Kwarcinski et al. hypothesized that type I½ antagonists that bind to the αC_{out} conformation may be more selective than type I or II blockers [51]. Abemaciclib, ribociclib, and palbociclib (all CDK4/6 antagonists) are US FDA-approved αC_{out} inhibitors. Kwarcinski et al. suggested that all protein kinases are able to assume the DFG-D_{out} conformation while they inferred that not all protein kinases are able to adopt the αC_{out} conformation [51]. In contrast, Hari et al. reported that many protein kinases are unable to adopt the DFG-D_{out} conformation [21]. A survey of more than 1250 protein kinase X-ray crystal structures in 2014 found that 5% exhibit a DFG-D dilated conformation, 10% exhibit a DFG-D_{out} conformation, and 85% exhibit a DFG-D_{in} conformation [13]. It must be noted that this is a biased representation because considerable effort has been made to study therapeutically targeted protein kinases and not a random assortment of enzymes that occur throughout the kinome.

We previously classified type I½ and type II antagonists into A and B subtypes [25]. Type A inhibitors are drugs that extend past the gatekeeper residue into the back cleft. Contrariwise, type B inhibitors are drugs that do not extend into the back cleft. Based upon preliminary results, the potential importance of this difference is that type B inhibitors bind to their target enzyme with shorter residence times [25] as compared with type A inhibitors [53]. Sunitinib is a VEGFR type IIB inhibitor that is approved by the FDA for the treatment of renal cell carcinomas. Sorafenib is a VEGFR type IIA inhibitor that is also approved by the FDA for the treatment of renal cell carcinomas. The type IIB inhibitor has a residence time of less than 2.9 min while that of the type IIA inhibitor has a residence time greater than 64 min [25].

Ung et al. examined several structural features of the protein kinase catalytic domain using the relative location of the αC-helix and the DFG-motif to define its conformational space [46]. Their studies describe the movement of the αC-helix from its active αC_{in} location to the inactive αC_{out} position by rotating and tilting. Correspondingly, the DFG motif can move from its active DFG-D_{in} location to the dormant DFG-D_{out} location. The catalytic domain of protein kinases under physiologic conditions exists in an equilibrium of inactive and active states. These workers described five different protein kinase conformations; they listed these as (i) αC_{in}-DFG-D_{in} (CIDI), (ii) αC_{in}-DGF-D_{out} (CIDO), (iii) αC_{out}-DFG-D_{in} (CODI), (iv) αC_{out}-DFG-D_{out} (CODO), and (v) ωCD; the ωCD designation signifies structures with variable DFG-D or αC-helix conformations. CIDI describes the active enzyme with a linear R-spine while CIDO describes the inactive DFG-D_{out} structure that results in the disassembly of the R-spine and the generation a new hydrophobic pocket. CODI refers to the inactive αC_{out} and DFG-D_{in} configuration. This structure may form because a drug or ligand induces the

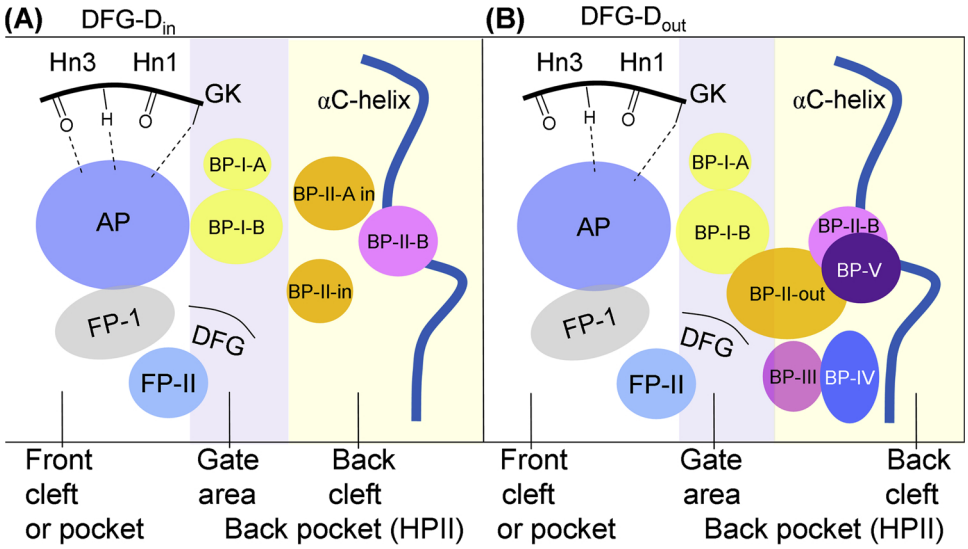

Fig. 3. Structure of the protein kinase domain drug-binding pockets. AP, adenine pocket; BP, back pocket; FP, front pocket; GK, gatekeeper; Hn, hinge; HPII, hydrophobic pocket II. Adapted from Ref. [26].

movement of the αC-helix outward. Alternatively, formation of a helix within the proximal portion of the activation segment may move the αC-helix to the αC_{out} position. The CODO conformation is an unusual structure that rarely occurs. ωCD structures represent a heterogeneous group with diverse DFG-D transitional states and variable αC-helix positioning.

4. Drug-ligand binding pockets

Liao [54] and van Linden et al. [26] divided the region between the small and large lobes of protein kinases into the front pocket (front cleft), the gate area, and the back cleft. The gate area and back cleft make up HPII (hydrophobic pocket II) or the back pocket (Fig. 3). The hinge residues, the adjacent adenine-binding pocket, the catalytic loop ($HRD(x)_4N$) residues, and the glycine-rich loop constitute the front cleft. The β3-strand of the small lobe and the proximal section of the activation segment including DFG of the large lobe make up the gate area. The αC-β4 back loop, the β4- and β5-strands of the small lobe, and the αE-helix within the large lobe constitute the back cleft. One of the challenges in the design of therapeutic small molecule protein kinase antagonists is to achieve selectivity in order to reduce undesirable off-target adverse events [14], a process that is facilitated by investigating drug interactions with their target protein kinases [4,55,56]. The binding pockets within the catalytic cleft play important roles in protein kinase inhibitor design and in maximizing drug affinity. In addition to exploiting hydrogen bonding and hydrophobic interactions, halogen bonding [57] may be used to increase ligand-binding affinity.

van Linden et al. described several regions that occur in the front pocket, gate area, and back cleft (Table 4) [26]. Thus, the front pocket contains residues that make up an adenine-binding pocket (AP) along with two adjacent front pockets (FP-I and FP-II). Most steady-state ATP-competitive inhibitors have a core pharmacophoric scaffold that interacts with key features of the adenine binding pocket. This core platform is adorned with various chemical fragments that interact with adjacent binding pockets. FP-I occurs between the large lobe xDFG motif (where x is the amino acid residue immediately before the activation segment DFG signature) and the solvent-exposed hinge residues and FP-II occurs between the small lobe β3-strand near the ceiling of the cleft and the glycine-rich loop. BP-I-A and BP-I-B occur within the gate area between the αC-helix, the β3- and β4-strands, the conserved β3-strand K of the AxK signature of the small lobe, and the xDFG-motif of the large lobe. The smaller BP-I-A pocket, which occurs near the top

Table 4
Location of selected catalytic cleft residues.

Description	Location	KLIFS residue no.[a]
GxGxΦG	Front cleft	4–9
β2-strand V (CS7)	Front cleft	11
β3-strand A (CS8)	Front cleft	15
HRD with $DFG\text{-}D_{in}$	Front cleft	68–70
$HRD(x)_4N$-N	Front cleft	75
β7-strand CS6	Front cleft	77
β3-strand K; three residues before the αC-helix	Gate area	17
αC-β4 penultimate back loop residue	Gate area	36
Gatekeeper	Gate area	45
The x of xDFG	Gate area	80
DFG	Gate area	81–83
αC-helix E	Back cleft	24
RS3	Back cleft	28
HRD with $DFG\text{-}D_{out}$	Back cleft	68–70

[a] Ref. [26].

of the gate area, is enclosed by residues of the αC-helix and the β5- and adjacent β3-strands including the β3-strand AxK residues. The larger BP-I-B, which allows for access to the back cleft, occurs in the center of the gate area. Both the smaller BP-I-A and larger BP-I-B occur in both the $DFG\text{-}D_{in}$ and the $DFG\text{-}D_{out}$ protein kinase structures. The gatekeeper residue as well as the x residue of the xDFG signature often bridge the C- and R-spines (Fig. 1B) [26].

As shown in Fig. 3A, BP-II-in and BP-II-A-in occur within the back cleft of the $DFG\text{-}D_{in}$ protein kinase conformation [54]. These subpockets are enclosed by the small lobe αC-β4 back loop, the αC-helix, and the β5- and β4-strands and the large lobe DFG-motif. Pivotal structural changes of BP-II-in and BP-II-A-in create BP-II-out that is found only in the $DFG\text{-}D_{out}$ conformation; this structural change is a consequence of the movement of DFG-F. This movement results in the formation of back pocket II-out (BP-II-out); it is found where the DFG-F occurs in the $DFG\text{-}D_{in}$ conformation. BP-II-B is bordered by the β4-strand and the adjacent αC-helix in both the $DFG\text{-}D_{in}$ and $DFG\text{-}D_{out}$ structures. In contrast, Back Pocket III (BP-III) is a structure that is found only in the $DFG\text{-}D_{out}$ conformation (Fig. 3B). This region occurs on the floor of BP-II-out between the αC-helix and the αC-β4 back loop of the N-terminal lobe, the β6-strand residues, the conserved catalytic loop HRD-H, the activation segment $DFG\text{-}D_{out}$ motif, and the αE-helices of the C-terminal lobe. BP-IV and BP-V are two pockets that are partially solvent exposed and they occur between the C-terminal lobe $DFG\text{-}D_{out}$ motif, the

catalytic loop, the β6-strand residues, the activation segment, and N-terminal lobe αC-helix (Fig. 3B).

van Linden et al. established an all-inclusive formulation of ligand and drug binding to more than twelve hundred human and mouse protein kinases [26]. Their kinase–ligand interaction fingerprint and structure (KLIFS) formulary includes an arrangement of 85 potential ligand binding-site residues occurring in both lobes. Their formulary helps in the discovery of related interactions and enables the classification of agents based upon their binding properties. Moreover, these investigators formulated a generalized amino acid residue numbering system that facilitates the comparison of different drug-enzyme interactions. Table 3 indicates the correspondence between the KLIFS database residue numbers and the regulatory spine, shell, and catalytic spine amino acid residue nomenclature. Moreover, these authors established a useful non-commercial and searchable web site that is regularly updated and describes the interaction of human and mouse protein kinases with bound drugs and ligands (klifs.vu-compmedchem.nl/). Moreover, the Blue Ridge Institute for Medical Research website, which is regularly updated, depicts the structures and key properties of all small molecule protein kinase inhibitors that are approved by the US FDA (http://www.brimr.org/PKI/PKIs.htm). Additionally, Carles et al. formulated an all-inclusive directory of small molecule protein kinase and phosphatidylinositol 3-kinase inhibitors that are or have been in clinical trials [3]. They developed a non-commercial and searchable web site, which is also regularly updated, that includes inhibitor physicochemical properties and structures, their protein kinase targets, therapeutic indications, the year of first approval (if applicable), and trade names (http://www.icoa.fr/pkidb/).

5. Type I drug-enzyme inhibitor structures and interactions

Bosutinib is an anilino-quinoline derivative (Fig. 4A) that is one of five small molecule protein kinase inhibitors (dasatinib, imatinib, nilotinib, ponatinib) that is approved for the treatment of Philadelphia chromosome-positive chronic myelogenous leukemias (CML) [58]. The drug is a potent inhibitor of Abl, which is the presumed target in the treatment of this illness. Bosutinib is a multikinase inhibitor with IC_{50} values in the nanomolar range for Src and Src family kinases including Fyn, Hck, Lck and Yes. It is also a potent inhibitor of Abl, Abl2, BLK, BMX, FGR, BTK, Frk, ErbB3, M3K5, ephrin-A3/8, and ephrin-B2/4 (ChEMBL ID: CHEMBL288441). The therapeutic efficacy of bosutinib may be related to inhibition of protein kinases in addition to Abl. The X-ray crystal structure with Src shows that the *N*1-quinoline makes a hydrogen bond with the backbone amide of M341, the third hinge residue (Fig. 4A). Bosutinib makes hydrophobic contact with four spine (RS3, CS6/7/8) and all three shell residues of Src (Table 5). The antagonist makes additional hydrophobic contact with the β1-strand residue that occurs immediately before the glycine-rich loop (L273); the residue in this position corresponds to KLIFS-3 (kinase–ligand interaction fingerprint and structure residue-3). It also makes hydrophobic contact with I294 of the β3-strand, K295 of the AxK signature, E310 and M314 of the αC-helix, I336 and V337 of the β5-strand, E339 and Y340 of the hinge, S342 and K343 before the αD-helix, A403 (the x of xDFG) and DFG-D404 of the activation segment. The 4-chlorine atom of the drug forms a halogen bond with the E310 carboxylate group within the α-helix. The quinoline group is found within the adenine pocket and the 2,4-dichloro-anilino group extends into BP-I-A and BP-I-B (Table 6). Bosutinib binds to the active form of Src with an open activation segment, αC_{in}, and a linear R-spine; it is therefore classified as a type I inhibitor [25]. The interaction of bosutinib with Abl has not been described (www.rcsb.org/).

Crizotinib is a pyrazole–pyridine amine derivative (Fig. 4B) that is used in the treatment of ALK-positive and ROS1-positive NSCLC [27,28,59,60]. Four other drugs are approved for the treatment of ALK-driven NSCLC including alectinib, brigatinib, ceritinib, and lorlatinib. Crizotinib is a multikinase inhibitor with IC_{50} values in the nanomolar range for ALK, ROS1, c-Met (hepatocyte growth factor receptor), and MST1R (CHEMBL601719). The X-ray crystal structure with ROS1 shows that the pyridine *N*1 forms a hydrogen bond with the backbone amide of M2029 (the third hinge residue) and the amino group forms a hydrogen bond with the carbonyl group of E2027 (the first hinge residue). The drug makes hydrophobic contact with three spine residues (CS6/7/8) and two shell residues (Sh1/2) (Table 5). Crizotinib also makes hydrophobic contact with the β1-strand L1951 (KLIFS-3), K1980 of the AxK signature, L2010 of the αC–β4 back loop, E2027 and L2028 of the hinge, D2033 before the αD-helix, R2083 and N2084 of the catalytic loop, and DFG-D2102. The 2-chlorine atom makes van der Waals contact with the carbonyl oxygen of G2101 (the x residue of xDFG). The pyrimidine occurs within the adenine pocket and the dichlorofluorophenyl group occurs within the front pocket and FP-I. Crizotinib binds to the active form of ROS and is classified as a type I inhibitor [25].

Brigatinib is a 2,4-diamino-pyrimidine derivative (Fig. 4C) that is used for the treatment of crizotinib-resistant ALK-positive NSCLC [61]. Brigatinib is a multikinase inhibitor with activity against ALK, ROS1, insulin-like growth factor-1 receptor (IGF-1R), Flt3, and EGFR (ChEMBL ID: CHEMBL354311). The X-ray crystal structure demonstrates that the amino group forms a hydrogen bond with the carbonyl oxygen of M1199 and the *N*1 pyrimidine forms a hydrogen bond with the N–H group of this third hinge residue. The drug makes hydrophobic contact with four spine residues (RS3, CS6/7/8) and the gatekeeper (Sh2). The antagonist makes additional hydrophobic contact with the β1-strand L1122 (KLIFS-3) as well as E1197, L1198, and A1200 within the hinge, E1210 in the αD–αE loop, R1253 and N1254 within the catalytic loop, and DFG-D1270. The amino-pyrimidine is found within the adenine pocket and the phosphoryl-phenyl group extends into the front pocket and FP-I. Brigatinib binds to the active form of ALK and is classified as a type I inhibitor [25].

Dasatinib is an amino-thiazole pyrimidine derivative (Fig. 4D) that is used in the treatment of Philadelphia chromosome-positive (i) chronic myelogenous leukemias and (ii) acute lymphoblastic leukemias [62]. The drug is a potent inhibitor of Abl, which is the presumed primary target in the treatment of this illness. The drug is a multikinase inhibitor with activity against BCR-Abl, Abl2, BTK, CSF1, CSK, DDR1/2, FGR, GAK, ephrin-A2/3/4/5/8, ephrin-B1/2/3/4, Kit, Src, and PDGFRα/β. Dasatinib is also a potent inhibitor of Src and Src family kinases including Fyn, Frk, and Hck (CHEMBL1421). Owing to the large number of enzymes inhibited by this drug, the therapeutic efficacy of dasatinib may be related to inhibition of protein kinases in addition to Abl. The X-ray crystal structure with Abl shows that one amino group forms a hydrogen bond with the carbonyl group of M318 and the *N*3 of the thiazole forms a hydrogen bond with the N–H group of this third hinge residue. The amino group of the carboxamide moiety forms a hydrogen bond with the –OH group of the gatekeeper T315. Dasatinib makes hydrophobic contact with four spine residues (RS3, CS1/2/3) and all three shell residues including the gatekeeper. The drug makes hydrophobic contact with the β1-strand L248 (KLIFS-3), V270 and K271 of the AxK signature, E286 of the αC-helix, I313 of the β5-strand, F317 of the hinge, T319, Y320, and G321 before the αD-helix, and A380 (the x of xDFG). The chlorine atom of the drug forms a halogen bond with the amide nitrogen of the AxK-K271. The amino-thiazole occurs in the adenine pocket and the anilino group is found in FP-I-A/B. Dasatinib binds to the active form of Abl and is classified as a type I inhibitor [25].

Fostamatinib is a 2-anilino-pyrimidine derivative that is approved for the second-line treatment of chronic immune thrombocytopenia [63]. This is a bleeding disorder that is characterized by low platelet values and a normal bone marrow. It is an autoimmune disease with antibodies directed against various platelet surface antigens. Fostamatinib is a prodrug that results in the formation of R406 following the cleavage of the methylphosphate (Fig. 4E) [64]. R406 is a multikinase inhibitor that targets the non-receptor protein-tyrosine kinase Syk

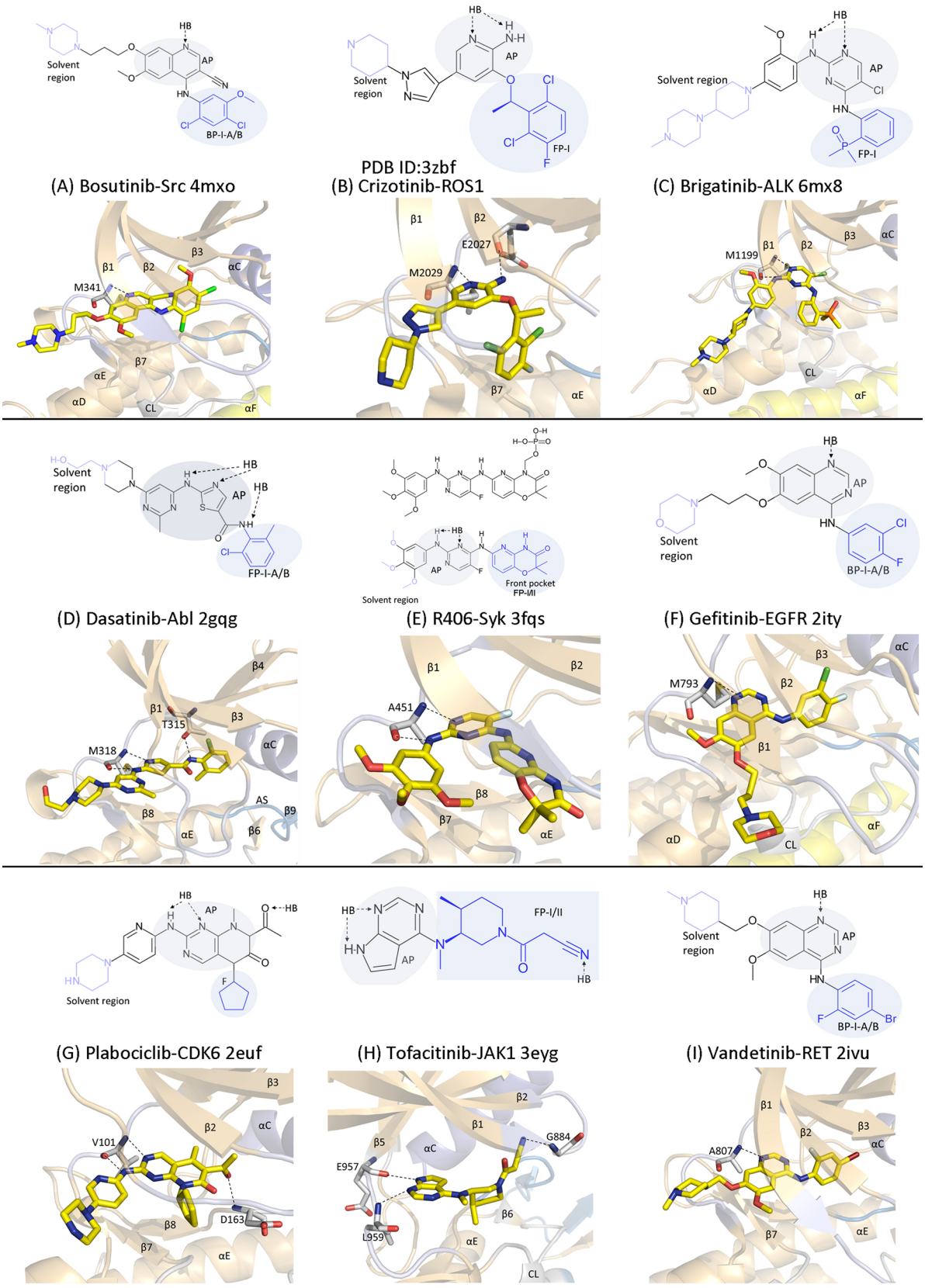

Fig. 4. Structures of drugs and drug-enzyme complexes of type I inhibitors. HB, atoms that participate in hydrogen-bond formation. The PDB ID is given in the title. The gray-shaded areas represent portions of the drug in the adenine pocket (AP) and the blue-shaded area occur within other pockets that are depicted in Fig. 3. BP, back pocket; FP, front pocket; GK, gatekeeper. These same descriptors are used in Figs. 5–9.

Table 5
Drug-enzyme hydrophobic (Φ) and hydrogen bonding (HB) interactions based upon their common KLIFS residue numbers[a,b]

	PDB ID	RS1	RS2	RS3	RS4	Sh1	Sh2	Sh3	CS3	CS4	CS5	CS6	CS7	CS8	KLIFS-3[e]
KLIFS no.		68	82	28	38	36	45	43	53	78	76	77	11	15	3
Drug-enzyme															
Type I inhibitors															
Bosutinib-Src	4mxo			Φ		Φ	Φ	Φ				Φ	Φ	Φ	Φ
Brigatinib-ALK	6mx8			Φ,HB			Φ					Φ	Φ	Φ	Φ
Crizotinib-ROS	3zbf					Φ	Φ					Φ	Φ	Φ	Φ
Dasatinib-Abl	2gqg			Φ		Φ	Φ,HB	Φ				Φ	Φ	Φ	Φ
Erlotinib-EGFR	1m17						Φ	Φ				Φ	Φ	Φ	Φ
Gefitinib-EGFR	2ity			Φ			Φ	Φ				Φ	Φ	Φ	Φ
Imatinib-Syk[c]	1xbb					Φ	Φ					Φ	Φ	Φ	Φ
Palbociclib-CDK6	2euf					Φ	Φ					Φ	Φ	Φ	Φ
R406 (fostamatinib)	3fqs					Φ	Φ					Φ	Φ	Φ	Φ
Tofacitinib-JAK1	3eyg					Φ	Φ					Φ	Φ	Φ	Φ
Tofacitinib-JAK3	3lxk					Φ	Φ				Φ	Φ	Φ	Φ	Φ
Vandetanib-RET	2ivu				Φ	Φ	Φ	Φ				Φ	Φ	Φ	Φ
Type I½A inhibitors															
Dabrafenib–B-Raf	5csw		Φ,HB	Φ	Φ	Φ	Φ	Φ				Φ	Φ	Φ	Φ
Lapatinib-EGFR	1xkk		Φ	Φ	Φ	Φ	Φ	Φ				Φ	Φ	Φ	Φ
Lenvatinib-VEGFR	3wzd		Φ	Φ		Φ	Φ					Φ	Φ	Φ	Φ
Palbociclib-CDK6	5l2i					Φ	Φ					Φ	Φ	Φ	Φ
Vemurafenib-B-Raf	3og7		Φ	Φ	Φ	Φ	Φ	Φ				Φ	Φ	Φ	Φ
Type I½B inhibitors															
Abemeciclib-CDK6	5l2s					Φ	Φ					Φ	Φ	Φ	Φ
Alectinib-ALK	3aox					Φ	Φ					Φ	Φ	Φ	Φ
Ceritinib-ALK	4mkc			Φ,HB		Φ						Φ	Φ	Φ	Φ
Crizotinib-ALK	2xp2			Φ			Φ					Φ	Φ	Φ	Φ
Crizotinib-Met	2wgj			Φ,HB		Φ	Φ					Φ	Φ	Φ	Φ
Erlotinib-EGFR	4hjo			Φ,HB		Φ	Φ					Φ	Φ	Φ	Φ
Ribociclib-CDK6	5l2t			HB		Φ	Φ					Φ	Φ	Φ	Φ
Type IIA inhibitors															
Axitinib-VEGFR	4ag8		Φ	Φ		Φ	Φ	Φ				Φ	Φ	Φ	Φ
Imatinib-Abl[d]	1iep	Φ,HB	Φ	Φ		Φ	Φ,HB	Φ				Φ	Φ	Φ	Φ
Imatinib-Kit	1t46	Φ	Φ	Φ		Φ	Φ,HB	Φ				Φ	Φ	Φ	Φ
Nilotinib-Abl	3cs9	Φ	Φ	Φ		Φ	Φ,HB	Φ				Φ	Φ	Φ	Φ
Ponatinib-Abl[d]	3oxz	Φ,HB	Φ	Φ		Φ	Φ	Φ				Φ	Φ	Φ	Φ
Ponatinib-Kit	4u0i	Φ,HB	Φ	Φ		Φ	Φ	Φ				Φ	Φ	Φ	Φ
Ponatinib-B-Raf	1uwh	Φ	Φ	Φ		Φ	Φ					Φ	Φ	Φ	Φ
Sorafenib-CDK8	3rgf	Φ	Φ	Φ		Φ	Φ					Φ	Φ	Φ	Φ
Sorafenib-VEGFR	4asd	Φ	Φ	Φ		Φ	Φ					Φ	Φ	Φ	Φ
Type IIB inhibitors															
Bosutinib-Abl	3ue4		Φ	Φ		Φ	Φ	Φ				Φ	Φ	Φ	Φ
Sunitinib-Kit	3g0e		Φ			Φ						Φ	Φ	Φ	Φ
Sunitinib-VEGFR	4agd		Φ			Φ	Φ					Φ	Φ	Φ	Φ
Type III and VI inhibitors															
Cobimetinib-MEK1	4an2		Φ	Φ		Φ	Φ	Φ				Φ	Φ	Φ	Φ
Afatinib-EGFR	4g5j			Φ			Φ	Φ				Φ	Φ	Φ	Φ
Ibrutinib-BTK	5p9j		Φ	Φ		Φ	Φ	Φ				Φ	Φ	Φ	Φ

[a] klifs.vu-compmedchem.nl/.
[b] Human enzyme unless otherwise noted.
[c] Not a therapeutic target for this drug.
[d] Mouse enzyme.
[e] KLIFS-3, kinase-ligand interaction fingerprint and structure residue-3.

(spleen tyrosine kinase) as well as BLK, CDC7, CSNK2A1, EGFR, ErbB2, FER, FGFR3, Flt1/3, Frk, IRAK1, LRRK2, Lyn, MAPK8/10, MAP3K10, PDGFRβ, PDPK1, PLK3/4, RET, ROS1, SIK2, SLK, Src, STK17A, Tyk2, and VEGFR1/2/3 (CHEMBL475251). Syk plays an important role in B-cell receptor signaling [63]. Binding of antiplatelet antibodies to surface antigens makes the platelets prone to phagocytosis by macrophages in a Syk-dependent Fcγ receptor (FcγR)-mediated process. Inhibition of Syk inhibits this activity, which results in improved platelet counts in patients with chronic immune thrombocytopenia. The X-ray crystal structure of R406 with Syk shows that the anilino nitrogen forms a hydrogen bond with the carbonyl group of A451 and the pyrimidine *N1* forms a hydrogen bond with the N–H group of the same third hinge residue. The drug makes hydrophobic contact with three spine residues (CS6/7/8) and two shell residues (Sh1/2) (Table 5). The drug also makes hydrophobic contact with the β1-strand L377 (KLIFS-3), the glycine-rich loop residue S379 as well as E449, M450, A451, and E452 of the hinge region, and P455 immediately before the αD-helix. The drug occupies only the front pocket and FP-I/II. R406, the active metabolite of fostamatinib, binds to the active form of Syk and is classified as a type I inhibitor [25]. See Ref. [65] for a summary of the clinical trials that led to the approval of fostamatinib. It is conceivable that the efficacy of fostamatinib against chronic immune thrombocytopenia is related to the inhibition of protein kinases in addition to Syk.

Gefitinib is an anilino-quinazoline derivative (Fig. 4F) that is approved for the treatment of *EGFR* mutation-positive NSCLC [66,67]. The drug inhibits EGFR with IC_{50} values in the subnanomolar range; it has activity against several other protein kinases, but the IC_{50} values are in the micromolar range (ChEMBL ID: CHEMBL939). The X-ray crystal structure with EGFR demonstrates that the *N*1 quinazoline forms a hydrogen bond with the backbone amide of M793. The drug makes hydrophobic contact with four spine residues (RS3, CS6/7/8) and two shell residues (Sh2/3) including the T790 gatekeeper residue. The drug also makes hydrophobic contact with the β1-strand L718 (KLIFS-3), the AxK-K745 signature residue, E762 of the αC-helix, Q791, L792, P794 of

Table 6
Drug-protein kinase interactions.

Drug-enzyme[a]	PDB ID	DFG-D	AS[b]	αC	R-Spine	GK[c]	Inhibitor class	Pockets and sub-pockets occupied[d]
Type I inhibitors								
Bosutinib-Src	4mxo	in	open	in	linear	T	I	F, G, BP-I-A/B
Brigatinib-ALK	6mx8	in	?	in	linear (?)	L	I (?)	F, FP-I
Crizotinib-ROS1	3zbf	in	open	in	linear	L	I	F, FP-I
Dasatinib-Abl	2gqg	in	open	in	linear	T	I	F, FP-I-A/B
Erlotinib-EGFR	1m17	in	open	in	linear	T	I	F, G, B, BP-I-A/B
Gefitinib-EGFR	2ity	in	open	in	linear	T	I	F, G, BP-I-A/B
Palbociclib-CDK6	2euf	in	open	in	linear	F	I	F
R-406 (fostamatinib)	3fqs	in	open	in	linear	M	I	F, FP-I/II
Tofacitinib-JAK1	3eyg	in	open	in	linear	M	I	F, FP-I/II
Vandetanib-RET	2ivu	in	open	in	linear	V	I	F, G, BP-I-A/B
Type I½A inhibitors								
Dabrafenib–B-Raf	5csw	in	?	out	RS3→	T	I½A	F, G, B, FP-II, BP-I-A/B, BP-II-in, BP-II-A-in
Lapatinib-EGFR	1xkk	in	closed	out	RS2/3→	T	I½A	F, G, B, BP-I-A/B, BP-II-in, BP-II-A-in
Lenvatinib-VEGFR	3wzd	in	?	in	RS3/4 up	V	I½A	F, G, B, BP-I-B, BP-II-in
Vemurafenib-B-Raf	3og7	in	?	out	RS3→	T	I½A	F, G, B, FP-I, BP-I-A/B, BP-II-in, BP-II-A-in
Type I½B inhibitors								
Abemeciclib-CDK6	5l2s	in	?	out	RS3→	F	I½B	F, FP-II
Alectinib-ALK	3aox	in	closed	in	RS3/4 up	L	I½B	F, BP-I-B
Ceritinib-ALK	4mkc	in	open	in	RS3/4 up	L	I½B	F, FP-I
Crizotinib-ALK	2xp2	in	closed	in	linear	L	I½B	F, FP-I
Erlotinib-EGFR	4hjo	in	closed	out	RS2/3→	T	I½B	F, G, BP-I-A/B
Palbociclib-CDK6	5l2i	in	?	out	RS3→	F	I½B	F
Ribociclib-CDK6	5l2t	in	?	out	RS3→	F	I½B	F, G, FP-I
Type IIA and IIB inhibitors								
Axitinib-VEGFR	4ag8	out	closed	in	←RS2	V	IIA	F, G, B, BP-I-B, BP-II-out
Imatinib-Abl[e]	1iep	out	closed	in	←RS2	T	IIA	F, G, B, BP-I-A/B, BP-II-out, BP-IV
Nilotinib-Abl	3cs9	out	closed	in	←RS2	T	IIA	F, G, B, BP-I-A/B, BP-II-out, BP-III, BP-V
Ponatinib-Abl[e]	3oxz	out	closed	in	←RS2	T	IIA	F, G, B, BP-I-A/B, BP-II-out, BP-III, BP-IV
Sorafenib-VEGFR	4asd	out	closed	in	←RS2	V	IIA	F, G, B, BP-I-B, BP-II-out, BP-III
Bosutinib-Abl	3ue4	out	open	in	←RS2	T	IIB	F, G, BP-I-A/B
Sunitinib-VEGFR2	4agd	out	closed	in	←RS2	V	IIB	F, BP-I-B
Sunitinib-Kit	3g0e	out	closed	in	←RS2	T	IIB	F
Type III and VI inhibitors								
Cobimetinib-MEK1	4an2	in	closed	out	RS2/3/4→	M	III	F, G, B, BP-II-in
Afatinib-EGFR	4g5j	in	open	in	linear	T	VI	F, G, BP-I-A/B
Ibrutinib-BTK	5p9j	in	closed	out	RS3/4 up	T	VI	F, G, B, BP-I-B

[a] All human proteins unless otherwise noted.
[b] Activation segment.
[c] Gatekeeper residue.
[d] F, front cleft; G, gate area; B, back cleft; from http://klifs.vu-compmedchem.nl/.
[e] Mouse enzyme.

the hinge region, and T854 (the x residue of xDFG). The gefitinib chlorine atom makes van der Waals contact with the carbonyl group of L788 within the β5-strand while the fluoride atom makes van der Waals contact with the L788 side chain. The quinazoline occurs in the adenine pocket and the anilino group occurs in the gate area (BP-I-A, BP-I-B). Gefitinib binds to the active form of EGFR and is classified as a type I inhibitor [25].

Palbociclib is a pyrido[2,3-*d*]pyrimidine derivative (Fig. 4G) that is approved for the treatment of estrogen receptor-positive and ErbB2/HER2-positive breast cancer [15,29,68–70]. The inhibitory power of the drug has been tested against a variety of protein kinases, but its therapeutic targets (CDK4/6) are the only enzymes that are inhibited by low concentrations of the agent (CHEMBL189963). The X-ray crystal structure with CDK6 shows that the amino group forms a hydrogen bond with the carbonyl group of V101 and the *N*1 of the pyrimidine forms a hydrogen bond with the N–H group of V101, the third hinge residue. The 6-acetyl oxygen forms a hydrogen bond with the N–H group of DFG-D163. The drug interacts hydrophobically with three spine residues (CS6/7/8) and two shell residues (Sh1/2). It also makes hydrophobic contact with the β1-strand I19 (KLIFS-3) immediately before the glycine-rich loop, the AxK-K43 signature residue, and H100, V101, D102, Q103 within the hinge. Palbociclib also makes hydrophobic contact with T107 within the αD-helix, Q149 and N150 within the catalytic loop, A162 (the x of xDFG), and DFG-D163. The pyridopyrimidine is found in the adenine pocket and the cyclopentane moiety occurs in the front pocket. Palbociclib binds to the active form of CDK6 and is classified as a type I inhibitor [25].

Tofacitinib is a pyrrolo[2,3-*d*]pyrimidine derivative that is used in the treatment of rheumatoid arthritis, psoriatic arthritis, and ulcerative colitis; it is a potent JAK1/2/3 and Tyk2 antagonist, but it has little effect on other protein kinases (CHEBL221959) [33,71]. The X-ray crystal structure with JAK1 demonstrates that the pyrrolo N–H group forms a hydrogen bond with the carbonyl oxygen of E957 and the *N*1 of the pyrimidine group forms a hydrogen bond with the amide nitrogen of L959, the third hinge residue (Fig. 4H). The nitrile nitrogen forms a polar bond with G884 within the glycine-rich loop. The drug makes hydrophobic contact with three spine residues (CS6/7/8) and two shell residues (Sh1/2). Tofacitinib also makes hydrophobic contact with the β1-strand L881 (KLIFS-3), E883 of the glycine-rich loop, the AxK-K908 signature residue, F958 and L959 of the hinge region, S963 immediately before the αD-helix, and DFG-D1021. The pyrrolopyrimidine occurs within the adenine pocket and the piperidinyl-oxopropanenitrile occupies FP-I and FP-II. Tofacitinib binds to the active form of JAK1 and is classified as a type I inhibitor [25]. Tofacitinib also binds to the active form of JAK2 (PDB ID: 3fup), JAK3 (PDB ID: 3lxk), and Tyk2 (PDB ID: 3lxn) – all members of the JAK family – making it a type I inhibitor of

these enzymes.

Vandetanib is an anilino-quinazoline derivative (Fig. 4I) that is approved for the treatment of medullary thyroid cancers [40,72]; it is a multikinase inhibitor with activity against Abl, Abl2, BLK, PDGFRβ, ephrin-A6/8, BRK, DDR2, EGFR, Lck, MAP2K5, RET, Src, STK2/35, ROCK2, RIPK2, TYRO3, VEGFR1/2 (CHEMBL24828); its target in medullary thyroid cancer appears to be RET [40]. It is conceivable that the inhibition of other enzymes may play a role in its therapeutic efficacy. The X-ray crystal structure shows that the quinazoline *N*1 forms a hydrogen bond with the backbone amide nitrogen of third hinge residue of RET (A807). The drug makes hydrophobic contact with four spine residues (RS4, CS6/7/8) and all three shell residues (Sh1/2/3) (Table 5). Vandetanib also makes hydrophobic contact with the β1-strand L730 (KLIFS-3), the entire AxK signature (A756, V757, K758), E775 of the αC-helix, I778 of the αC–β4 back loop, E805, Y806, A807, K808, and Y809 of the hinge region. The quinazoline group occupies the adenine pocket and the substituted anilino group is found in BP-I-A and BP-I-B of the gate area. Vandetanib binds to the active form of RET and is classified as a type I inhibitor [25].

All of the type I inhibitors described in this section are found in the front pocket and gate area and do not extend into the back cleft. All of them form hydrogen bonds with the third hinge residue. Like ATP, crizotinib and tofacitinib form hydrogen bonds with the first and third hinge residues. All of the type I inhibitors make hydrophobic contact with the Sh2 gatekeeper, CS6/7/8, and KLIFS-3 of the β1-strand and most of these antagonists (except for gefitinib and erlotinib) interact with Sh1. All of these small molecule inhibitors, with the exception of erlotinib and tofacitinib, have six-membered polar rings that extend into the solvent region.

6. Type I½A inhibitors

Dabrafenib is an amino-pyrimidine derivative (Fig. 5A) that is approved as a single agent for the treatment of advanced melanomas with a *BRAF*^{V600E} mutation or in combination with trametinib (a MEK1/2 inhibitor) for the treatment of *BRAF*^{V600E} mutation-positive advanced melanomas or NSCLC [37,73,74]. There is little data on the range of other protein kinases in addition to B-Raf that are inhibited by dabrafenib (ChEMBL ID: CHEMBL2028663). Binimetinib, encorafenib, and vemurafenib are three additional B-Raf inhibitors that are approved for the treatment of melanomas. The X-ray crystal structure shows that the dabrafenib amino group forms a hydrogen bond with the carbonyl oxygen of B-Raf C532 and the *N*1 of the pyrimidine moiety form a hydrogen bond with the N–H group of this same third hinge residue. Furthermore, one of the sulfonamide oxygen atoms forms a hydrogen bond with the N–H group of DFG-F595. The drug makes hydrophobic contact with six spine residues (RS2/3/4, CS6/7/8) and all three shell residues (Sh1/2/3). Dabrafenib also makes hydrophobic contact with the β1-strand I463 (KLIFS-3), S465 within the glycine-rich loop, AxK-K483, W531 and C532 of the hinge, DFG-D594 and DFG-F595. The 2-fluoride atom of dabrafenib forms a halogen bond with the phenyl group of DFG-F595. The amino-pyrimidine occupies the adenine pocket and the fluorophenyl group occupies BP-I-A and BP-I-B within the gate area while the difluorobenzenesulfonamide occupies BP-II-in and BP-II-A-in within the back cleft of the DGF-D_{in}–αC_{out} enzyme structure (Table 6). Dabrafenib binds to an inactive (αC_{out}) structure and it extends into the back cleft and is classified as a type I½A inhibitor [25].

Lenvatinib is a quinoline derivative (Fig. 5B) that is used in the treatment of differentiated thyroid cancers, hepatocellular carcinomas, and the second-line treatment of renal cell carcinomas in combination with everolimus; the drug is a multikinase inhibitor that targets VEGFR2/3, RET, PDGFR, and Kit (CHEMBL1289601) [40,75–77]. Its effectiveness in these disorders may be the result of the inhibition of all of these enzyme targets. The X-ray crystal structure with VEGFR2 demonstrates that the quinoline *N*1 forms a hydrogen bond with the N–H group of C919, the third hinge residue. The ureido nitrogen atoms form polar bonds with αC-E885 and the ureido oxygen forms a hydrogen bond with the N–H group of DFG-D1046. Lenvatinib makes hydrophobic contact with five spine residues (RS2/3, CS6/7/8) and two shell residues (Sh1/2). The compound also makes hydrophobic contact with the β1-strand L840 (KLIFS-3), AxK-K868, E885 and I888 of the αC-helix, E917, F918, K920 of the hinge region, C1045 (the x of xDFG), DFG-D1046, DFG-F1047, and L1049 of the activation segment. The quinoline group occupies the adenine pocket and the cyclopropylcarbamoylamino-phenoxy group is found in BP-I-B and BP-II-in; the drug occupies the front pocket, gate area, and back pocket. The enzyme displays an inactive conformation owing to the subluxation of the R-spine between RS2 and RS3. Lenvatinib is classified as a type A inhibitor because of the extension of the drug into the back pocket. Because of the inactive DFG-D_{in} enzyme conformation, lenvatinib is classified as a type I½A inhibitor of VEGFR2 [25].

Vemurafenib is a pyrrolo[2,3-*b*]pyridine derivative (Fig. 5C) that is used in the treatment of advanced *BRAF*^{V600E}-mutant melanoma and Erdheim-Chester disease [78,79]. There is little data on the spectrum of

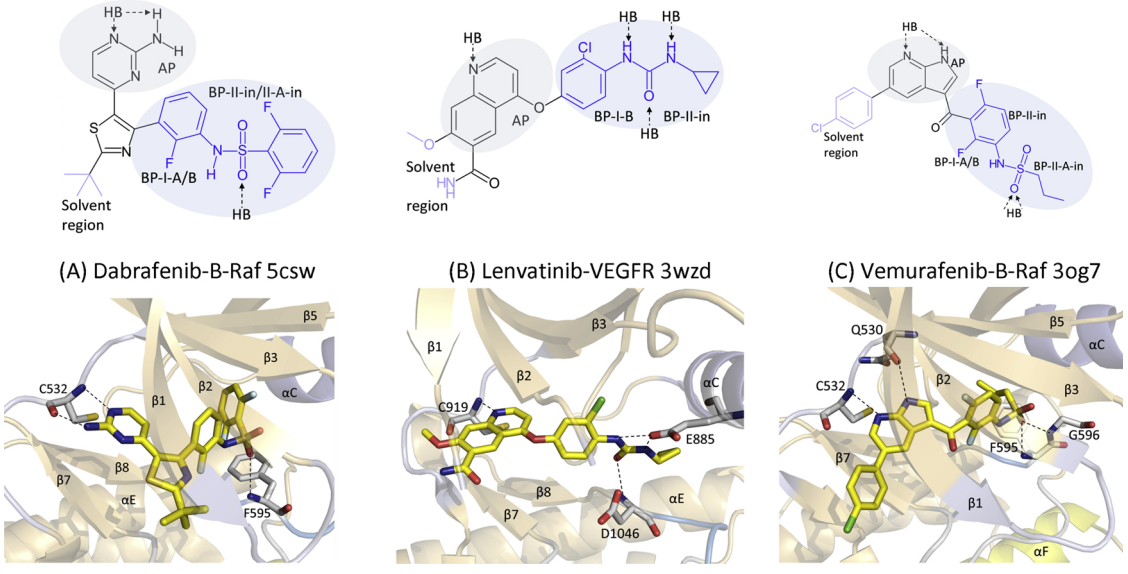

Fig. 5. Structures of drugs and drug-enzyme complexes of type I½A inhibitors. HB, atoms that participate in hydrogen-bond formation.

other protein kinases in addition to B-Raf that are inhibited by vemurafenib (CHEMBL1229517). Erdheim-Chester disease is a rare form of non-Langerhans cell histiocytosis that exhibits xanthogranulomatous infiltrations of multiple organs by lipid-laden histiocytes. The pathogenesis of this disease is unclear. However, there is increasing evidence supporting a clonal neoplastic process vs. inflammatory activity. The X-ray crystal structure with B-Raf shows that the *N*1 pyridine forms a hydrogen bond with the N–H group of C532 (third hinge residue) and the N–H group of the pyrrolo moiety forms a hydrogen bond with the carbonyl oxygen of Q530 (the first hinge residue). Moreover, one of the sulfonamide oxygen atoms forms hydrogen bonds with the N–H groups of both DFG-F595 and DFG-G596. The drug makes hydrophobic contact with six spine residues (RS2/3/4, CS6/7/8) and three shell residues. The compound also makes hydrophobic contact with the β1-strand I463 (KLIFS-3), the AxK signature (A481, V482, K483), L515 in the αC–β4 back loop, Q530, W531, and C532 of the hinge region as well as DFG-D594 and DFG-F595. The pyrrolopyridine occurs within the adenine pocket and the 2,4-difluorophenyl propane-1-sulfonamide occupies the gate area (BP-I-A, BP-I-B), BP-II-in and BP-II-A-in. Because the drug occurs in the back cleft, the inhibitor belongs to the A sub-grouping. B-Raf exists in an inactive αC_{out} configuration with DFG-D_{in} and the overall classification of the B-Raf – vemurafenib complex conforms to that of a type I½A antagonist [25].

7. Type I½B inhibitors

Abemaciclib is an amino-pyrimidine-benzimidazole derivative (Fig. 6A) that is used in the treatment of hormone receptor-positive and ErbB2/HER2-negative advanced breast cancer [15,80–83]. There is very little information on the range of protein kinases that are inhibited by this drug. This agent and palbociclib and ribociclib are CDK4/6 antagonists that are approved for the treatment of advanced breast cancers. The X-ray crystal structure with CDK6 shows that the amino group of abemaciclib forms a hydrogen bond with the carbonyl oxygen of V101 and the pyridine *N*1 forms a hydrogen bond with the N–H group of this same third hinge residue. Moreover, the benzimidazole *N*1 forms a hydrogen bond with the β3-strand K43. The agent makes hydrophobic contact with three spine residues (CS6/7/8) and two shell residues (Sh2/3). Abemaciclib also makes hydrophobic contact with the β1-strand I19 (KLIFS-3), Y24 of the glycine-rich loop, V27 of the β2-strand, AxK-K43, E99, H100, V101, D102 of the hinge, Q103 and D104 before the αD-helix, Q149 of the catalytic loop, A162 (the x of xDFG), and DFG-D163. The amino-pyridine occurs within the adenine pocket of the cleft and the benzimidazole occupies the front pocket and FP-II. The drug binds to an inactive αC_{out} structure with DFG-D_{in} and it does not enter the back pocket. These properties classify abemaciclib as a type I½B inhibitor [25].

Alectinib is a benzo[*b*]carbazole derivative (Fig. 6B) that is used in the treatment of ALK mutation-positive NSCLC; this medicine targets ALK and RET (ChEMBL ID: CHEMBL1738798) [40,84–87]. The X-ray crystal structure with ALK demonstrates that the alectinib carbonyl oxygen forms a hydrogen bond with the M1199 N–H group, the third hinge residue. The drug makes hydrophobic contact with three hinge residues (CS6/7/8) and two shell residues (Sh1/2). The medicinal also makes hydrophobic contact with the β1-strand R1120 and L1122 (KLIFS-3), AxK-K1150 as well as L1198, M1199, and A1200 of the hinge region, and D1203 before the αD-helix. The drug occupies the adenine pocket, the front pocket, and BP-I-B. It does not extend past the gate area making it a type B inhibitor; the enzyme exists in an inactive DFG-D_{in} conformation with a subluxation between RS2 and RS3 of the R-spine. These properties indicate that alectinib is a type I½B inhibitor of ALK [25].

Ceritinib is a 2,4-dianilino-pyrimidine derivative (Fig. 6C) that is used as a first-line or second-line treatment of ALK-positive NSCLC [88–91]; this multikinase inhibitor has activity against ALK, Flt3, IGF-1R, the insulin receptor, and ROS1 (CHEMBL2403108). It is possible that its therapeutic effects are related to the inhibition of several protein kinases in addition to ALK. The X-ray crystal structure with ALK demonstrates that the ceritinib amino group makes a hydrogen bond with the carbonyl group of M1199 and the *N*1 of the pyrimidine group makes a hydrogen bond with the backbone amide group of this same third hinge residue. The drug makes hydrophobic contact with four spine residues (RS3, CS6/7/8) and with one shell residue (Sh1) (Table 5). The drug also makes hydrophobic contact with the β1-strand L1122 (KLIFS-3), H1124 of the glycine-rich loop, the β2-strand L1132, the AxK-K1150 as well as E1197, L1198, A1200 of the hinge region, D1203 before the αD-helix, S1206 within the αD-helix, and DFG-D1270. The amino-pyrimidine occupies the adenine pocket and the propane sulfonylphenyl group occupies the front pocket and FP-I. There is a subluxation between RS2 and RS3 of the regulatory spine indicating that this DFG-D_{in} structure is dormant. Furthermore, the compound does not extend into the back pocket. These properties indicate the ceritinib is a type I½B inhibitor of ALK [25].

Crizotinib is a pyrazole-pyridine derivative (Fig. 6D) that is approved for the treatment of ALK-positive and ROS1-positive NSCLC [27,28,41,59,60,91–93]. The agent is a multikinase inhibitor as described in Section 5 (CHEMBL601719). Its therapeutic effectiveness may be related to the inhibition of enzymes in addition to ALK. The X-ray structure with ALK shows that the *N*1 pyridine forms a hydrogen bond with the N–H group of M1199 and the amino group forms a hydrogen bond with the carbonyl group of E1197; these are the third and first hinge residues, respectively. This hydrogen-bonding pattern mimics the binding of ATP to the hinge region of this enzyme. The drug makes hydrophobic contact with four spine residues (RS3, CS6/7/8) and one shell residue (Sh2, the gatekeeper). Crizotinib also makes hydrophobic contact with the β1-strand L1122 (KLIFS-3), the AxK-K1150 as well as L1198, M1199, A1200 of the hinge, D1203 before the αD-helix, R1253 and N1254 of the catalytic loop, and DFG-D1270. The amino-pyridine group occurs within the adenine pocket and the dichlorofluorophenyl group occupies the front pocket and FP-I. Crizotinib binds to an inactive enzyme (DFG-D_{in} with a closed activation segment) and it does not extend into the back pocket (making it a type B inhibitor); the drug is therefore classified as a type I½B inhibitor [25].

Ribociclib is a 2-amino-pyrrolo[2,3-*d*]pyrimidine derivative (Fig. 6E) that is used in the treatment of hormone receptor-positive ErbB2/HER2-negative advanced breast cancer; the drug targets CDK4/6 (ChEMBL ID: CHEMBL3545110) [15,29,94–97]. Very little data are available on the spectrum of protein kinases that are inhibited by this drug. The X-ray crystal structure with CDK6 shows that the amino group forms a hydrogen bond with the carbonyl group of V101 and the *N*1 of the pyrimidine forms a hydrogen bond with the N–H group of V101, the third hinge residue. Moreover, the carboxamide oxygen forms a polar bond with the N–H group of DFG-D163. The drug makes hydrophobic contact with three spine residues (CS6/7/8) and two shell residues (Sh1/2). The drug makes additional hydrophobic contact with the β1-strand I19 (KLIFS-3), the AxK-K43 signature, E99 and H100 of the hinge region, D104 before the αD-helix, N150 of the catalytic loop, A162 (the x of xDFG), and DFG-D163. The amino-pyrrolopyrimidine occurs within the adenine pocket and gate area while the cyclopentyl group occupies FP-I. The enzyme occurs in an inactive DFG-D_{in}–αC_{out} configuration and the drug does not extend into the back cleft. Accordingly, the drug is classified as a type I½B inhibitor [25].

Palbociclib is an amino-pyrido[2,3-*d*]pyrimidine derivative (Fig. 6F) that is used as part of a combination therapy for the treatment of advanced estrogen receptor-positive ErbB2/HER2-negative breast cancer [15,29,69,70,98,99]. The drug is a potent inhibitor of CDK4/6 and CLK4 (CHEMBL189963). Very little data are available on the range of protein kinases that are inhibited by this drug. The X-ray crystal structure with CDK6 shows that the amino group makes a hydrogen bond with the carbonyl oxygen of V101 and the *N*1 of the pyridopyrimidine forms a hydrogen bond with the N–H group of V101, the third hinge residue. The acetyl oxygen forms a hydrogen bond with the N–H

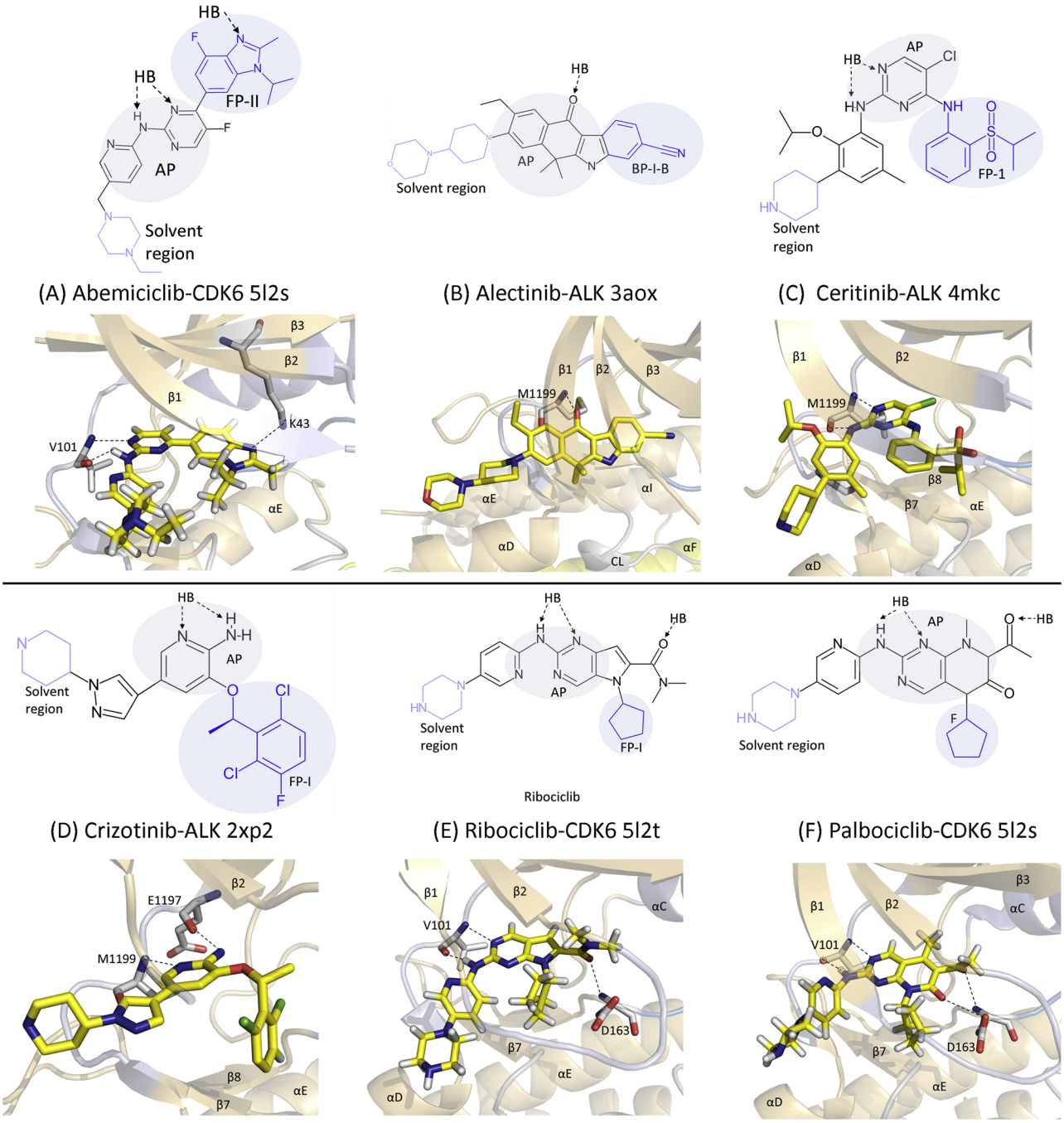

Fig. 6. Structures of drugs and drug-enzyme complexes of type I½B inhibitors. HB, atoms that participate in hydrogen-bond formation.

group of DFG-D163 and the carbonyl oxygen forms a polar bond with the R-group of DFG-D163. The drug makes hydrophobic contact with three spine residues (CS6/7/8) and two shell residues (Sh2/3). The drug also makes hydrophobic contact with the β1-strand I19 (KLIFS-3), AxK-K43, H100 of the hinge, Q103 and D104 before the αD-helix. Palbociclib also makes hydrophobic contact with T107 within the αD-helix, Q149 and N150 of the catalytic loop, A162 (the x residue of xDFG), and DFG-D163. The amino-pyridopyrimidine moiety occurs within the adenine pocket and the cyclopentyl group occurs in the front pocket. The drug is a type B inhibitor because it does not enter the back cleft and CDK6 has a DFG-D_{in} conformation along with the dormant αC_{out} structure; the drug is classified as a type I½B inhibitor [25].

8. Epidermal growth factor receptor-drug complexes

The EGFR family is among the most investigated protein-tyrosine kinases owing to its widespread role in signal transduction and in oncogenesis [30–32]. This family of enzyme receptors is implicated in the pathogenesis of a large fraction of lung and breast cancers, which number first and second, respectively, in the incidence of all types of malignancies worldwide (excluding skin). The ErbB family of proteins function physiologically as homo and heterodimers. The ErbB nomenclature is derived from the avian viral erythroblastosis oncogene to which these receptors are related. Five of the FDA-approved drugs target this family for the treatment of NSCLC and one (lapatinib) is used in the treatment of ErbB2/HER2-positive breast cancer. These drugs are among the more commonly prescribed agents owing to the sizable incidence of these malignancies. For example, nearly 20% of NSCLC

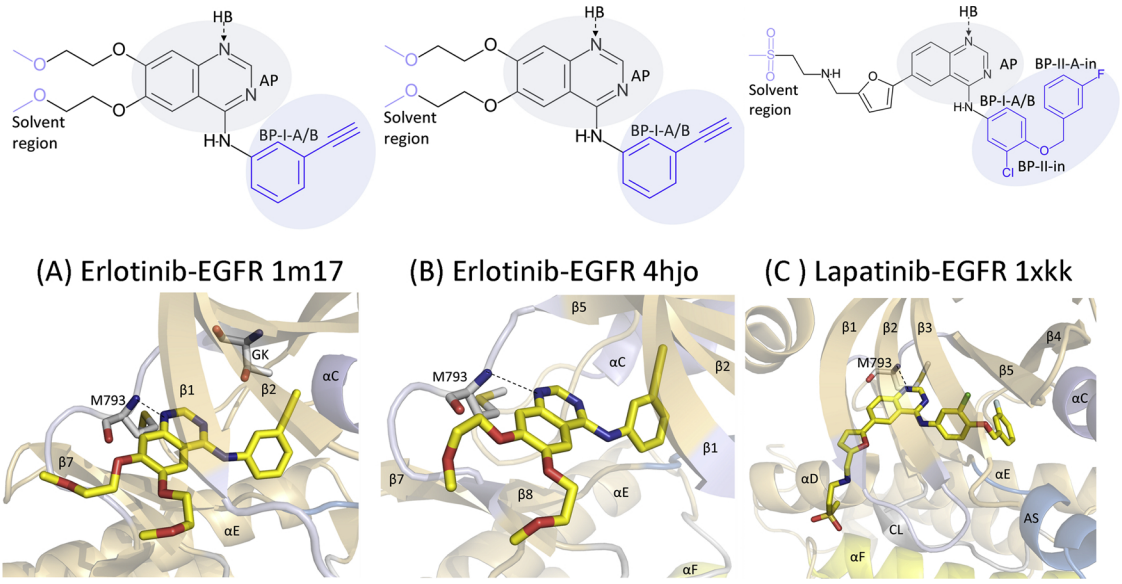

Fig. 7. Structures of drugs and drug-EGFR complexes. HB, atoms that participate in hydrogen-bond formation.

patients harbor activating mutations in *EGFR*. Moreover, nearly 20% of breast cancer patients exhibit *ErbB2/HER2* gene amplification on chromosome 17q. Erlotinib binds to EGFR as both a type I and type I½B inhibitor and lapatinib binds to EGFR as a type I½A inhibitor.

Erlotinib, which contains an anilino-quinazoline scaffold (Fig. 7A), is an effective EGFR antagonist that is used in the treatment of NSCLC and pancreatic cancer [30–32,100,101]. Its activity has been tested against a broad spectrum of enzymes; EGFR and GAK (cyclin G-associated kinase) are the only protein kinases displaying significant inhibition in the low nanomolar range (CHEMBL553). The X-ray crystal structure with EGFR indicates that the quinoline *N*1 forms a hydrogen bond with the backbone amide nitrogen of M793, the third hinge residue. Erlotinib makes hydrophobic contact with three spine residues (CS6/7/8) and two shell residues (Sh2/3) including the gatekeeper (Table 5). The agent also makes hydrophobic contact with the β1-strand L718 (KLIFS-3), K745 of the AxK signature, Q791, L792, M793, P794 and F795 before the αD-helix, T854 (the x of xDFG) and DFG-D855. The quinoline group occupies the adenine pocket and the ethynylphenyl group is found in the gate area (BP-I-A, BP-I-B). Erlotinib binds to the active form of EGFR and is classified as a type I inhibitor [25].

Erlotinib is also a type I½B inhibitor of EGFR. The X-ray crystal structure of erlotinib with EGFR indicates that the quinoline *N*1 forms a hydrogen bond with the backbone amide of M793, the third hinge residue (Fig. 7B) The agent makes hydrophobic contact with CS6/7/8. As a type I½B inhibitor erlotinib makes hydrophobic contact with RS3, Sh1 and Sh2; as a type I inhibitor, the drug makes hydrophobic contact with Sh2 and Sh3. Erlotinib makes hydrophobic contact with the β1-strand L718 (KLIFS-3), the AxK signature residues (A743, I744, K745), I789 immediately before the gatekeeper residue, T790 (the gatekeeper), Q791, L792, M793, P794, F795, C797 of the hinge region, D766 within the αD-helix, T854 (the x residue of xDFG), and DFG-D855. All of these contacts occur with active EGFR with the exception of C797 and T790. The main difference between the active and dormant enzyme is the occurrence of a short α-helix (the AL helix) in the proximal portion of the activation segment that prevents protein substrate binding and pushes the αC-helix to the out position. As described above for the prototype of type I inhibition, the quinoline group occupies the adenine pocket while the ethynylphenyl group is found in the gate area (BP-I-A and BP-I-B). Park et al. used a L834R EGFR mutant for the studies on the binding of erlotinib to a dormant enzyme; this mutation prevents the formation of homodimers that lead to the formation of an active enzyme and explains in part the ability to obtain a structure of a dormant enzyme with erlotinib [102].

Lapatinib is an anilino-quinazoline derivative (Fig. 7C) that is used in the treatment of ErbB2/HER2-positive breast cancer in combination with capecitabine or letrozole [103,104]; the drug targets only EGFR and ErbB2/HER2 of many tested enzymes (CHEMBL554). The X-ray crystal structure with EGFR shows that the quinazoline *N*1 forms a hydrogen bond with the N–H group of M793, the third hinge residue. Lapatinib makes hydrophobic contact with six spine residues (RS2/3/4, CS7/8/9) and all three shell residues (Sh1/2/3). The drug also makes hydrophobic contact with the β1-strand L718 (KLIFS-3), the AxK signature (A743, I744, K745), R766 of the αC–β4 back loop, L777 of the β4-strand, I789 of the β5-strand within the small lobe and Q791 of the hinge region. Lapatinib also makes hydrophobic contact with C797 before the αD-helix, L799 and D800 of the αD-helix, R841 of the catalytic loop, T854 (the x of xDFG), DFG-D855, DFG-F856, and L858 of the activation segment within the large lobe. The chlorine atom of lapatinib makes van der Waals contact with the carbonyl oxygen of L788 within the β4-strand and the fluorine atom makes a halogen bond with the backbone amide nitrogen of T790, the gatekeeper residue. The quinazoline group occurs in the adenine pocket and gate area (BP-I-A and BP-I-B) while the chlorophenyl group occupies BP-II-in while the fluorophenyl group is found in BPII-A-in. Lapatinib binds to an inactive DFG-D_{in}–αC_{out} conformation of EGFR and it extends into the back cleft and is classified as a type I½A inhibitor [25].

9. Type II inhibitors

Axitinib is an indazole derivative (Fig. 8A) that is approved for the second-line treatment of advanced renal cell carcinomas [105,106]. Six other small molecule protein kinase inhibitors are approved for the treatment of renal cell carcinomas including cabozantinib, everolimus, pazopanib, sorafenib, sunitinib, and temsiroliumus. Axitinib is a potent multikinase inhibitor of VEGFR1/2/3, PDGFRα/β, Kit (the stem cell growth factor receptor), Abl, and aurora-C (ChEMBL ID: CHEMBL289926). Its therapeutic efficacy may involve the inhibition of several of these enzymes. The X-ray crystal structure with VEGFR2 shows that the indazole *N*1 N–H group forms a hydrogen bond with the carbonyl group of the first hinge residue (E917) and the indazole *N*2 forms a hydrogen bond with the N–H group of the third hinge residue (C919). Moreover, the benzamide nitrogen forms a hydrogen bond with the αC-helix E885 and the benzamide oxygen forms a hydrogen bond with the N–H group of DFG-D1046, which is in the DFG-D_{out}

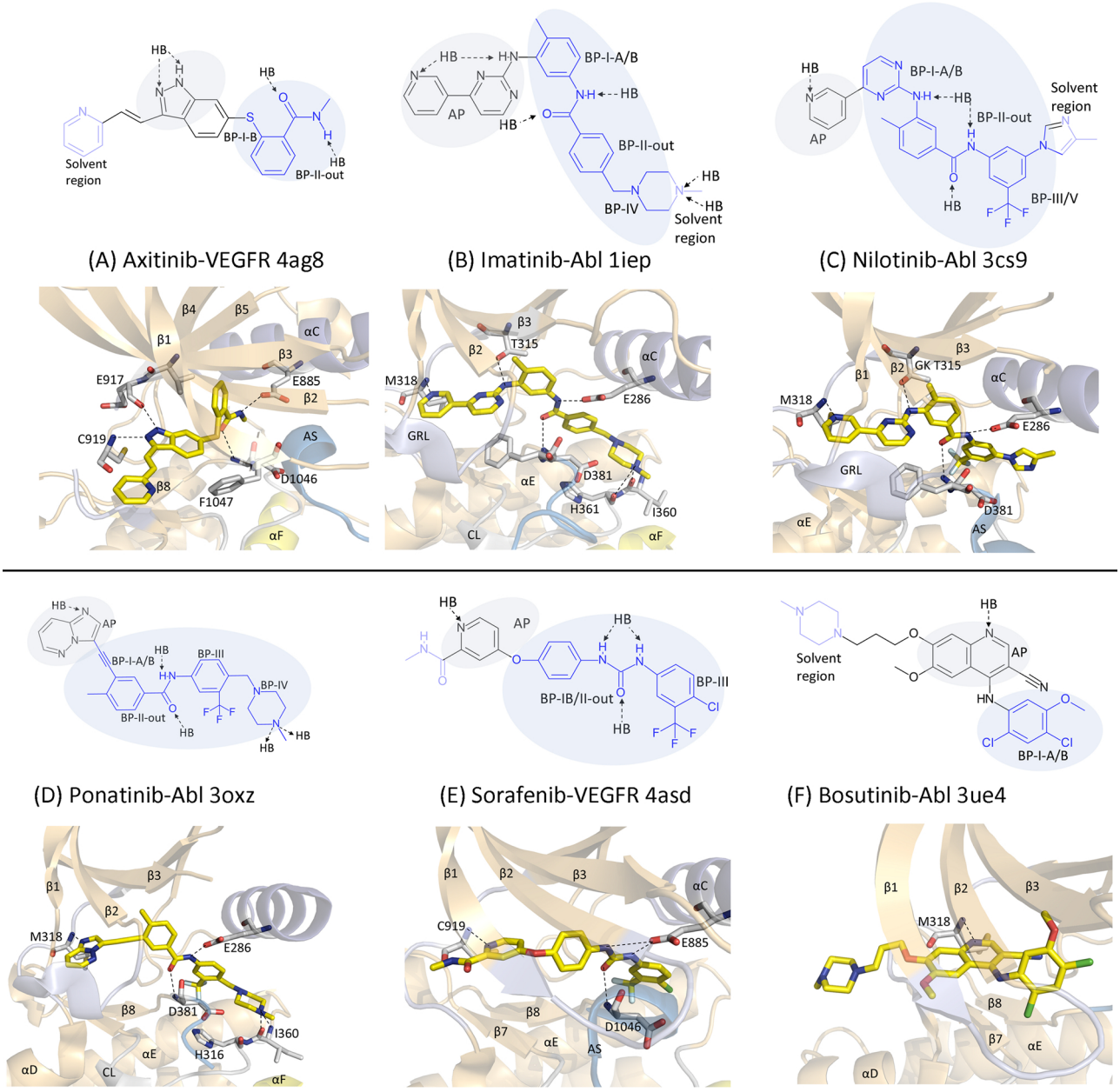

Fig. 8. Structures of drugs and drug-enzyme complexes of type II inhibitors. HB, atoms that participate in hydrogen-bond formation.

configuration. Type IIA inhibitors characteristically form a hydrogen bond with a hinge residue, the αC-helix glutamate, and the DFG-D_{out} residue as observed here. The drug makes hydrophobic contact with five spine residues (RS2/3, CS6/7/8) and all three shell residues. Moreover, the drug makes additional hydrophobic contact with the β1-strand L840 (KLIFS-3), the AxK signature (A866, V867, K868), E885 of the αC-helix, E917, F918, C919, K920, F921 of the hinge region, C1045 (the x of xDFG), DFG-D1046, and DFG-F1047. The indazole group is found within the adenine pocket and the benzamide moiety occupies the BP-I-B and BP-II-out. The drug binds to a dormant VEGFR2 with DFG-D_{out} and it extends into the back pocket; these are the properties of a type IIA inhibitor [25].

Imatinib is an 2-amino-4-pyrido-pyrimidine derivative (Fig. 8B) that is FDA-approved for the first-line treatment of Philadelphia chromosome-positive chronic myelogenous leukemias, Kit mutation-positive gastrointestinal stromal tumors, dermatofibrosarcoma protuberans, myelodysplastic/myeloproliferative diseases with PDGFR gene-rearrangements, chronic eosinophilia leukemias, hypereosinophilic syndrome, and as a second-line treatment for aggressive systemic mastocytosis without the KIT^{D816V} mutation and acute lymphoblastic leukemias [1,4,25,36,107]. The drug is a multikinase inhibitor with activity against Abl, Abl2, CSF1, DDR1, PDGFRα/β, and Kit (CHEMBL941). The X-ray crystal structure of imatinib bound to Abl demonstrates that the pyridine *N*1 forms a hydrogen bond with the N–H group of M318 and the amino group forms a hydrogen bond with the hydroxyl group of the gatekeeper T315. Moreover, the benzamide N–H group forms a hydrogen bond with the αC-E286 and the benzamide oxygen forms a polar bond with the N–H group of DFG-D381. The piperazine *N*4 forms polar bonds with the carbonyl groups of I360 and HRD-H361. The drug makes hydrophobic contact with six spine residues (RS2/3/4, CS6/7/8) and all three shell residues. Imatinib makes additional hydrophobic contact with the β1-strand L248 (KLIFS-3), Y253 of the glycine-rich loop, the three AxK signature residues (A269, V270, K271), E286 and V289 of the αC-helix, I293 of the back loop within the amino-terminal lobe, and F317 and M318 within the hinge region. It also makes hydrophobic contact with F359 and I360 of the

β6-strand, HRD-H361 and HRD-R362, A380 (the x of xDFG), and DFG-D381 and DFG-F382 within the carboxyterminal lobe. The amino-pyrimidine-pyridine moiety is found in the adenine pocket and the remainder of the drug occupies the gate area (BP-I-A, BP-I-B), BP-II-out, and BP-IV. The drug binds to dormant Abl with DFG-D_{out} and it extends into the back pocket; these properties are those of a type IIA inhibitor [25]. The approval of imatinib for the treatment of chronic myelogenous leukemias in 2001 paved the way for the development of all of the small molecule protein kinase inhibitors considered in this review with the exception of the indirect mTOR inhibitors.

Nilotinib is a 2-amino-4-pyrido-pyrimidine derivative (Fig. 8C) that is used as a first-line or second-line treatment of Philadelphia chromosome-positive chronic myelogenous leukemias [62,108,109]. The drug is a BCR-Abl, PDGFRα/β, and DDR1/2 (discoidin domain-containing receptor-1/2) antagonist (CHEMBL255863) with BCR-Abl being its prime target for this illness. The X-ray crystal structure with Abl demonstrates that the drug pyridine *N*1 forms a hydrogen bond with the N–H group of M318 (the third hinge residue), the amino group forms a hydrogen bond with the hydroxyl group of the gatekeeper (T315), the benzamide nitrogen forms a polar bond with the αC-helix E286 while the benzamide oxygen forms a hydrogen bond with the N–H group of DFG-D381. The drug makes hydrophobic contact with six spine residues (RS1/2/3, Cs6/7/8) and all three shell residues. Nilotinib makes additional hydrophobic contact with the β1-strand L248 (KLIFS-3), the glycine-rich loop Y253, the AxK signature (A269, V270, K271), K285, E286, V289, and M290 of the αC-helix, I293 and L298 of the back loop, V313 of the β5-strand within the small lobe and F317 and M318 within the hinge. It also makes hydrophobic contact with L354 of the αE-helix, F359 of the β6-strand, HRD-H361, V379 of the β8-strand, A380 (the x of xDFG), DFG-D381 and DFG-F382 within the large lobe. The pyridine moiety occupies the adenine pocket and the remainder of the drug is found in the gate area (BP-I-A, BP-I-B), BP-II-out, BP-III, and BP-V. As with the previous case, nilotinib binds to a dormant Abl with DFG-D_{out} and it extends into the back pocket; these properties are those of a type IIA inhibitor [25].

Ponatinib is an imidazole[1,2-*b*]pyridazine derivative (Fig. 8D) that is approved as a second-line treatment for chronic myelogenous leukemias and Philadelphia chromosome-positive acute lymphoblastic leukemias [110,111]. The drug is a multikinase inhibitor with activity against BCR-Abl, BCR-Abl^{T315I}, FGFR1, Flt3, Kit, RET, Src, and VEGFR2 (CHEMBL1171837); BCR-Abl represents the prime target in the treatment of CML and ALL. The X-ray structure with Abl demonstrates that the imidazole *N*1 forms a hydrogen bond with the N–H group of M318 (the third hinge residue), the benzamide nitrogen forms a hydrogen bond with the αC-helix E286, and the benzamide oxygen forms a polar bond with N–H group of DFG-D381. Moreover, the piperazine *N*4 nitrogen forms polar bonds with the carbonyl oxygen atoms of I360 and HRD-H361. The drug makes hydrophobic contact with six spine residues (RS1/2/3, CS6/7/8) and with all three shell residues. Ponatinib also makes hydrophobic contact with the β1-strand L248 (KLIFS-3), Y253 of the glycine-rich loop, the AxK triad signature sequence (A269, V270, K271), E786 and V789 of the αC-helix, I293 and L298 of the back loop, I313 of the β5-strand within the amino-terminal lobe and E316, F317, M318 within the hinge. It makes additional hydrophobic contact with F359, I360 of the β6-strand, HRD-H361 and HRD-R362 within the catalytic loop, V379 of the β8-strand, A380 (the x residue of xDFG), DFG-D381, and DFG-F382 within the carboxyterminal lobe. The imidazole-pyridazine component occupies the adenine pocket and the remainder of the drug is found in the gate area (BP-I-A, BP-I-B), BP-II-out, BP-III, and BP-IV. As with the previous two cases, ponatinib binds to a dormant Abl with DFG-D_{out} and it extends into the back pocket; these are the properties of a type IIA inhibitor [25].

Sorafenib is a pyridine-2-carboxamide derivative (Fig. 8E) that is used in the treatment of renal cell carcinomas, hepatocellular carcinomas, and differentiated thyroid cancers [112–115]. The drug is a multikinase inhibitor and its targets include VEGFR1/2/3, DDR2, EGFR, FGFR, HIPK4, Kit, B-Raf, Flt3, PDGFRβ, and RET (ChEMBL ID: CHEMBL1336). Its prime targets include VEGFR1/2/3, but inhibition of the other enzymes may play a role in its therapeutic efficacy. The X-ray structure with VEGFR2 shows that the pyridine *N*1 forms a hydrogen bond with the C919 N–H group (third hinge residue), the two ureido nitrogen N–H groups form hydrogen bonds with the carboxylate groups of αC-E885 and the ureido oxygen atom forms a hydrogen bond with the N–H group of DFG-D1046. The drug makes hydrophobic contact with six spine residues (RS1/2/3, CS1/2/3) and two shell residues (Sh1/2). Sorafenib also makes hydrophobic contact with the β1-strand L840 (KLIFS-3), AxK-K868, E885 and I888 of the αC-helix of the amino-terminal lobe and E917, F918, C919, and K920 of the hinge region. Furthermore, sorafenib makes hydrophobic contact with HRD-H1026 of the catalytic loop, I1044 of the β8-strand, C1045 (the x of xDFG), DFG-D1046 and DFG-F1047 within the carboxyterminal lobe. The pyridine group occupies the adenine pocket and the remainder of the drug is found in the gate area (BP-I-B), BP-II-out, and BP-III. Sorafenib binds to a dormant VEGFR2 with DFG-D_{out} and it extends into the back pocket; these properties are those of a type IIA inhibitor [25].

Bosutinib is a quinoline derivative (Fig. 8F) that is used for the treatment of chronic myelogenous leukemias [58]. The drug is a potent multikinase inhibitor of Abl, Src, Src family kinases, and several other protein kinases that are listed at the beginning of Section 5. The X-ray crystal structure with Abl shows that the *N*1-quinoline makes a hydrogen bond with the backbone amide of M318, the third hinge residue. Bosutinib makes hydrophobic contact with five Abl spine (RS2/3, CS6/7/8) and all three shell residues (Table 5). Bosutinib also makes contact with the β1-strand L248 (KLIFS-3), the AxK signature (A269, V270, K271), I313 and I314 of the β5-strand, F317, M318, T319, Y320 in the hinge region, A380 (the x of xDFG), and DFG-F382. The quinoline group occupies the adenine pocket and the 2,4-dichloro-5-methoxyanilino moiety is found in BP-I-A and BP-I-B within the gate area. Bosutinib binds to a dormant form of Abl with αC_{out} and DFG-$D_{out;}$ it is therefore classified as a type II inhibitor [25]. Because the drug does not extend into the back pocket, it receives a B designation (IIB).

Sunitinib is an indole derivative (Fig. 9A) that is used for the

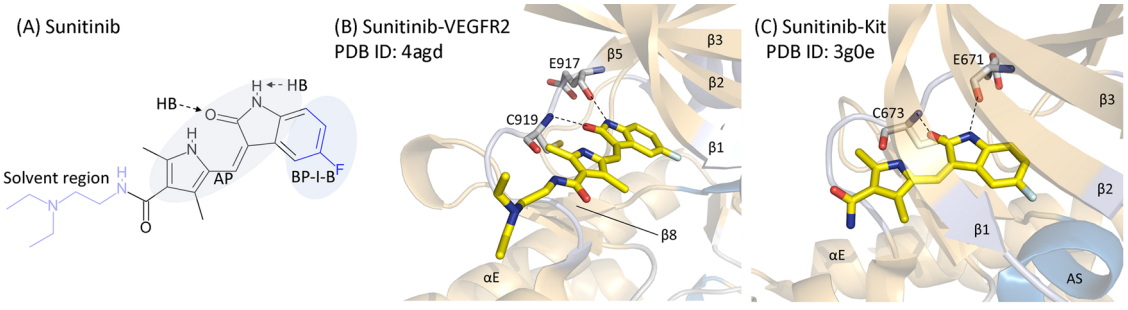

Fig. 9. (A) Sunitinib. (B) Sunitinib-VEGFR2 complex. (C) Sunitinib-Kit complex; not all of the drug atoms could be localized. AS, activation segment. HB, atoms that participate in hydrogen-bond formation.

treatment of renal cell carcinomas, pancreatic neuroendocrine tumors, and gastrointestinal stromal tumors [1,25,36,40]. The drug is a potent multikinase inhibitor of VEGFR2/3, PDGFRα/β, Kit, Flt3, LRRK2, BMP2K, Lck, CSF1R, CHK2 (CHEMBL535), and Axl [6]. Its effectiveness against renal cell carcinomas may be related to its inhibition of VEGFR2/3 and PDGFR while its effectiveness against gastrointestinal stromal tumors may be related to its inhibition of Kit [36]. The X-ray crystal structure with VEGFR2 (Fig. 9B) shows that the indole N–H group of sunitinib forms a hydrogen bond with the backbone carbonyl group of E917 (the first hinge residue) and the drug carbonyl oxygen forms a hydrogen bond with the N–H group of C919 (the third hinge residue). The drug makes hydrophobic contact with four spine residues (RS2, CS6/7/8) and two shell residues (Sh1/2) (Table 5). The drug also makes contact with the β1-strand L840 (KLIFS-3), the AxK-K868 signature residue, F918, C919, and K920 within the hinge, C1045 (the x of xDFG), and D1046 and F1047. The indole group occupies the adenine pocket and the 5-fluoro group extends into BP-I-B of the gate area. Sunitinib binds to a dormant form of VEGFR2 with DGF-D_{out} making it a type II inhibitor; the drug does not extend into the back pocket leading to the overall classification as a type IIB inhibitor [25].

Sunitinib was the standard of care for the first-line treatment of renal cell carcinomas from 2007 until 2015. The checkpoint inhibitor nivolumab became the preferred method of treatment of this disease in 2015. In 2018 the combination of nivolumab and ipilimumab (which targets CTLA-4) were shown to be more efficacious than sunitinib; the combination of the two monoclonal antibodies is the current standard of care for patients with advanced renal cell carcinomas.

The X-ray crystal structure of sunitinib with Kit (Fig. 9C) shows that the indole N–H group forms a hydrogen bond with the backbone carbonyl group of E671 (the first hinge residue) and the drug carbonyl oxygen forms a hydrogen bond with the N–H group of C673 (the third hinge residue). Owing to disorder, not all of the atoms of the drug could be traced. The drug makes hydrophobic contact with four spine residues (RS2, CS6/7/8) and one shell residue (Sh1). The drug also makes hydrophobic contact with the β1-strand L595 (KLIFS-3), the β3-strand AxK-K623, Y672, C673, C674 of the hinge region, C809 (the x of xDFG) as well as DFG-D810 and DFG-F811. The indole group occupies the adenine pocket and the drug occupies only the front pocket of this DFG-D_{out} conformation making it a type IIB inhibitor. The interaction of sunitinib with Kit closely mimics its interaction with VEGFR2.

10. Type III and VI inhibitors

Cobimetinib is an anilino-benzene derivative (Fig. 10A) that is approved as a first-line treatment of *BRAF*^{V600E}-mutant melanomas in combination with vemurafenib [74,116–118]. Its inhibitory potency against very few other protein kinases has been tested (CHEMBL2146883). Cobimetanib is a MEK1/2 antagonist while vemurafenib is a B-Raf inhibitor. The X-ray crystal structure of cobimetanib with MEK1 shows that the 3-hydroxyl group makes hydrogen bonds with the side-chain amide nitrogen of N195 at the end of the catalytic loop and with the carboxylate group of HRD-D190. The piperidine *N*1 makes a hydrogen bond with the HRD-D190 carboxylate group and the carbonyl oxygen makes a polar bond with AxK-K97 of the β3-strand. The drug makes hydrophobic contact with five spine residues (RS2/3, CS6/7/8) and all three shell residues. Additionally, cobimetanib also makes hydrophobic contact with the β1-strand L74 (KLIFS-3), A76 and N78 of the glycine-rich loop, AxK-K97, L115 and L118 of the αC-helix, and I141 of the β5-strand within the amino-terminal lobe along with E144, H145, M146 of the hinge region. Cobimetanib also makes additional hydrophobic contact with S150 before the αD-helix, Q153 within the αD-helix, HRD-D190, and K192 and N195 of the catalytic loop, DFG-D208, DFG-F209, and activation segment residues V211 and S212 within the carboxyterminal lobe. The drug occurs in the front pocket and the gate area and the diarylamino group occurs in the back pocket including BP-II-in. Note that the drug does not occupy the adenine pocket but it does occur in the deep cleft between the small and large lobes. It is therefore classified as a type III allosteric inhibitor [25].

Afatinib is an anilino-quinazoline derivative (Fig. 10B) that is approved for the first-line treatment of patients with NSCLC harboring *EGFR*-mutations or as a second-line treatment for patients with advanced NSCLC progressing after platinum-based chemotherapy [119–122]. The drug inhibits EGFR/ErbB1 and ErbB2, but its inhibitory power against very few other protein kinases has been examined (CHEMBL1173655). The X-ray structure with EGFR shows that the quinazoline *N*1 forms a hydrogen bond with the N–H group of M793 (the third hinge residue). The drug makes hydrophobic contact with four spine residues (RS3, CS6/7/8) and with two shell residues (Sh2/3). Afatinib makes hydrophobic contact with the β1-strand L781 (KLIFS-3), K728 and AxK-K745 of the β3-strand, E762 and M766 of the αC-helix, L788 of the β5-strand of the small lobe and it makes hydrophobic contact with L792, M793, P794, and F795 of the hinge region. The drug makes additional hydrophobic contract with C797 before the αD-helix, D800 of the αD-helix, R841 of the catalytic loop, and T854 (the x of xDFG) within the large lobe. The drug also forms a covalent bond with C797, which occurs just before the αD-helix. The quinazoline group is found in the adenine pocket and the 3-chloro-4-fluoroanilino group occurs in the gate area (BP-I-A and BP-I-B). The drug is bound to an active conformation of EGFR. However, it is classified as a type VI inhibitor because the drug is covalently bound to its target [25].

Ibrutinib is an amino pyrazolo[3,4-*d*]-pyrimidine derivative (Fig. 10C) that is used in the treatment of mantle cell lymphomas, chronic lymphocytic leukemias, Waldenström macroglobulinemia, and graph vs. host disease [123–126]. Its inhibitory power against very few other protein kinases has been examined (CHEMBL3747532). The drug is a covalent (type VI) inhibitor of Bruton tyrosine kinase. The X-ray structure with BTK shows that the pyrimidine *N*3 forms a hydrogen bond with the N–H group of M477 (the third hinge residue) and the 4-amino group forms a hydrogen bond with E475 (the first hinge residue) as well as the hydroxyl group of T474 (the gatekeeper residue). The carbonyl oxygen of the drug forms a hydrogen bond with the backbone amide of C481 and the drug forms a covalent Michael adduct with the same residue, which occurs before the αD-helix. The drug makes hydrophobic contact with five spine residues (RS2/3, CS6/7/8) and all three shell residues. Ibrutinib makes hydrophobic contact with the β1-strand L408 (KLIFS-3), AxK-K430, M499 of the αC-helix, I472 of the β5-strand of the small lobe and E475, Y476, and M477 of the hinge region. It also makes hydrophobic contact with C481 immediately before the αD-helix, S538 (the x of xDFG), DFG-D539, DFG-F540, and L542 of the activation segment within the large lobe. The amino-pyrimidine occurs within the adenine pocket and the phenoxyphenyl group occupies BP-I-B within the gate area. Table 6 contains a summary of the pockets and subpockets occupied by all of the drugs considered thus far. Ibrutinib assumes an inactive structure with DFG-D_{in}, but with αC_{out}. However, ibrutinib is classified as a type VI covalent inhibitor [25].

11. Additional drugs approved for the treatment of malignancies with unknown drug-enzyme binding properties

Dacomitinib is an anilino-quinazoline derivative [127] (Fig. 11A) that was approved by the FDA in 2018 for the first-line treatment of patients with advanced NSCLC with *EGFR* exon-21 L858R mutations or exon-19 deletions (see Supplementary material). The drug is a second-generation, irreversible type VI EGFR protein-tyrosine kinase antagonist that forms a covalent bond with C797 as described for afatinib. The inhibitory power of dacomitinib against a spectrum of protein kinases has not been reported. Clinical studies demonstrated that dacomitinib improved progression-free survival over gefitinib (14.7 months vs. 9.2 months) [128]. Moreover, dacomitinib increased overall survival over gefitinib (34.1 months vs. 26.8 months) [129]. Studies performed with cultured cells not derived from patient samples suggest that resistance

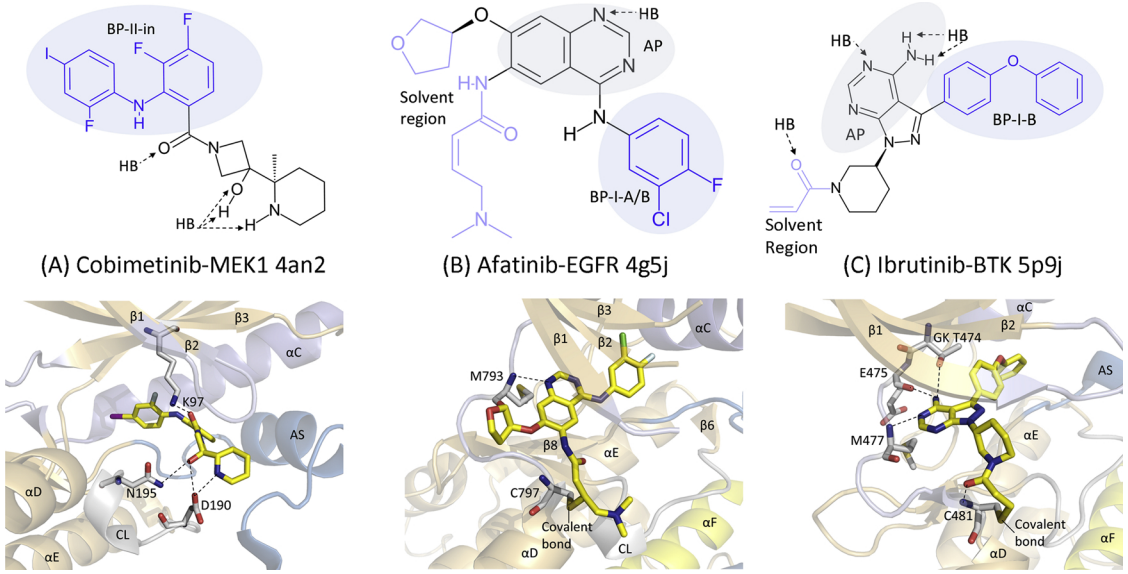

Fig. 10. Structures of drugs and drug-enzyme complexes of type III and VI inhibitors. HB, atoms that participate in hydrogen-bond formation.

to this agent may be related to either C797S *EGFR* or T790M mutations [130]. The ability of this drug to inhibit EGFR (ErbB1), ErbB2, and ErbB4 may add to its therapeutic efficacy [127]. Like the other quinazoline derivatives (gefitinib, vandetanib, erlotinib, lapatinib, and afatinib), the *N*1 of dacomitinib may form a hydrogen bond with the third hinge residue of EGFR.

Osimertinib is a 3-pyrimido-indole derivative (Fig. 11B) that was FDA-approved in 2015 for the first-line treatment of patients with metastatic NSCLC with *EGFR* exon-21 L858R or exon-19 deletions [131,132]. It is therapeutically advantageous that this agent has almost two hundred times greater affinity for the EGFR L858R/T790 mutant than it has for the wild type enzyme (CHEMBL3353410). However, the inhibitory power of osimertinib against a range of protein kinases has not been reported. The drug is also approved for the second-line treatment of individuals with *EGFR* T790M mutation-positive metastatic NSCLC whose disease became resistant to prior EGFR inhibitor therapy. Furthermore, osimertinib was the first drug approved for the treatment of patients with the EGFR T790M gatekeeper mutation. Like afatinib and dacomitinib, this agent is a type VI inhibitor that irreversibly inhibits EGFR by forming a covalent bond with C797. The first-line treatment with osimertinib was associated with an overall response rate of 67% and a median progression-free survival of 22.1 months [133]. This compares with previous clinical trials of erlotinib and gefitinib with a progression-free survival lasting 8.4 to 13.1 months [134]. Mechanisms of resistance to osimertinib include the *EGFR* C797S mutation or *KRAS* amplification [133]. Clinical trials comparing osimertinib vs. afatinib, erlotinib, or gefitinib are planned or are underway (www.clinicaltrials.gov). See Ref. [131] for a comprehensive discussion of the clinical trials that led to its approval. Based upon the inspection of the drug structure, the amino-pyrimidine group of the drug may form hydrogen bonds with EGFR hinge residues.

Neratinib is an anilino-quinoline derivative (Fig. 11C) that is used for the extended adjuvant therapy of women with early stage HER2/ErbB2-amplified/overexpressed breast cancer; the extended adjuvant therapy follows adjuvant trastuzumab-based treatment [135]. Adjuvant therapy refers to treatments given after surgery and extended adjuvant therapy follows adjuvant therapy. Neratinib contains an acrylamide group that forms a covalent bond with C805 near the ErbB2/HER2 ATP-binding site [136], making it a type VI inhibitor. Its affinity for a large number of protein kinases has been tested, but it interacts mainly with EGFR/ErbB1 and ErbB2 (CHEMBL180022). The efficacy of neratinib in treating HER2-positive breast cancer alone or in combination with trastuzumab has been studied in several clinical trials (clinicaltrials.gov). Neratinib was effective alone or in combination with other chemotherapeutic agents in the treatment of ErbB2/HER2-positive metastatic breast cancer patients. Refs. [135,137,138] summarize the clinical trials that led to the approval of this drug. See Ref. [136] for an account of the development of this ErbB2/HER2 inhibitor. The X-ray crystal structure of neratinib with EGFR is known (PDB ID: 2jiv). The quinoline *N*1 forms a hydrogen bond with the N–H group of the third hinge residue (M793). It is likely that this same interaction occurs with ErbB2.

Pazopanib is a 6-amino-indazole derivative (Fig. 11D) that is approved for the first-line treatment of advanced renal cell carcinomas and for the second-line treatment of soft tissue sarcomas [139–142]. The drug inhibits VEGFR1/2/3, PDGFRα/β, DDR2, and Kit (ChEMBL ID: CHEMBL477772). Its effectiveness against renal cell carcinomas may be the result of the inhibition of each of these enzymes. Sternberg et al. reported that pazopanib increased progression-free survival in patients with advanced renal cell carcinomas from 9.2 months compared with 4.2 months for a placebo [143]. It also produced an objective response rate of 30% compared with 3% for a placebo. Moreover, Motzer et al. reported that the response rates of sunitinib and pazopanib were equivalent [144]. However, they found that the patients who received pazopanib experienced less fatigue and fewer side effects than those who received sunitinib. van der Graaf et al. reported that progression-free survival rates in sarcoma patients treated with pazopanib were 4.6 months vs. 1.6 months in patients treated with a placebo [145]. Overall survival rates of patients treated with pazopanib were 12.5 months compared vs. 10.7 months for the placebo cohort. See Ref. [140] for a description of the development of this VEGFR inhibitor. It is conceivable that either an indazole nitrogen atom or the amino-pyrimidine nitrogen atoms form hydrogen bonds with the hinge residues of its target enzymes.

Regorafenib is a pyridine-2-carboxamide derivative containing a diaryl urea moiety (Fig. 11E) that was FDA-approved initially as a third or fourth-line treatment for advanced colorectal cancers [146,147]. It has subsequently been approved as a third-line treatment for gastrointestinal stromal tumors following imatinib and sunitinib and as a second-line treatment of hepatocellular carcinomas following sorafenib treatment [148,149]. The medication was initially developed as an angiogenesis inhibitor with activity against several receptor protein-tyrosine kinases including VEGFR1/2, PDGFRβ, Kit, and RET as well as the B-Raf protein-serine/threonine kinase [146,150]. Its clinical

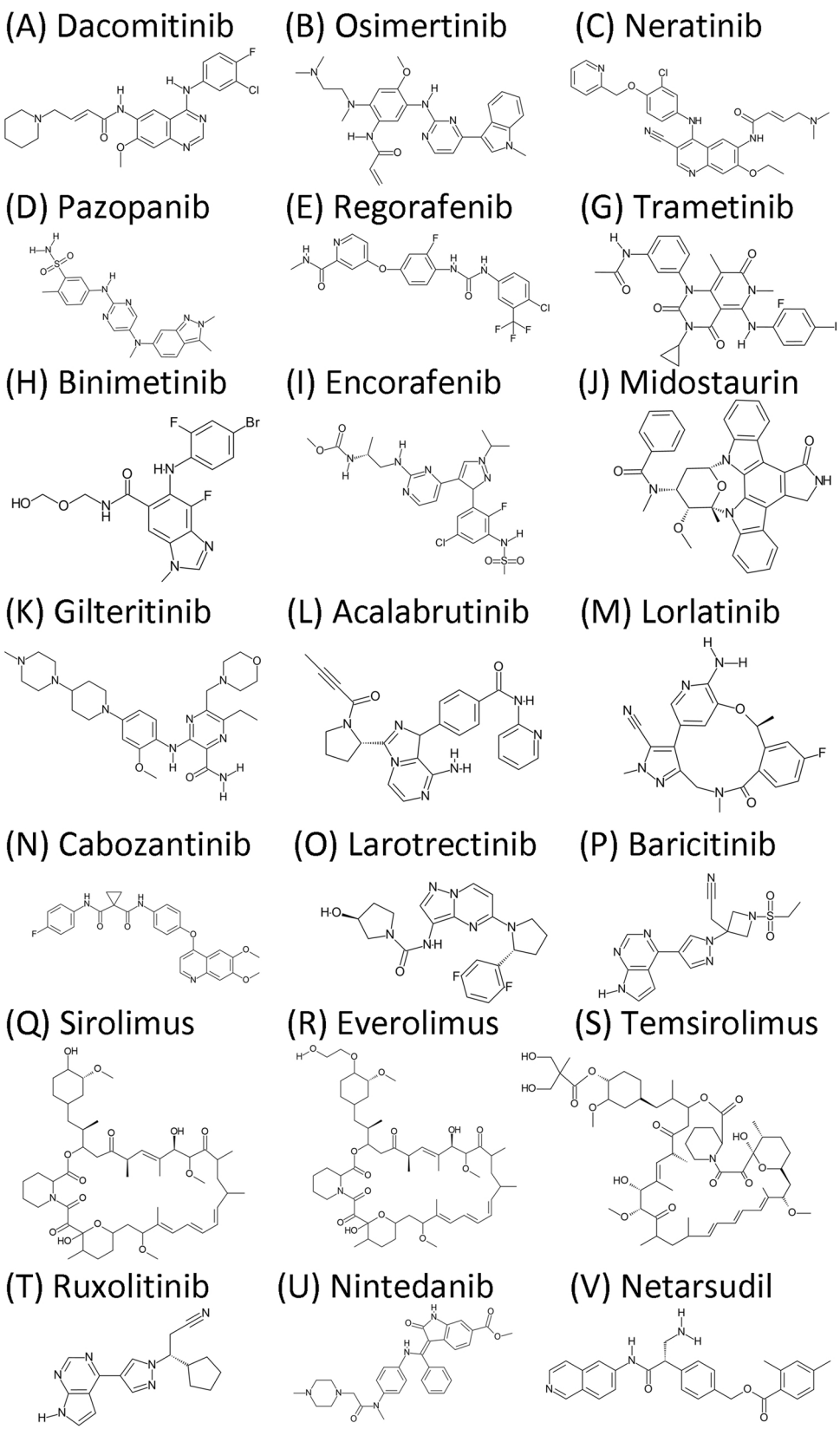

Fig. 11. Structures of FDA-approved small molecule protein-kinase inhibitors lacking drug-enzyme X-ray crystal structures.

effectiveness against these three tumor types may result from its multikinase inhibitor activity. Regorafenib is a sorafenib derivative that differs by the addition of a fluorine atom to the anilino group; both drugs were developed by Bayer. Regorafenib is also in clinical trials in patients with renal cell carcinomas, soft tissue sarcomas, and medullary thyroid cancers. See Refs. [146–149] for a summary of the clinical trials that led to its approval. The pyridine-2-carboxamide nitrogen atoms may form hydrogen bonds with hinge residues of its target enzymes that mimic those formed by sorafenib.

The Ras-Raf-MEK-ERK map kinase pathway is activated by several

mechanisms that lead to the production of many malignancies including melanomas [39]. The FDA has approved three protein kinase inhibitor protocols for the treatment of patients with metastatic/advanced skin melanomas that have a $BRAF^{V600}$ mutation (about 50% of all advanced melanoma patients). These approvals include a combination of a B-Raf and MEK1/2 inhibitors including: (i) encorafenib and binimetinib, (ii) vemurafenib and cobimetanib, and (iii) dabrafenib and trametinib. Studies are underway to determine whether one of these drug combinations is superior to the others.

Trametinib is a pyrido[4,3-*d*]pyrimidine derivative (Fig. 11G) that is approved in combination with dabrafenib for the treatment of melanomas and NSCLC harboring $BRAF^{V600E}$ mutations [151]. The drug is an allosteric antagonist and type III inhibitor of MEK1/2 (CHEMBL2103875). Its effect against a range of protein kinases has not been examined. It was initially developed by Japan Tobacco and was further developed by GlaxoSmithKline. Flaherty et al. compared trametinib and dabrafenib monotherapy with the combination of these two drugs in a clinical trial involving 247 patients with advanced melanoma with $BRAF^{V600}$ mutations [152]. They observed that the median progression-free survival was 9.4 months for the combination therapy group while it was 5.8 months for the monotherapy groups. Moreover, they reported that the frequency of complete or partial responses was 76% for the combination group while it was 54% for monotherapy groups. Current clinical trials are testing the efficacy of B-Raf and MEK inhibitors with immune checkpoint inhibitors [151]. Preliminary studies have found that such combinations are highly toxic and this finding has led to sequential rather than parallel administration of the drugs. Ref. [151] provides a comprehensive summary that led to the approval of trametinib in combination with dabrafenib. As a type III allosteric inhibitor, the drug is not expected to form hydrogen bonds with the hinge residues.

Binimetinib is a 6-anilino-benzimidazole derivative (Fig. 11H) that is approved in combination with encorafenib for the treatment of $BRAF^{V600E}$ mutant melanomas [153]. Encorafenib is a pyrazole-pyrimidine amine derivative (Fig. 11I) that inhibits B-Raf $^{V600E/K}$ while binimetinib is an allosteric Type III antagonist of MEK1/2. The inhibitory effects of these drugs against a spectrum of protein kinases has not been reported (CHEMBL3187723 and CHEMBL3301612). Dummer et al. reported on the findings of a clinical trial involving 577 patients with advanced/metastatic $BRAF^{V600}$ mutation-positive melanoma that had progressed on or after first-line immunotherapy or was previously untreated [153]. The patients were randomly assigned to receive either (i) binimetinib and encorafenib, (ii) vemurafenib, or (iii) encorafenib. With a median follow-up of 16.6 months, median progression-free survival was 14.9 months in the binimetinib plus encorafenib cohort and 7.3 months in the vemurafenib cohort; progression-free survival of the encorafenib group was not reported. These investigators concluded that encorafenib plus binimetinib combination therapy and encorafenib monotherapy showed favorable efficacy when compared with vemurafenib. Furthermore, they concluded that binimetinib and encorafenib combination therapy appears to have an improved tolerability profile compared with vemurafenib or encorafenib. The FDA approved the combination of binimetinib and encorafenib for the treatment of $BRAF^{V600E/K}$-positive advanced melanoma in 2018 [154]. As a type III allosteric inhibitor, binimetinib is not expected to make hydrogen bonds with the hinge residues of B-Raf. There are several possible ways that encorafenib might form hydrogen bonds with the hinge residues of B-Raf, but it would be preferable to examine the X-ray crystal structure of such complexes to give a definitive answer.

Midostaurin is a triazaoctacyclo derivative (Fig. 11J) that is approved for the treatment of *FLT3* mutation-positive acute myelogenous leukemias in combination with cytarabine and daunorubicin [155]. Flt3 is a receptor protein-tyrosine kinase that is activated by the FLT3LG cytokine. The drug is a multikinase inhibitor with activity against Flt3, TRKA/C, VEGFR2, PRKG2, RPS6KA2/3/6, MAP3K11, and MST1 [156]. Whether inhibition of enzymes other than Flt3 plays a therapeutic role in the treatment of this malignancy is unclear. *FLT3* mutations are found in about 30% of adults with newly diagnosed acute myelogenous leukemias. Nearly three quarters of such patients harbor a *FLT3* internal tandem duplication mutation. As a consequence, the duplication of between 3 and more than 100 amino acids occurs in the juxtamembrane region. Moreover, about 8% of patients with newly diagnosed disease harbor a *FLT3* point mutation in the tyrosine kinase domain. Both of these *FLT3* mutations produce proteins that spontaneously dimerize leading to ligand-independent activation. Talati and Sweet showed that the addition of midostaurin to chemotherapy resulted in a 22% lower risk of death when compared with patients who received chemotherapy plus placebo [155]. Moreover, overall four-year survival was longer in the midostaurin group than in the placebo group (51% vs. 44%). See Refs. [155,157,158] for a summary of the clinical trials that led to the approval of midostaurin. The X-ray crystal structure of midostaurin with human DYRK1A shows that the pyrrole N–H group forms a hydrogen bond with the carbonyl group of the first hinge residue and the adjacent drug carbonyl oxygen forms a hydrogen bond with the N–H group of the third hinge residue. DYRK1A is a dual specificity protein kinase. It is conceivable that the interaction of midostaurin with Flt3 is similar.

Gilteritinib is a 3-anilino-pyrazine derivative (Fig. 11K) that is an approved monotherapy for the treatment of *FLT3* mutation-positive acute myelogenous leukemias [159]. The drug is a multikinase inhibitor with activity against Flt3, ALK, Axl, RET, and ROS (ChEMBL ID: CHEMBL3301622). Whether inhibition of enzymes other than Flt3 plays a therapeutic role in the treatment of this malignancy is unknown. Perl et al. conducted a phase I–II clinical trial in patients with relapsed or refractory acute myeloid leukemias who received the drug [160]. They found that the overall response rate was 49% in patients with *FLT3* mutations vs. 12% of patients without the mutation. They found that the rates of complete remission and partial remission were greater in patients with *FLT3* mutations than in patients lacking the mutation (9% vs. 2% and 23% vs. 3%), respectively. Note that fewer than one-quarter of patients exhibit even a partial remission in patients harboring a *FLT3* mutation; such results are not uncommon in the cancer setting indicating that additional strategies should be developed to decrease primary drug resistance. Perl et al. reported that the adverse events including anemia, anorexia, and diarrhea could be easily managed in the outpatient setting. These findings led to the approval of gilteritinib in 2018 [160]. There are several possible ways that gilteritinib could interact with hinge residues of its target enzymes, but it would be preferable to examine the X-ray crystal structure of such complexes to give definitive answers.

Acalabrutinib is an imidazo[1,5-*a*]pyrazine derivative (Fig. 11L) that is approved for the second-line treatment of mantle cell lymphomas [161]. The drug is an irreversible type VI inhibitor that forms a Michael adduct with target –SH groups including C481 of Bruton tyrosine kinase (BTK). BTK is an essential component in the B cell receptor (BCR) signaling pathway and a driving force for chronic lymphocytic leukemias and other B cell malignancies [162]. In contrast to ibrutinib, acalabrutinib has much higher IC_{50} values (> 1000 nM) or virtually no inhibition on the protein kinase activities of BLK, ErbB1/2/3, FGR, Fyn, Hck, ITK, JAK3, Lck, Lyn, Src, and Yes [163]. In a clinical trial involving 124 patients with relapsed or refractory mantle cell lymphomas, Wang et al. reported that the overall response rate to acalabrutinib treatment was 81% with 40% achieving a complete response and 41% achieving a partial response [164]. They reported that there were fewer adverse events in comparison with the findings from ibrutinib clinical trials and this may be due to the lack of inhibition of BLK and the other enzymes listed. There are several conceivable ways that acalabrutinib could interact with hinge residues of its target enzymes, but it would be better to study actual X-ray crystal structures for clarification.

Lorlatinib is a macrocyclic pyrazole-pyridine derivative (Fig. 11M) that is approved for the second- and third-line treatment of ALK-positive NSCLC [165]. The drug is a multikinase inhibitor of ALK, FER, FES,

LTK, NRTK1, PTK2, and TNK2 (CHEMBL3286830). It is a derivative of crizotinib that was specifically designed to penetrate the blood-brain barrier to increase its effect on brain metastases frequently experienced by patients with lung cancers [166]. In a phase I clinical trial, Shaw et al. reported that the proportion of ALK-positive patients who achieved an objective response was 46% (19 of 41 patients). In ROS1-positive patients, including seven crizotinib-pretreated patients, an objective response was observed in six of 12 patients (50%) [167]. In a subsequent phase II study, Solomon et al. reported that ALK-positive patients who had been previously treated with at least one ALK protein-tyrosine kinase inhibitor, objective responses were observed in 93 of 198 (47%) patients and an objective intracranial response in those with measurable baseline central nervous system lesions was seen in 51 of 81 (63%) patients [168]. They reported that objective responses were achieved in 41 of 59 (69.5%) patients who had only received previous crizotinib therapy. Moreover, objective intracranial responses were achieved in 20 of 23 (87%) patients with measurable baseline central nervous system lesions. Based upon these studies, lorlatinib was approved in 2018 [165]. The amino-pyridine nitrogen atoms (as observed with crizotinib; PDB ID: 3zbf) represent possible sites of hydrogen bond formation with the hinge residues of its target enzymes.

Cabozantinib is a quinoline derivative (Fig. 11N) that is approved for the treatment of advanced medullary thyroid, renal cell, and hepatocellular carcinomas [169,170]. The drug is a multikinase inhibitor with activity against Axl, Flt3, FGFR1, Kit, c-Met, RET, Tie-2, and VEGFR1/2 (ChEMBL ID: CHEMBL2105717). Its clinical effectiveness against these three malignancies may result from the inhibition of a combination of these enzymes. Markowitz et al. reported that the approval for the treatment of medullary thyroid cancers was based on a phase III randomized double-blind placebo controlled international trial of 330 patients with documented radiographic progression of the disease [169]. The median duration of progression-free survival was 11.2 months in the cabozantinib group and 4.0 months in the placebo group. In a clinical trial comparing the efficacy of cabozantinib and everolimus in the treatment of advanced renal cell carcinomas, Singh et al. reported that progression-free survival increased from 7.4 months in patients receiving cabozantinib compared with 3.8 months in patients receiving everolimus [171]. Moreover, the overall response rate was 17% in the cabozantinib cohort compared with 3% in the everolimus group. Progression-free survival in previously treated patients with advanced hepatocellular carcinomas was studied in a double-blind, randomized phase III trial (CELESTIAL trial) that compared cabozantinib with a placebo [172]. Of the 707 patients that were studied, the results showed that the median overall survival was 10.2 months for the cabozantinib cohort compared with 8.0 months for the placebo cohort. Median progression-free survival was 5.2 months for cabozantinib vs. 1.9 months for the placebo. As a result of these and other studies, cabozantinib gained FDA approval for the first-line treatment of medullary thyroid and renal cell carcinomas and for the second-line treatment of advanced hepatocellular carcinomas in patients previously treated with sorafenib. The *N*1 of the cabozantinib quinazoline has the potential to form a hydrogen bond with hinge residues of its target enzymes as described above for gefitinib; whether or not this is the case must be verified experimentally.

Larotrectinib is a pyrazolo[1,5-*a*]pyridine derivative (Fig. 11O) that is approved for the first-line treatment of solid tumors bearing *NTRK* gene fusion proteins [173]. This drug was the first tissue-agnostic small molecule protein kinase inhibitor approved by the FDA for the treatment of solid tumors in adults and children that harbor a high-affinity nerve growth factor receptor protein-tyrosine kinase (*NTRK*) gene fusion protein; a tissue-agnostic inhibitor is so named because it is used for the treatment of any cancer harboring the gene fusion protein regardless of the organ, tissue, or anatomical location. Larotrectinib inhibits TRKA/B/C, but its inhibition of very few other enzymes has been examined (CHEMBL3889654). Oncogenic gene fusions involving *NTRK* result in constitutively activated, growth factor-independent downstream signaling of TRKs in a diverse spectrum of solid malignancies in adult and pediatric patients. These receptors play a physiological role in the growth, development, and survival of neurons. *NTRK* gene fusions involve chromosomal rearrangements involving an expressed 5′ partner (more than 60 have been identified) and a 3′ partner encoding NTRK. These fusion proteins may occur in up to 1% of all solid tumors. Drilon et al. reported on the efficacy of larotrectinib in a clinical trial involving both adult and pediatric patients bearing the NTRK gene fusion proteins (TRKA, 45%; TRKB, 2%, TRKC, 53%) [174]. The overall response rate was 80% with 17% complete responses and 63% partial responses. Patients had 17 different tumor types including infantile fibrosarcoma, melanoma, and thyroid, colon, lung, and gastrointestinal tumors. As a result of these and other studies, larotrectinib gained FDA approval for the treatment of solid tumors bearing *NTRK* gene fusion proteins in 2018 [173]. It is possible that the amino group and the pyridine ring nitrogen form hydrogen bonds with the hinge residues of its NTRK fusion protein targets, but it would be better to study actual X-ray crystal structures for definitive answers.

Sirolimus (rapamycin) is a natural occurring macrolide compound (Fig. 11Q) obtained from *Streptomyces hygroscopicus*. The macrolides contain a large macrocyclic lactone ring and they belong to the polyketide class of natural products. Sirolimus is a macrolide compound that is used to coat coronary stents, prevent kidney transplant rejection, and to treat a rare lung disease called lymphangioleiomyomatosis (LAM). Sirolimus binds to the FK Binding Protein-12 (FKBP-12 with a molecular weight of 12 kDa) to generate a complex that binds to and inhibits the activation of the mammalian Target Of Rapamycin (mTOR). mTOR is a protein-serine/threonine kinase that is a component of a complex signaling pathway involved in cell growth and metabolism [175]. mTOR exists in two multiprotein complexes, mTORC1 and mTORC2; the former, but not the latter, is sirolimus sensitive. Allosteric inhibitors are those that do not bind to the active site of their target enzyme [176]. In contrast to type III allosteric inhibitors that bind within the deep cleft of protein kinases, sirolimus is a type IV allosteric inhibitor that produces inhibition by binding elsewhere to non-active site residues. Sirolimus binds to FKBP-12, which then binds to mTOR to produce inhibition. Through its downstream effectors 4E-BP1 and S6K, mTOR participates in the initiation of the ribosomal translation of mRNA into proteins required for cell growth, cell cycle progression, and metabolism.

There are numerous modulators that control the activity of mTOR [175]. Positive regulators, such as growth factors and their corresponding receptors (e.g., IGF-1R, EGFR, VEGFR1/2/3), transmit signals to activate the PI3K–Akt–mTOR pathway. Negative regulators include phosphatase and tensin homolog (PTEN), TSC1 (tuberous sclerosis complex-1 or hamartin), and TSC2 (tuberin). TSC1 and TSC2 form a complex that inhibits mTOR. The inhibition of mTOR by sirolimus results in (i) the inhibition of T lymphocyte activation and proliferation that occurs in response to antigenic and cytokine (IL-2, IL-4, and IL-15) stimulation and (ii) the inhibition of antibody production.

An early phase I/II dose escalation trial involving HLA-mismatched living donor kidney transplant recipients demonstrated that sirolimus with corticosteroids and cyclosporine decreased organ rejection to 7.5% over three years in comparison with 32% in patients who received only the steroid and cyclosporine [177]. In a large phase III study involving more than thirteen hundred patients comparing sirolimus vs. azathioprine and corticosteroids plus cyclosporine, the incidence of rejection in the sirolimus cohorts was 12–17% compared with 30% for the azathioprine cohort. Moreover, clinical studies for the treatment of coronary artery stenosis using sirolimus-eluting stents vs. bare metal stents with the aim of improving outcomes by reducing the incidence of restenosis have been successful [178].

Lymphangioleiomyomatosis (LAM) is an uncommon disorder that produces diffuse cystic changes in the lung and occurs primarily in women [179]. The disease can be sporadic or occur in patients with tuberous sclerosis (which refers to the hard swelling in the brains of

these patients). Tuberous sclerosis is a rare multisystem genetic disorder that results in the formation of non-malignant tumors in the liver, kidney, heart, lungs, and skin [180]. It results from mutations in *TSC1* and *TSC2*, which encode hamartin and tuberin, respectively. Following *TSC1* or *TSC2* gene mutation, the resulting protein complex is no longer effective as an upstream negative regulator of mTOR and the mutation produces the constitutive activation of the mTOR pathway, which leads to unregulated cell growth. The pathogenesis of sporadic LAM often follows *TSC2* gene mutations that activate the mTOR pathway. Bissler et al. published the findings of the first clinical trial on the use of sirolimus for renal angiomyolipomas in patients with tuberous sclerosis as well as patients with sporadic LAM [180]. In a one year-treatment period, sirolimus significantly reduced the size of the tumors. Moreover, the pulmonary function of the patients in the study with LAM improved as well. Subsequently, a randomized placebo-controlled study of sirolimus for LAM enrolled 89 patients [181]. The forced expiratory volume at 1 s (FEV1) increased or remained stable during the one year's treatment. Moreover, the level of serum VEGF-D, a biomarker reflecting disease activity, decreased significantly during sirolimus treatment. These studies led to its approval for the treatment of lymphangioleiomyomatosis in 2015. The drug makes hydrophobic contact with several residues and it forms six hydrogen bonds with FKBP-12 (PDB ID: 1c9h).

Everolimus is a macrolide mTOR inhibitor (Fig. 11R) indicated for the treatment of (i) postmenopausal women with advanced hormone receptor-positive, ErbB2/HER2-negative breast cancer in combination with exemestane after failure of treatment with letrozole or anastrozole (the latter three drugs are aromatase inhibitors), (ii) adults with progressive neuroendocrine tumors of pancreatic origin (PNET) that are unresectable, locally advanced, or metastatic, (iii) adults with advanced renal cell carcinomas after failure of treatment with sunitinib or sorafenib. (iv) adults with renal angiomyolipomas and tuberous sclerosis not requiring immediate surgery, and (v) pediatric and adult patients with tuberous sclerosis who have subependymal giant cell astrocytomas (SEGA). Unlike temsirolimus, this drug is not converted to sirolimus in vivo.

O'Shaughnessy et al. reported on the results of clinical trials on hormone receptor-positive ErbB2/HER2-negative breast cancer patients comparing everolimus, exemestane, and a combination of these two drugs [182]. These postmenopausal women had locally advanced or metastatic breast cancer that had recurred or progressed on prior nonsteroidal aromatase inhibitor therapy. The combination of everolimus and exemestane more than doubled median progression-free survival when compared with exemestane alone (7.8 vs. 3.2 months, respectively). These studies led to the regulatory approval of this combination of drugs. Motzer et al. reported on a clinical trial involving 410 patients with advanced renal cell carcinomas who had previously received sunitinib, sorafenib, or both agents [183]. These patients received everolimus or placebo. Progression-free survival was greater in the former group (4.0 months) compared with those in the latter group (1.9 months). These studies led to the approval of everolimus as a second-line treatment following sunitinib or sorafenib. Later studies are comparing everolimus as second- and third-line therapies after treatment with additional small molecule protein kinase inhibitors including lenvatinib and cabozantinib [184].

Neuroendocrine tumors make up of a diverse group of malignancies [185]. These tumors are derived from neuroendocrine cells, most commonly those originating from the gastroenteropancreatic tract. As a group, neuroendocrine tumors are more indolent than epithelial tumors and they are characterized by median survival rates of longer than 30 months. The upregulation of the mTOR pathway has been shown to play a pivotal role in the pathogenesis of neuroendocrine tumors. In a phase III clinical trial involving 410 patients who were randomly assigned to monotherapy with everolimus or placebo, Gajate et al. reported that patients treated with everolimus had a significantly longer progression-free survival than the placebo cohort (11.4 versus 5.4 months) [185]. The data indicated that the benefit was observed irrespective of age, sex, race, geographic region, prior chemotherapy, or tumor grade. In 2011, based on the findings of this and similar studies, the US FDA and EMA (European Medical Agency) approved the use of everolimus for the treatment of progressive, advanced neuroendocrine tumors.

Tuberous sclerosis is an autosomal-dominant multisystem neurocutaneous disorder characterized by tissue dysplasia and cellular hyperplasia [186]. Its underlying pathophysiology involves critical intracellular signaling cascades that regulate many cellular functions, including cell growth, proliferation, and intermediary metabolism. Based on the genetics of the tuberous sclerosis, there was a strong scientific rationale to investigate mTOR inhibition as a therapeutic strategy for its treatment. Prior to the approval of everolimus, there were no treatment options for patients with tuberous sclerosis other than surgery. In a large double-blind, placebo-controlled, phase III clinical trial conducted in tuberous sclerosis patients, everolimus was shown to be an effective and safe treatment option for pediatric and adult patients with the disease who have SEGA (subependymal giant cell astrocytomas) [187]. In another trial, 117 patients with tuberous sclerosis and the astrocytoma received oral everolimus or placebo [187]. The primary endpoint was the SEGA response, which was defined as at least a 50% reduction in the volume of the astrocytoma compared with the initial baseline. Of the 78 patients randomized to receive everolimus, 35% of patients in the everolimus group responded, compared with 0% receiving placebo. Of the 110 patients with at least one baseline skin lesion, 42% of the everolimus group and 11% of the placebo group had a positive skin-lesion response. Moreover, of the 44 patients with at least one renal angiomyolipoma lesion at baseline, 53% of the everolimus group and none in the placebo group had a positive response. These and other clinical studies led to the approval of everolimus for the treatment of pediatric and adult patients with tuberous sclerosis who have subependymal giant cell astrocytomas. There are no available X-ray crystal structures of everolimus with FKBP-12. However, it is likely that its interaction with the target involves hydrogen bonding and hydrophobic interactions as reported for sirolimus.

Temsirolimus is an ester analog of sirolimus (Fig. 11S) that is approved for the treatment of advanced renal cell carcinomas [188]. This small molecule protein kinase inhibitor is not orally effective, but it must be given by intravenously. This drug inhibits the mTOR pathway as described for sirolimus; hydrolysis of the ester linkage of temsirolimus yields sirolimus. Kwitkowski et al. reported on the results of a clinical trial in 626 treatment-naïve patients with advanced renal cell carcinomas comparing temsirolimus, interferon-α, or the combination of the two drugs [189]. There was a statistically significant longer median overall survival in the temsirolimus cohort than in the interferon cohort monotherapy arm (10.9 months versus 7.3 months). There was also a statistically significant longer progression-free survival for the temsirolimus cohort than for the interferon-monotherapy cohort (median, 5.5 months versus 3.1 months). These and similar clinical trials led to the approval of temsirolimus for the treatment of renal cell carcinomas in 2007. Other small molecule protein kinase inhibitors approved for the treatment of renal cell carcinomas include axitinib, cabozantinib, everolimus, pazopanib, sorafenib, and sunitinib. Although there are no available X-ray crystal structures of temsirolimus bound to FKBP-12, it is likely that its interaction with the target involves hydrogen bonding and hydrophobic interactions as described for sirolimus.

12. Additional drugs approved for the treatment of miscellaneous diseases within unknown drug-enzyme binding properties

Baricitinib is a pyrrolo[2,3-*d*]pyrimidine derivative (Fig. 11P) like tofacitinib that is approved for the treatment of adult patients with moderate to severe rheumatoid arthritis who have had an inadequate

response to one or more tumor necrosis factor-α antagonist therapies such as adalimumab, certolizumab, or etanercept [190]. The drug is an inhibitor of the non-receptor protein-tyrosine kinases JAK1/2/3 and the related Tyk2 (CHEMBL2105759), which are the four members of the Janus kinase (JAK) family. Its inhibitory activity against other enzymes has not been reported. Whereas JAK1/2 and Tyk2 are ubiquitously expressed, JAK3 occurs predominantly in hematopoietic cells [35]. This enzyme family is regulated by numerous hormones such as erythropoietin, thrombopoietin, and growth hormone and numerous cytokines including various interleukins and interferons. Ligand binding to hormone and cytokine receptors results in the activation of associated Janus kinases, which then mediate the phosphorylation of the receptors. The SH2 domain of STATs (signal transducers and activators of transcription) binds to the receptor phosphotyrosines to promote STAT phosphorylation and activation by the Janus kinases. Following translocation to the nucleus, STAT dimers participate in the regulation of the expression of numerous proteins. JAK-STAT dysregulation results in autoimmune disorders such as Crohn disease, ulcerative colitis, and rheumatoid arthritis. JAK-STAT dysregulation also plays a role in the pathogenesis of polycythemia vera and myelofibrosis.

Taylor et al. reported on the results of a baricitinib clinical trial on 1307 patients with rheumatoid arthritis who were receiving methotrexate [191]. These patients were randomly assigned to receive baricitinib, adalimumab (an anti-tumor necrosis factor-α monoclonal antibody), or a placebo. The primary end point was a 20% improvement according to the criteria of the American College of Rheumatology (ACR20 response). More patients (70%) had an ACR20 response at week 12 with baricitinib than with adalimumab (61%) or placebo (40%). Significant decreased radiographic progression was observed after 24 weeks with both baricitinib and adalimumab as compared to a placebo. These investigators reported that infections were more frequent with the adalimumab and baricitinib cohorts than with the placebo cohort. Adalimumab and baricitinib reduced the levels of circulating neutrophils, but they increased serum aminotransferase, creatinine, LDL, and HDL cholesterol levels. See Ref. [190] for additional details that led to the approval of baricitinib as a monotherapy for the treatment of rheumatoid arthritis in 2018. Based upon the inspection of the drug structure, it is possible that the pyrrolo[2,3-*d*] pyrimidine of baricitinib forms hydrogen bonds with its target enzymes similar to those formed by tofacitinib with the JAK family as described in Section 5.

Ruxolitinib is a pyrrolo[2,3-*d*]pyrimidine derivative (Fig. 11T) like baricitinib and tofacitinib that is used in the treatment of patients with (i) intermediate or high-risk myelofibrosis, including primary myelofibrosis, post-polycythemia vera myelofibrosis, and post-essential thrombocythemia myelofibrosis and (ii) polycythemia vera who have had an inadequate response to or are intolerant of hydroxyurea [192,193]. The drug is a JAK1/2/3 and Tyk2 inhibitor, although the reported effects on the degree of JAK3 inhibition have been variable (CHEMBL1789941). The inhibitory power of ruxolitinib has not been tested in a wide range of other protein kinases. Primary myelofibrosis is a myeloproliferative neoplasm in which the production of an abnormal clone of hematopoietic stem cells in the bone marrow results in fibrosis or the replacement of the marrow with scar tissue. As a result of bone marrow fibrosis, blood cell formation occurs outside of the bone marrow in extramedullary sites such as the spleen and liver. Polycythemia vera is a condition in which the bone marrow produces too many red blood cells and possibly the overproduction of white cells and platelets. The *V617F* mutation of the JAK2 protein is found in approximately half of the individuals with primary myelofibrosis and 95% of patients with polycythemia vera [35]. Harrison et al. reported on the results of a clinical trial involving 219 patients with primary myelofibrosis, post-essential thrombocythemia myelofibrosis, or post-polycythemia vera myelofibrosis that received oral ruxolitinib or the best available therapy [194]. They reported that a total of 28% of the patients in the ruxolitinib group had at least a 35% reduction in spleen volume after 48 weeks as compared with 0% in the group receiving the best available therapy. Moreover, the mean palpable spleen length in the ruxolitinib cohort decreased by 56%, but it increased by 4% in the other group. Patients in the ruxolitinib group experienced a reduction in symptoms associated with myelofibrosis and had an improvement in overall quality-of-life measures. The most common grade 3 or higher hematologic abnormalities in either group were anemia and thrombocytopenia; these were managed by dose reduction, interruption of treatment, or transfusion. See Ref. [192] for additional information on the approval of ruxolitinib for the treatment of myelofibrosis and polycythemia vera. It is possible that the pyrrolo[2,3-*d*]pyrimidine of baricitinib forms hydrogen bonds with its target enzymes similar to those formed by tofacitinib with the JAK family as described in Section 5.

Nintedanib is an indole derivative (Fig. 11U) that is used for the treatment of idiopathic pulmonary fibrosis [195]. The drug is a multikinase inhibitor with activity against FGFR1/2, Flt3, Lck, MELK, PDGFRα/β, and VEGFR1/2/3 (CHEMBL502835). Richeldi et al. performed a clinical trial involving 1066 patients with idiopathic pulmonary fibrosis comparing nintedanib with a placebo [196]. They measured the rate of decline in the forced vital capacity over a one-year period. The rate of change of this parameter for the placebo group was 240 ml vs. 115 for the nintedanib cohort. These studies demonstrated that nintedanib reduced the rate of decline in this measurement, which is consistent with a decrease in the rate of disease progression. In follow-up studies, Rodrıguez-Portal reported that nintedanib continued to slow disease progression for periods of up to three years [195]. Pirfenidone (5-methyl-1-phenylpyridin-2-one) is an orally effective drug used in the treatment of idiopathic pulmonary fibrosis; it decreases the production of growth factors and procollagens I and II. These are the only two drugs that are approved for the treatment of this disorder, but there have been no head-to-head clinical trials comparing these two agents [197]. There are several possible ways that the amino-indole derivative could form hydrogen bonds with the hinge residues of its target enzymes, but it would be better to study the actual X-ray crystal structures for edification.

Netarsudil is an amino-isoquinoline derivative (Fig. 11V) that is an eye-drop approved for the treatment of open-angle glaucoma [198]. This disease is characterized by an increased intraocular pressure and is one of the most common causes of blindness worldwide owing to the degeneration of retinal ganglion cells [199]. Common medical treatments for glaucoma include carbonic anhydrase inhibitors (e.g., dorzolamide) and β-adrenergic receptor blockers (e.g., timolol). The most commonly prescribed medications are the prostaglandin F2α analogs (e.g., latanoprost) that reduce intraocular pressure by increasing aqueous humor outflow through the uveoscleral pathway. Netarsudil is a Rho associated protein serine/threonine kinase (ROCK1/2) inhibitor that lowers intraocular pressure by increasing aqueous humor outflow through the trabecular meshwork [198]. The inhibitory power of this drug has not been tested against a spectrum of protein kinases (CHEMBL3545127). ROCK1/2 are involved in cell contraction and cell stiffness in the Schlemm canal and the trabecular meshwork; these protein kinases are downstream from Rho-GTPases. Inhibiting ROCK1/2 reduces cell stiffness and cell contraction and decreases fibrous-related protein expression. As a result, ROCK1/2 blockade increases aqueous humor outflow resulting in decreased intraocular pressure. Netarsudil is a pro-drug that undergoes hydrolysis of the 2,4 dimethylbenzoyl group as catalyzed by corneal esterases to yield a more active form [200]. Clinical trials demonstrated that netarsudil was effective in lowering intraocular pressure and was equivalent (noninferior) to timolol [198]. There are several possible ways that the amino-isoquinoline derivative could form hydrogen bonds with the hinge residues of its target enzymes, but it would be better to examine the results of actual X-ray crystal structures for clarification.

13. Analyses of the physicochemical properties of orally effective drugs

13.1. Lipinski's rule of five

Medicinal chemists and pharmacologists have searched for advantageous drug-like chemical properties that result in agents with oral therapeutic efficacy in a foreseeable manner. Lipinski's "rule of five" is an experimental and computational method to estimate solubility, membrane permeability, and efficacy in the drug development setting [201]. It is a rule of thumb that evaluates drug-likeness and determines whether a chemical compound with specific pharmacological activities has physical and chemical properties that would make it an orally active drug in humans. The rule was based upon the observation that most orally effective drugs are relatively small and moderately lipophilic molecules. It is used during drug development when pharmacologically active lead structures are optimized step-wise to increase their activity and selectivity as well as to ensure that their drug-like physicochemical properties are maintained.

The rule of 5 indicates that poor absorption is more likely to occur when there are more than (i) 5 hydrogen-bond donors, (ii) 10 (5 × 2) hydrogen-bond acceptors, (iii) a molecular weight greater than 500 (5 × 100), and (iv) a calculated Log P (cLogP) greater than 5. The partition coefficient (P) is the ratio of the solubility of the un-ionized drug in the organic phase of 1-octanol saturated with water divided by its solubility in the aqueous phase. A larger P value correlates with greater hydrophobicity. The number of hydrogen-bond donors is the sum of OH and NH groups and the number of hydrogen-bond acceptors includes any heteroatom without a formal positive charge with the exception of heteroaromatic oxygen and sulfur, pyrrole nitrogen, halogens, and higher oxidation states of nitrogen, phosphorus, and sulfur but including the oxygens bonded to them. Lipinski's rule was based on the chemical properties of more than two thousand drugs that served as references [201].

As shown in Table 7 and excluding the macrolides, the average molecular weight of the small molecule inhibitors is 480 with a range from 306 (ruxolitinib) to 615 (trametinib). Moreover, 38 of the 48 approved drugs have a cLogP of less than five and dabrafenib, fostamatinib, and the three macrolides (sirolimus, everolimus, and temsirolimus) have more than ten hydrogen bond acceptors. The compounds with a molecular weight greater than 500 include abemaciclib, bosutinib, brigatinib, cabozantinib, ceritinib, cobimetinib, dabrafenib, encorafenib, fostamatinib (a prodrug that is converted to R406 with a molecular weight of 470), gilteritinib, lapatinib, midostaurin, neratinib, nilotinib, nintedanib, ponatinib, trametinib, and the three macrolides. Thus, a total of 20 of the 48 FDA-approved small molecule protein kinase inhibitors fail to conform to the rule of five. The data indicate that there is a tendency for orally effective small molecule protein kinase inhibitors to exceed the 500 Da molecular weight criterion.

13.2. Lipophilic efficiency, LipE

After the appearance of the rule of five in 1997 [201], subsequent work on the physicochemical properties of effective drugs has led to various refinements [202–210]. The property of lipophilic efficiency, or LipE, is a parameter used in drug discovery that links potency and lipophilicity-driven binding as a strategy to increase potency. The formula for calculating lipophilic efficiency is given by the following equations:

$$\text{LipE} = \text{pIC}_{50} - \text{cLogD} \text{ or } \text{LipE} = pK_i - \text{cLogD}$$

Paralleling its usage in expressing the hydrogen ion concentration as pH, the operator p represents the negative of the Log_{10} of the IC_{50} or the K_i. cLogD is the calculated logarithm of the Distribution coefficient, which is the ratio of the drug solubility (both ionized and un-ionized) in the organic phase to the aqueous phase of immiscible 1-octanol/water at a specified pH, usually 7.4.

The second term (–cLogD or minus cLogD) represents the lipophilicity of a drug or compound where c indicates that the value is calculated using an algorithm based upon the behavior of thousands of reference organic compounds. The more soluble the compound is in the organic phase of an immiscible 1-octanol/water mixture, the greater is its lipophilicity and the greater is the value of – cLogD. Leeson and Springthorpe propose that compound lipophilicity, as assessed by – cLogP, is one of the most important chemical properties to consider during drug discovery and development [204]. Their use of – cLogP was based upon studies performed before the use of D, the distribution coefficient, was developed. For practical purposes, either cLog_{10}D or cLog_{10}P can be used to compare a series of compounds. A higher lipophilicity may play a significant role in promoting binding to unwanted drug targets leading to increased toxicities. One goal for optimizing drug properties during development is to increase potency without simultaneously increasing lipophilicity. LipE assists in lead optimization by permitting a direct comparison of drug congeners based upon the use of the same assay in making comparisons [208].

cLogD can be determined for several compounds by computer in a matter of minutes. Because the experimental determination of LogD is labor intensive, it is performed only in select cases. Recommended optimal values of LipE range from 5–10 [203]. Decreasing the lipophilicity and increasing potency during drug development usually produces medications with more optimal properties. The average value of LipE for the FDA-approved small molecule protein kinase inhibitors is 4.99 with a range from 2 (vandetanib) to 8.5 (tofacitinib) (Table 8). Nearly half of the antagonists (23) have values that are less than 5 while the recommended optima range from 5–10.

13.3. Ligand efficiency, LE

The ligand efficiency (LE) is a property that relates the potency or binding affinity per heavy atom (non-hydrogen atom) of a drug. It is given by the following equation:

$$\text{LE} = \Delta G^{\circ\prime}/N = -RT \ln K_{eq}/N = -2.303 RT Log_{10} K_{eq}/N$$

$\Delta\mathring{G}'$ represents the standard free energy change of the drug binding to its target at neutral pH, N is the number of heavy atoms (non-hydrogen atoms) in the drug, R is the universal gas constant or universal temperature-energy coefficient, (0.00198 kcal/degree-mol), T is the absolute temperature in degrees Kelvin, and K_{eq} is the equilibrium constant. Recommended optimal values of LE are greater than 0.3 kcal/mol [202,207]. The K_i or IC_{50} values are used as a substitute for the equilibrium constant. At 37 °C, or 310 K, this equation becomes – (2.303 × (0.00198 kcal/mol-K) × 310 K Log_{10} K_{eq})/N or – 1.41 Log_{10} K_{eq}/N. LE was first suggested as a procedure for comparing drugs according to their average binding energy per atom. This property is used in the selection of lead compounds and is especially valuable in fragment-based drug discovery protocols [208].

LE represents the binding affinity per heavy atom of the ligand or drug of interest. The value of N serves as a surrogate for the molecular weight. The defining equation of LE indicates that it is inversely proportional to the value of N and is directly proportional to the binding affinity and – Log_{10} K_{eq} (a positive number). The values of LE calculated on the basis of representative IC_{50} values for the small molecule protein kinase inhibitors are provided in Table 8. With the exception of fostamatinib, midostaurin, neratinib, nilotinib, and nintedanib, the LE values fall into a satisfactory range and are greater than 0.3. The values for ligand efficiency (LE) or lipophilic efficiency (LipE) listed in Table 8 were calculated from experiments performed under different conditions. Accordingly, LE and LipE values alone cannot be used to make a direct comparison of the drugs because different assays were used. The examples provided, which were derived from various drug discovery projects, are meant to provide representative values.

Table 7
Properties of FDA-approved small molecule inhibitors[a]

Drug	PubMED CID	Formula	MW (Da)	HD[b]	HA[c]	cLogP[d]	Rotatable bonds	PSA[e] (Å^2)	Ring count	Complexity[f]
Abemaciclib	462620502	$C_{27}H_{32}F_2N_8$	507	1	9	5.2	7	75	5	723
Acalabrutinib	71226662	$C_{26}H_{23}N_7O_2$	466	2	6	1.1	4	119	5	845
Afatinib	10184653	$C_{24}H_{25}ClFN_5O_3$	486	2	8	4.0	8	88.6	4	702
Alectinib	49806720	$C_{30}H_{34}N_4O_2$	483	1	5	4.7	3	72.4	6	867
Axitinib	6450551	$C_{22}H_{18}N_4OS$	386	2	4	3.8	5	96	4	557
Baricitinib	44205240	$C_{16}H_{17}N_7O_2S$	371	1	7	0.3	5	129	4	678
Binimetinib	10288191	$C_{17}H_{15}BrF_2N_4O_3$	441	3	7	2.6	6	88.4	3	521
Bosutinib	5328940	$C_{26}H_{29}Cl_2N_5O_3$	530	1	8	5.0	9	82.9	4	734
Brigatinib	68165256	$C_{29}H_{39}ClN_7O_2P$	584	2	9	5.2	8	85.9	5	835
Cabozantinib	25102847	$C_{28}H_{24}FN_3O_5$	501	2	7	4.5	8	98.8	4	795
Ceritinib	57379345	$C_{28}H_{36}ClN_5O_3S$	558	3	8	6.0	9	114	4	835
Cobimetinib	16222096	$C_{21}H_{21}F_3IN_3O_2$	531	3	7	5.1	4	64.6	4	624
Crizotinib	11626560	$C_{21}H_{22}Cl_2FN_5O$	450	2	6	4.4	5	78	4	558
Dabrafenib	44462760	$C_{23}H_{20}F_3N_5O_2S_2$	520	2	11	4.5	6	148	4	817
Dacomitinib	11511120	$C_{24}H_{25}ClFN_5O_2$	470	2	7	4.8	7	79.4	4	665
Dasatinib	3062316	$C_{22}H_{26}ClN_7O_2S$	488	3	9	3.0	7	135	4	642
Encorafenib	50922675	$C_{22}H_{27}ClFN_7O_4S$	540	3	10	3.1	10	149	3	836
Erlotinib	176870	$C_{22}H_{23}N_3O_4$	393	1	7	3.1	11	74.7	3	525
Everolimus	6442177	$C_{53}H_{83}NO_{14}$	958	3	14	4.5	9	205	3	1810
Fostamatinib	11671467	$C_{23}H_{26}FN_6O_9P$	580	4	15	1.7	10	187	4	904
Gefitinib	123631	$C_{22}H_{24}ClFN_4O_3$	447	1	8	4.5	8	68.7	4	545
Gilteritinib	49803313	$C_{29}H_{44}N_8O_3$	553	3	10	3.0	9	121	5	785
Ibrutinib	24821094	$C_{25}H_{24}N_6O_2$	441	1	6	3.1	5	99.2	5	678
Imatinib	5291	$C_{29}H_{31}N_7O$	494	2	7	4.2	7	86.3	5	706
Lapatinib	208908	$C_{29}H_{26}ClN_4O_4S$	581	2	9	5.0	11	115	5	898
Larotrectinib	46188928	$C_{21}H_{22}F_2N_6O_2$	428	2	7	2.6	3	86	5	659
Lenvatinib	9823820	$C_{21}H_{19}ClN_4O_4$	427	3	5	3.6	6	116	4	634
Lorlatinib	71731823	$C_{21}H_{19}FN_6O_2$	406	1	7	2.0	0	110	3	700
Midostaurin	9829523	$C_{35}H_{30}N_4O_7$	571	1	4	5.3	3	77.7	5	1140
Neratinib	9915743	$C_{30}H_{29}ClN_6O_3$	557	2	8	5.1	11	112	4	881
Netarsudil	66599893	$C_{28}H_{27}N_3O_3$	453	2	5	4.2	8	94.3	4	678
Nilotinib	644241	$C_{28}H_{22}F_3N_7O$	530	2	9	5.0	6	97.6	5	817
Nintedanib	135423438	$C_{31}H_{33}N_5O_4$	540	2	7	3.9	8	102	5	947
Osimertinib	71496458	$C_{28}H_{33}N_7O_2$	500	2	7	3.4	10	87.6	4	752
Palbociclib	5330286	$C_{24}H_{29}N_7O_2$	447	2	8	0.3	5	103	5	775
Pazopanib	10113978	$C_{21}H_{23}N_7O_2S$	437	2	8	3.8	5	127	4	717
Ponatinib	24826799	$C_{29}H_{27}F_3N_6O$	533	1	8	4.7	6	65.8	5	910
R406	11213558	$C_{22}H_{23}FN_6O_5$	470	3	11	3.1	7	129	4	691
Regorafenib	11167602	$C_{21}H_{15}ClF_4N_4O_3$	483	3	8	4.8	5	92.4	3	686
Ribociclib	44631912	$C_{23}H_{30}N_8O$	435	2	7	2.6	5	91.2	5	636
Ruxolitinib	25126798	$C_{17}N_{18}N_6$	306	1	4	2.0	4	83.2	4	453
Sirolimus	5284616	$C_{51}H_{79}NO_{13}$	914	3	13	4.5	6	195	3	1760
Sorafenib	216239	$C_{21}H_{16}ClF_3N_4O_3$	465	3	7	3.2	5	92.4	3	646
Sunitinib	5329102	$C_{22}H_{27}FN_4O_2$	398	3	4	3.2	7	77.2	3	636
Temsirolimus	6918289	$C_{56}H_{87}NO_{16}$	1029	4	16	4.3	11	242	3	2010
Tofacitinib	9926791	$C_{16}H_{20}N_6O$	312	1	5	1.0	3	88.9	3	488
Trametinib	11707110	$C_{26}H_{23}FlN_5O_4$	615	2	6	2.8	5	102	4	1090
Vandetanib	3081361	$C_{22}H_{24}BrFN_4O_2$	475	1	7	5.3	6	59.5	4	539
Vemurafenib	42611257	$C_{23}H_{18}ClF_2N_3O_3S$	489	2	7	4.9	7	100	4	790

[a] All data from NIH PubChem except for cLogP (the calculated Log_{10} of the partition coefficient, which was computed using MedChem Designer™, version 2.0, Simulationsplus, Inc. Lancaster, CA 93534).
[b] No. of hydrogen bond donors.
[c] No. of hydrogen bond acceptors.
[d] Calculated Log_{10} of the partition coefficient.
[e] (PSA) Polar surface area.
[f] Values obtained from https://pubchem.ncbi.nlm.nih.gov/.

13.4. Additional chemical descriptors of druglike properties

In an effort to improve the predictors of oral effectiveness, not-surprisingly, the rules have generated many corollaries and extensions. Veber et al. reported that the number of rotatable bonds and the polar surface area (PSA) have been found to discriminate between compounds that are orally active and those that are not for a large series of compounds in rat [209]. These investigators concluded that the recommended number of rotatable bonds should be less than or equal to 10. This descriptor is related to molecular flexibility (degrees of freedom) that is considered as an important factor in passive membrane permeation. Moreover, the number of degrees of freedom correlates with the change of entropy upon binding, which is related to the binding affinity of drugs to their targets. Additionally, these investigators have reported that compounds with polar surface area (PSA) values less than or equal to 140 Å^2 exhibit good oral bioavailability. The polar surface area is the surface sum over all polar atoms, primarily oxygen and nitrogen, but also including their attached hydrogen atoms. Moreover, Oprea reported that the number of rings in most orally effective drugs is three or greater [210]. With the exception of the

Table 8
Selected FDA-approved drug lipophilic efficiency (LipE) and ligand efficiency (LE) values.

Drug	Targets	K_i (nM)[a]	pK_i	cLogP[b]	LipE[c]	No. of heavy atoms	LE[d]
Abemaciclib	CDK4	0.6	9.22	5.2	4.02	37	0.351
Acalbrutinib	BTK	3.1	8.51	1.1	7.41	35	0.343
Afatinib	EGFR	0.5	9.33	4.0	5.33	34	0.387
Alectinib	ALK	1.9	8.72	4.7	4.02	36	0.342
Axitinib	VEGFR	0.25	9.6	3.8	5.80	28	0.483
Baricitinib	JAK2	7	8.15	0.3	7.85	26	0.442
Binimetinib	MEK1	?	?	2.6	?	27	?
Bosutinib	BCR-Abl	20	7.7	5.0	2.70	36	0.302
Brigatinib	ALK	0.398	9.4	5.2	4.20	40	0.331
Cabozantinib	RET	5	8.3	4.5	3.80	37	0.316
Ceritinib	ALK	0.2	9.7	6.0	3.70	38	0.360
Cobimetinib	MEK1	0.79	9.1	5.1	4.00	30	0.427
Crizotinib	ALK	0.63	9.2	4.4	4.80	30	0.432
Dabrafenib	B-Raf	0.4	9.4	4.5	4.90	35	0.379
Dacomitinib	EGFR	2.0	8.7	4.8	3.90	33	0.372
Dasatinib	BCR-Abl	0.16	9.8	3.0	6.80	33	0.419
Encorafenib	B-Raf	0.30	9.52	3.1	6.42	36	0.373
Erlotinib	EGFR	0.32	9.5	3.1	6.40	29	0.462
Everolimus	FKBP12/ mTOR	?	?	4.5	?	68	?
Fostamatinib	Syk	17	7.77	1.7	6.07	40	0.274
Gefitinib	EGFR	0.5	9.3	4.5	4.80	31	0.432
Gilteritinib	Flt3	0.41	9.39	3.0	6.39	40	0.331
Ibrutinib	BTK	?	?	3.1	?	33	?
Imatinib	BCR-Abl	1	9.0	4.2	4.80	37	0.433
Lapatinib	EGFR	1	9.0	5.0	4.00	40	0.317
Larotrectinib	TRK	9.7	8.01	2.6	5.41	31	0.364
Lenvatinib	VEGFR2	3.98	8.4	3.6	4.80	30	0.395
Lorlatinib	ALK	9	8.05	2.0	6.05	30	0.378
Midostaurin	Flt3	37	7.43	5.3	2.13	43	0.243
Neratinib	ErbB2/ HER2	59	7.23	5.1	2.13	40	0.255
Netarsudil	ROCK1/2	?	?	4.2	?	34	?
Nilotinib	BCR-Abl	12.5	7.9	5.0	2.90	39	0.286
Nintedanib	FGFR	39.8	7.4	3.9	3.50	40	0.261
Osimertinib	EGFR	7	8.15	3.4	4.75	37	0.311
Palbociclib	CDK4	10	8	0.3	7.70	33	0.342
Pazopanib	VEGFR	30	7.52	3.8	3.72	31	0.342
Ponatinib	BCR-Abl	1	9	4.7	4.30	39	0.326
Regorafenib	VEGFR	?	?	4.8	?	33	?
Ribociclib	CDK4	10	8	2.6	5.40	32	0.353
Ruxolitinib	JAK1	1.2	8.92	2.0	7.92	23	0.608
Sirolimus	FKBP12/ mTOR	?	?	4.5	?	65	?
Sorafenib	VEGFR1	15.8	7.8	3.2	6.60	32	0.432
Sunitinib	VEGFR2	3.98	8.4	3.2	5.20	29	0.408
Temsirolimus	FKBP12/ mTOR	?	?	4.3	?	73	?
Tofacitinib	JAK1	0.79	9.1	1.0	8.50	23	0.582
Trametinib	MEK1	3.4	8.47	2.8	6.00	37	0.335
Vandetanib	RET	50	7.3	5.3	2.00	30	0.343
Vemurafenib	B-Raf	3.98	8.4	4.9	3.50	33	0.359

[a] Representative values selected from https://www.ebi.ac.uk/chembl/.
[b] Calculated value of the partition coefficient using MedChem Designer™ version 2.0 Simulationsplus, Inc. Lancaster CA 93534, USA.
[c] LipE = pIC_{50}–cLogP, where cLogP is the calculated logarithm of the partition coefficient that was obtained using MedChem Designer™.
[d] LE = –2.303 RTLog$_{10}$ K_{eq}/N where N is the number of heavy (non-hydrogen) atoms in the drug.

macrolides, fostamatinib, encorafenib, and dabrafenib, all of the approved small molecule protein kinase inhibitors have a polar surface area less than 140 Å^2; the average is 105 and the range is from 59.5 (vandetanib) to 242 (temsirolimus) (Table 7). With the exception of erlotinib, lapatinib, neratinib and temsirolimus, which have 11 rotatable bonds, all of the other drugs have 10 or fewer rotatable bonds. The average number is 6.6 and the range is from 0 (lorlatinib) to 11. All of the drugs have 3 or more rings with an average of 4.1 and a range of 3 to 6 (alectinib). All of the drugs listed are given orally with the exceptions of netarsudil and temsirolimus.

The molecular complexity of a compound considers both the elements it contains and its structural features including symmetry. The molecular complexity rating of a compound is computed using the Bertz/Hendrickson/Ihlenfelt formula [211,212]. It considers the number and identity of atoms, their interconnections, and the nature of the chemical bonds. The molecular complexity is a floating-point value and it ranges from 0 (simple ions) to several thousand (complex natural products). Larger compounds are generally more complex than smaller ones. In contrast, highly symmetrical compounds and molecules with few distinct atom types or elements are rated lower in complexity. The values for molecular complexity were obtained from PubChem (https://pubchem.ncbi.nlm.nih.gov/). For all of the drugs listed in Table 7, the mean complexity is 799, the minimum is 453 (ruxolitinib), and the maximum is 2010 (temsirolimus). It is intuitive that the macrolide compounds exhibit the greatest complexity. There are no recommended values of complexity for drugs; it may be helpful as a loose correlation with the ease of synthesis, an important characteristic in the commercial production of medicinals.

14. Epilog and perspective

Although great strides have been made in the development of small molecule protein kinase inhibitors during the past 20 years, this field is still in its infancy. Most of the currently approved small molecule protein kinase inhibitors are directed toward the treatment of cancer and others target inflammatory diseases. Undoubtedly many more types of cancer will prove to be responsive to additional protein kinase antagonists. Owing to the genomic instability of malignant cells, resistance to kinase inhibitors occurs on a regular basis. This has led to the development of second and third generation drugs targeting the same disease. It is presently unclear whether secondary resistance occurs in the treatment of inflammatory disorders. The biomedical community would profit from the dissemination of the currently unavailable FDA-approved drug-enzyme X-ray crystal structures; these drugs are given in Sections 11 and 12.

Owing to the 244 protein kinases that map to disease loci or cancer amplicons [5], one can anticipate a substantial increase in the number of protein kinases that will be targeted for the treatment of many more illnesses. Near-term possibilities include targeting SPAK/OSR1 and Rho kinases (ROCK1/2) for the treatment of cardiovascular diseases including hypertension, cerebral vasospasm, coronary vasospasm, myocardial infarction and heart failure [213,214]. Other possibilities include targeting p38 MAP kinase for the treatment of asthma, atherosclerosis, Crohn disease, psoriasis, and rheumatoid arthritis [215], JAK1/2 for the treatment of lupus erythematosus [216], LRRK2 and glycogen synthase kinase-3β for Parkinson disease and amyotrophic lateral sclerosis [213,217], and TTMK1 for the treatment of Alzheimer disease and other neurodegenerative disorders [218]. The addition of new protein kinase targets to the therapeutic armamentarium will require the discovery of the signaling pathways that are responsible for the pathogenesis of currently untargeted sicknesses.

Table 9 provides a list and Fig. 12 depicts the structures of selected pharmacophores that make up the currently FDA-approved small molecule protein kinase antagonists. Many of the drugs consist of a small number of nitrogen-containing compounds such as quinazolines, quinolines, isoquinolines, pyrimidines, and indoles. Much of protein kinase inhibitor drug discovery has involved modifications of previously approved drugs. As the field matures during the next 20 years, one can

Table 9
Chemical composition of FDA-approved small molecule inhibitors.

Drug	Primary pharmacophore structures	Major secondary drug components
Afatinib	4-anilino-quinazoline	diaryl-amino group
Dacomitinib	4-anilino-quinazoline	diaryl-amino group
Erlotinib	4-anilino-quinazoline	diaryl-amino group
Lapatinib	4-anilino-quinazoline	diaryl-amino group
Neratinib	4-anilino-quinazoline	diaryl-amino group
Vandetanib	4-anilino-quinazoline	diaryl-amino group
Gefitinib	4-anilino-quinazoline	diaryl-amino group
Cabozantinib	quinoline	
Lenvatinib	quinoline	
Bosutinib	4-anilino-quinoline	diaryl-amino group
Netarsudil	6-amino-isoquinoline	
Vemurafenib	pyrrolo[2,3-*b*]pyridine	
Lorlatinib	macrocyclic pyrazole-pyridine	
Larotrectinib	pyrazolo[1,5-*a*]pyridine	
Regorafenib	pyridine-2-carboxamide	diaryl-urea group
Sorafenib	pyridine-2-carboxamide	diaryl-urea group
Crizotinib	pyrazole-pyridine amine	
Dabrafenib	2-amino-pyrimidine	
Encorafenib	pyrazole-pyrimidine amine	
Abemaciclib	amino-pyrimidine-benzimidazole	diaryl-amino group
Brigatinib	2,4-diamino-pyrimidine	diaryl-amino group
Fostamatinib	2-anilino-pyrimidine	diaryl-amino group
Ceritinib	2,4-dianilino-pyrimidine	diaryl-amino group
Palbociclib	amino-pyrido[2,3-*d*]pyrimidine	diaryl-amino group
Trametinib	pyrido[4,3-*d*]pyrimidine	diaryl-amino group
Baricitinib	pyrrolo[2,3-*d*]pyrimidine	
Tofacitinib	pyrrolo[2,3-*d*]pyrimidine	
Ibrutinib	amino-pyrazolo[3,4-*d*] pyrimidine	
Imatinib	2-amino-4-pyrido-pyrimidine	diaryl-amino group
Nilotinib	2-amino-4-pyrido-pyrimidine	diaryl-amino group
Ribociclib	2-amino-pyrrolo[2,3-*d*] pyrimidine	diaryl-amino group
Ruxolitinib	4-pyrazolo-pyrrolo[2,3-*d*] pyrimidine	
Dasatinib	amino-thiazole pyrimidine	diaryl-amino group
Axitinib	indazole	
Pazopanib	6-amino-indazole	diaryl-amino group
Ponatinib	imidazo[1,2-*b*]pyridazine	
Acalabrutinib	imidazo[1,5-*a*]pyrazine	
Cobimetinib	anilino-benzene	
Binimetinib	6-anilino-benzimidazole	diaryl-amino group
Gilteritinib	3-anilino-pyrazine	diaryl-amino group
Nintedanib	indole	
Sunitinib	indole	
Osimertinib	3-pyrimido-indole	diaryl-amino group
Alectinib	benzo[*b*]carbazole	

anticipate that protein kinase antagonists with a much larger number of scaffolds, chemotypes, and pharmacophores will be developed. There are currently only three approved type III allosteric inhibitors (binimetinib, cobimetinib and trametinib) and these inhibit MEK1/2. It is likely that additional allosteric inhibitors will be discovered that are directed against different enzymes in different signal transduction modules. It is also likely that additional irreversible inhibitors that target the dozens of enzymes with active thiols near the ATP-binding site will be forthcoming.

Although the development of therapeutic protein kinase antagonists represents a medical breakthrough, one of the adverse events associated with this class of drugs is that of financial toxicity [219]. One of the main drivers for the increase in cancer therapeutics in recent years has been the introduction of small molecule protein kinase inhibitors [220]. The cost of these drugs in the United States ranges from $5000–$10,000 per month or more. One of the arguments that drug companies provide for the high cost of these drugs is that a great deal of expense goes toward their development. In the case of imatinib (Gleevec), the drug was developed more than a decade ago, but the parent drug company increases the price about 10% per year so that its price has more than doubled in the past decade. Owing to the complexity of the health care market in the United States, it is unlikely that lower prices for these medicines will occur in the near or distant future. The problem is not confined to small molecule protein kinase antagonists, but it also includes biologics and monoclonal antibodies. Although not in the $10,000 per month cost category, even the price that patients or their insurers pay for insulin has dramatically increased from $200 to $500 per month over the past few years.

Because of the high cost of health insurance and required co-payments in the United States, health insurance per se does not eliminate this financial worry among patients receiving protein kinase antagonists. As a consequence of this financial burden, patients may become noncompliant and take less than the prescribed amount of their medications or they may take none at all [221,222]. If a patient fails to take the prescribed agent, the development of these targeted drugs helps neither the patient nor the drug company. Owing to the work of innumerable scientists worldwide in developing small molecule protein kinase inhibitors, it seems appropriate that more must be done to fairly distribute the fruits of these investigations to any patient who might benefit from the protein kinase-antagonist drug development-process.

Conflict of interest

The author is unaware of any affiliations, memberships, or financial holdings that might be perceived as affecting the objectivity of this review.

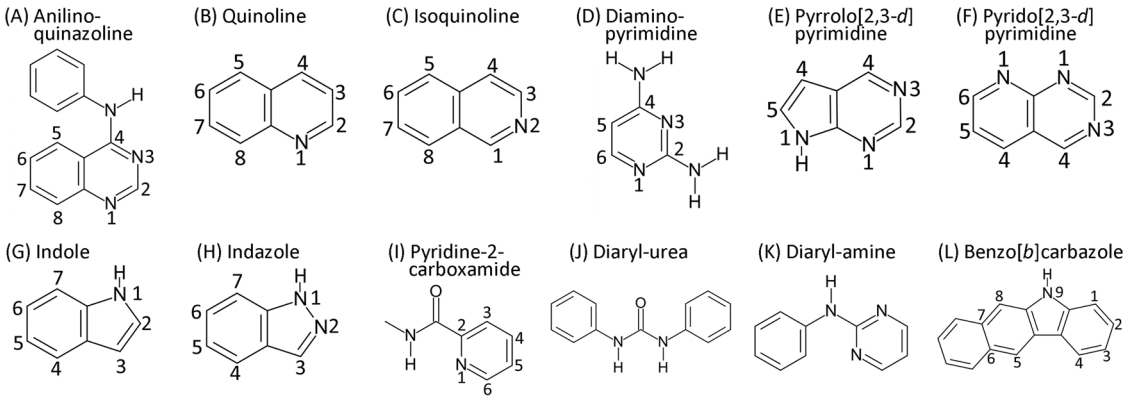

Fig. 12. Structures of selected pharmacophores that make up the FDA-approved small molecule protein kinase antagonists.

Acknowledgments

The author thanks Laura M. Roskoski for providing editorial and bibliographic assistance. I also thank Josie Rudnicki and Jasper Martinsek help in preparing the figures and Pasha Brezina and W.S. Sheppard for their help in structural analyses. The colored figures in this paper were evaluated to ensure that their perception was accurately conveyed to colorblind readers [223].

Appendix A. Supplementary data

Supplementary data associated with this article can be found, in the online version, at https://doi.org/10.1016/j.phrs.2019.03.006.

References

[1] R. Roskoski Jr., A historical overview of protein kinases and their targeted small molecule inhibitors, Pharmacol. Res. 100 (2015) 1–23.
[2] P. Cohen, Protein kinases – the major drug targets of the twenty-first century? Nat. Rev. Drug Discov. 1 (2002) 309–315.
[3] F. Carles, S. Bourg, C. Meyer, P. Bonnet, PKIDB: a curated, annotated and updated database of protein kinase inhibitors in clinical trials, Molecules 23 (4) (2018), https://doi.org/10.3390/molecules23040908 pii: E908.
[4] P.M. Fischer, Approved and experimental small-molecule oncology kinase inhibitor drugs: a mid-2016 overview, Med. Res. Rev. 37 (2017) 314–367.
[5] G. Manning, D.B. Whyte, R. Martinez, T. Hunter, S. Sudarsanam, The protein kinase complement of the human genome, Science 298 (2002) 1912–1934.
[6] S.H. Myers, V.G. Brunton, A. Unciti-Broceta, AXL inhibitors in cancer: a medicinal chemistry perspective, J. Med. Chem. 59 (2016) 3593–3608.
[7] B.L. Roth, D.J. Sheffler, W.K. Kroeze, Magic shotguns versus magic bullets: selectively non-selective drugs for mood disorders and schizophrenia, Nat. Rev. Drug Discov. 3 (2004) 353–359.
[8] P.L. Kaufman, M.E. Mohr, S.P. Riccomini, C.A. Rasmussen, Glaucoma drugs in the pipeline, Asia Pac. J. Ophthalmol. (Phila.) 7 (2018) 345–351.
[9] D.R. Knighton, J.H. Zheng, L.F. Ten Eyck, V.A. Ashford, N.H. Xuong, S.S. Taylor, et al., Crystal structure of the catalytic subunit of cyclic adenosine monophosphate-dependent protein kinase, Science 253 (1991) 407–414.
[10] D.R. Knighton, J.H. Zheng, L.F. Ten Eyck, N.H. Xuong, S.S. Taylor, J.M. Sowadski, Structure of a peptide inhibitor bound to the catalytic subunit of cyclic adenosine monophosphate-dependent protein kinase, Science 253 (1991) 414–420.
[11] S.S. Taylor, A.P. Kornev, Protein kinases: evolution of dynamic regulatory proteins, Trends Biochem. Sci. 36 (2011) 65–77.
[12] A.P. Kornev, S.S. Taylor, Dynamics-driven allostery in protein kinases, Trends Biochem. Sci. 40 (2015) 628–647.
[13] R.S. Vijayan, P. He, V. Modi, K.C. Duong-Ly, H. Ma, J.R. Peterson, et al., Conformational analysis of the DFG-out kinase motif and biochemical profiling of structurally validated type II inhibitors, J. Med. Chem. 58 (2015) 466–479.
[14] A.J. Kooistra, A. Volkamer, Kinase-centric computational drug development, Ann. Rep. Med. Chem. 50 (2017) 197–236.
[15] R. Roskoski Jr., Cyclin-dependent protein serine/threonine kinase inhibitors as anticancer drugs, Pharmacol. Res. 139 (2019) 471–488.
[16] S.K. Hanks, T. Hunter, Protein kinases 6. The eukaryotic protein kinase superfamily: kinase (catalytic) domain structure and classification, FASEB J. 9 (1995) 576–596.
[17] Madhusudan, E.A. Trafny, N.H. Xuong, J.A. Adams, L.F. Ten Eyck, S.S. Taylor, et al., cAMP-dependent protein kinase: crystallographic insights into substrate recognition and phosphotransfer, Protein Sci. 3 (1994) 176–187.
[18] J. Zhou, J.A. Adams, Participation of ADP dissociation in the rate-determining step in cAMP-dependent protein kinase, Biochemistry 36 (1997) 15733–15738.
[19] P.A. Schwartz, B.W. Murray, Protein kinase biochemistry and drug discovery, Bioorg. Chem. 39 (2011) 192–210.
[20] A.P. Kornev, S.S. Taylor, Defining the conserved internal architecture of a protein kinase, Biochim. Biophys. Acta 1804 (2010) 440–444.
[21] S.B. Hari, E.A. Merritt, D.J. Maly, Sequence determinants of a specific inactive protein kinase conformation, Chem. Biol. 20 (2013) 806–815.
[22] A.P. Kornev, N.M. Haste, S.S. Taylor, L.F. Eyck, Surface comparison of active and inactive protein kinases identifies a conserved activation mechanism, Proc. Natl. Acad. Sci. U. S. A. 103 (2006) 17783–17788.
[23] A.P. Kornev, S.S. Taylor, L.F. Ten Eyck, A helix scaffold for the assembly of active protein kinases, Proc. Natl. Acad. Sci. U. S. A. 105 (2008) 14377–14382.
[24] H.S. Meharena, P. Chang, M.M. Keshwani, K. Oruganty, A.K. Nene, N. Kannan, et al., Deciphering the structural basis of eukaryotic protein kinase regulation, PLoS Biol. 11 (2013) e1001690.
[25] R. Roskoski Jr., Classification of small molecule protein kinase inhibitors based upon the structures of their drug-enzyme complexes, Pharmacol. Res. 103 (2016) 26–48.
[26] O.P. van Linden, A.J. Kooistra, R. Leurs, I.J. de Esch, C. de Graaf, KLIFS: a knowledge-based structural database to navigate kinase-ligand interaction space, J. Med. Chem. 57 (2014) 249–277.
[27] R. Roskoski Jr., Anaplastic lymphoma kinase (ALK): structure, oncogenic activation, and pharmacological inhibition, Pharmacol. Res. 68 (2013) 68–94.
[28] R. Roskoski Jr., Anaplastic lymphoma kinase (ALK) inhibitors in the treatment of ALK-driven lung cancers, Pharmacol. Res. 117 (2017) 343–356.
[29] R. Roskoski Jr., Cyclin-dependent protein kinase inhibitors including palbociclib as anticancer drugs, Pharmacol. Res. 111 (2016) 784–803.
[30] R. Roskoski Jr., The ErbB/HER family of protein-tyrosine kinases and cancer, Pharmacol. Res. 79 (2014) 34–74.
[31] R. Roskoski Jr., ErbB/HER protein-tyrosine kinases: structures and small molecule inhibitors, Pharmacol. Res. 87 (2014) 42–59.
[32] R. Roskoski Jr., Small molecule inhibitors targeting the EGFR/ErbB family of protein-tyrosine kinases in human cancers, Pharmacol. Res. 139 (2019) 395–411.
[33] R. Roskoski Jr., ERK1/2 MAP kinases: structure, function, and regulation, Pharmacol. Res. 66 (2012) 105–143.
[34] R. Roskoski Jr., Targeting ERK1/2 protein-serine/threonine kinases in human cancers, Pharmacol. Res. 142 (2019) 151–168.
[35] R. Roskoski Jr., Janus kinase (JAK) inhibitors in the treatment of inflammatory and neoplastic diseases, Pharmacol. Res. 111 (2016) 784–803.
[36] R. Roskoski Jr., The role of small molecule Kit protein-tyrosine kinase inhibitors in the treatment of neoplastic disorders, Pharmacol. Res. 133 (2018) 35–52.
[37] R. Roskoski Jr., Allosteric MEK1/2 inhibitors including cobimetanib and trametinib in the treatment of cutaneous melanomas, Pharmacol. Res. 117 (2017) 20–31.
[38] R. Roskoski Jr., The role of small molecule platelet-derived growth factor receptor (PDGFR) inhibitors in the treatment of neoplastic disorders, Pharmacol. Res. 129 (2018) 65–83.
[39] R. Roskoski Jr., Targeting oncogenic Raf protein-serine/threonine kinases in human cancers, Pharmacol. Res. 135 (2018) 239–258.
[40] R. Roskoski Jr., A. Sadeghi-Nejad, Role of RET protein-tyrosine kinase inhibitors in the treatment RET-driven thyroid and lung cancers, Pharmacol. Res. 128 (2018) 1–17.
[41] R. Roskoski Jr., ROS1 protein-tyrosine kinase inhibitors in the treatment of ROS1 fusion protein-driven non-small cell lung cancers, Pharmacol. Res. 121 (2017) 202–212.
[42] R. Roskoski Jr., Src protein-tyrosine kinase structure, mechanism, and small molecule inhibitors, Pharmacol. Res. 94 (2015) 9–25.
[43] R. Roskoski Jr., Vascular endothelial growth factor (VEGF) and VEGF receptor inhibitors in the treatment of renal cell carcinomas, Pharmacol. Res. 120 (2017) 116–132.
[44] Y. Liu, K. Shah, F. Yang, L. Witucki, K.M. Shokat, A molecular gate which controls unnatural ATP analogue recognition by the tyrosine kinase v-Src, Bioorg. Med. Chem. 6 (1998) 1219–1226.
[45] A.C. Dar, K.M. Shokat, The evolution of protein kinase inhibitors from antagonists to agonists of cellular signaling, Annu. Rev. Biochem. 80 (2011) 769–795.
[46] P.M. Ung, R. Rahman, A. Schlessinger, Redefining the protein kinase conformational space with machine learning, Cell Chem. Biol. 25 (2018) 916-24.e2.
[47] F. Zuccotto, E. Ardini, E. Casale, M. Angiolini, Through the "gatekeeper door": exploiting the active kinase conformation, J. Med. Chem. 53 (2010) 2691–2694.
[48] L.K. Gavrin, E. Saiah, Approaches to discover non-ATP site inhibitors, Med. Chem. Commun. 4 (2013) 41.
[49] V. Lamba, I. Ghosh, New directions in targeting protein kinases: focusing upon true allosteric and bivalent inhibitors, Curr. Pharm. Des. 18 (2012) 2936–2945.
[50] T.K. Johnson, M.B. Soellner, Bivalent inhibitors of c-Src tyrosine kinase that bind a regulatory domain, Bioconjug. Chem. 27 (2016) 1745–1749.
[51] F.E. Kwarcinski, K.R. Brandvold, S. Phadke, O.M. Beleh, T.K. Johnson, J.L. Meagher, et al., Conformation-selective analogues of dasatinib reveal insight into kinase inhibitor binding and selectivity, ACS Chem. Biol. 11 (2016) 1296–1304.
[52] Z. Zhao, H. Wu, L. Wang, Y. Liu, S. Knapp, Q. Liu, N.S. Gray, Exploration of type II binding mode: a privileged approach for kinase inhibitor focused drug discovery? ACS Chem. Biol. 9 (2014) 1230–1241.
[53] R.A. Copeland, The drug-target residence time model: a 10-year retrospective, Nat. Rev. Drug Discov. 15 (2016) 87–95.
[54] J.J. Liao, Molecular recognition of protein kinase binding pockets for design of potent and selective kinase inhibitors, J. Med. Chem. 50 (2007) 409–424.
[55] D. Bajusz, G.G. Ferenczy, G.M. Keserá, Structure-based virtual screening approaches in kinase-directed drug discovery, Curr. Top. Med. Chem. 17 (2017) 2235–2259.
[56] P. Wu, T.E. Nielsen, M.H. Clausen, FDA-approved small-molecule kinase inhibitors, Trends Pharmacol. Sci. 36 (2015) 422–439.
[57] G. Cavallo, P. Metrangolo, R. Milani, T. Pilati, A. Priimagi, G. Resnati, et al., The halogen bond, Chem. Rev. 116 (2016) 2478–2601.
[58] J.E. Cortes, C. Gambacorti-Passerini, M.W. Deininger, M.J. Mauro, C. Chuah, D.W. Kim, et al., Bosutinib versus imatinib for newly diagnosed chronic myeloid leukemia: results from the randomized BFORE trial, J. Clin. Oncol. 36 (2018) 231–237.
[59] D.F. Heigener, M. Reck, Crizotinib, Recent Results Cancer Res. 211 (2018) 57–65.
[60] R. Puig de la Bellacasa, N. Karachaliou, R. Estrada-Tejedor, J. Teixidó, C. Costa, J.I. Borrell, ALK and ROS1 as a joint target for the treatment of lung cancer: a review, Transl. Lung Cancer Res. 2 (2013) 72–86.
[61] S. Zhang, R. Anjum, R. Squillace, S. Nadworny, T. Zhou, J. Keats, et al., The potent ALK inhibitor brigatinib (AP26113) overcomes mechanisms of resistance to first- and second-generation ALK inhibitors in preclinical models, Clin. Cancer Res. 22 (2016) 5527–5538.
[62] S. Ongoren, A.E. Eskazan, V. Suzan, S. Savci, I. Erdogan Ozunal, et al., Third-line treatment with second-generation tyrosine kinase inhibitors (dasatinib or nilotinib) in patients with chronic myeloid leukemia after two prior TKIs: real-life data on a single center experience along with the review of the literature, Hematology

23 (2018) 212–220.
[63] A. Markham, Fostamatinib: first global approval, Drugs 78 (2018) 959–963.
[64] S. Braselmann, V. Taylor, H. Zhao, S. Wang, C. Sylvain, M. Baluom, et al., R406, an orally available spleen tyrosine kinase inhibitor blocks Fc receptor signaling and reduces immune complex-mediated inflammation, J. Pharmacol. Exp. Ther. 319 (2006) 998–1008.
[65] J. Bussel, D.M. Arnold, E. Grossbard, J. Mayer, J. Treliński, W. Homenda, et al., Fostamatinib for the treatment of adult persistent and chronic immune thrombocytopenia: results of two phase 3, randomized, placebo-controlled trials, Am. J. Hematol. 93 (2018) 921–930.
[66] D. Kazandjian, G.M. Blumenthal, W. Yuan, K. He, P. Keegan, R. Pazdur, FDA approval of gefitinib for the treatment of patients with metastatic *EGFR* mutation-positive non-small cell lung cancer, Clin. Cancer Res. 22 (2016) 1307–1312.
[67] C.R. Kucharczuk, A. Ganetsky, J.M. Vozniak, Drug-drug interactions, safety, and pharmacokinetics of EGFR tyrosine kinase inhibitors for the treatment of non-small cell lung cancer, J. Adv. Pract. Oncol. 9 (2018) 189–200.
[68] F. Petrelli, A. Ghidini, R. Pedersini, M. Cabiddu, K. Borgonovo, M.C. Parati, et al., Comparative efficacy of palbociclib, ribociclib and abemaciclib for ER+ metastatic breast cancer: an adjusted indirect analysis of randomized controlled trials, Breast Cancer Res. Treat. (2019), https://doi.org/10.1007/s10549-019-05133-y.
[69] T.M. McShane, T.A. Wolfe, J.C. Ryan, Updates on managing advanced breast cancer with palbociclib combination therapy, Ther. Adv. Med. Oncol. 10 (2018), https://doi.org/10.1177/1758835918793849 1758835918793849; Erratum in: Ther Adv Med Oncol 2018;10:1758835918810117.
[70] J.A. Beaver, L. Amiri-Kordestani, R. Charlab, W. Chen, T. Palmby, A. Tilley, et al., FDA approval: palbociclib for the treatment of postmenopausal patients with estrogen receptor-positive, HER2-negative metastatic breast cancer, Clin. Cancer Res. 21 (2015) 4760–4766.
[71] S. Dhillon, Tofacitinib: a review in rheumatoid arthritis, Drugs 77 (2017) 1987–2001.
[72] P. Fallahi, S.M. Ferrari, E. Baldini, M. Biricotti, S. Ulisse, G. Materazzi, et al., The safety and efficacy of vandetanib in the treatment of progressive medullary thyroid cancer, Expert Rev. Anticancer. Ther. 16 (2016) 1109–1118.
[73] C. Luther, U. Swami, J. Zhang, M. Milhem, Y. Zakharia, Advanced stage melanoma therapies: detailing the present and exploring the future, Crit. Rev. Oncol. Hematol. 133 (2019) 99–111.
[74] S. Kakadia, N. Yarlagadda, R. Awad, M. Kundranda, J. Niu, B. Naraev, et al., Mechanisms of resistance to BRAF and MEK inhibitors and clinical update of US Food and Drug Administration-approved targeted therapy in advanced melanoma, Onco Targets Ther. 11 (2018) 7095–7107.
[75] S. Zschäbitz, C. Grüllich, Lenvantinib: a tyrosine kinase inhibitor of VEGFR 1-3, FGFR 1-4, PDGFRα, KIT and RET, Recent Results Cancer Res. 211 (2018) 187–198.
[76] M.E. Cabanillas, M.A. Habra, Lenvatinib: role in thyroid cancer and other solid tumors, Cancer Treat. Rev. 42 (2016) 47–55.
[77] M. Schlumberger, M. Tahara, L.J. Wirth, B. Robinson, M.S. Brose, R. Elisei, et al., Lenvatinib versus placebo in radioiodine-refractory thyroid cancer, N. Engl. J. Med. 372 (2015) 621–630.
[78] C. Garbe, T.K. Eigentler, Vemurafenib, Recent Results Cancer Res. 211 (2018) 77–89.
[79] F. Haroun, K. Millado, I. Tabbara, Erdheim-Chester disease: comprehensive review of molecular profiling and therapeutic advances, Anticancer Res. 37 (2017) 2777–2783.
[80] E.S. Kim, Abemaciclib: first global approval, Drugs 77 (2017) 2063–2070.
[81] J.M. Martin, L.J. Goldstein, Profile of abemaciclib and its potential in the treatment of breast cancer, Onco Targets Ther. 11 (2018) 5253–5259.
[82] M.P. Goetz, M. Toi, M. Campone, J. Sohn, S. Paluch-Shimon, J. Huober, et al., MONARCH 3: abemaciclib as initial therapy for advanced breast cancer, J. Clin. Oncol. 35 (2017) 3638–3646.
[83] A. McCartney, E. Moretti, G. Sanna, M. Pestrin, E. Risi, L. Malorni, et al., The role of abemaciclib in treatment of advanced breast cancer, Ther. Adv. Med. Oncol. 10 (2018) 1758835918776925.
[84] M. Herden, C.F. Waller, Alectinib, Recent Results Cancer Res. 211 (2018) 247–256.
[85] S. Peters, D.R. Camidge, A.T. Shaw, S. Gadgeel, J.S. Ahn, D.W. Kim, et al., Alectinib versus crizotinib in untreated ALK-positive non-small-cell lung cancer, N. Engl. J. Med. 377 (2017) 829–838.
[86] T. Vavalà, S. Novello, Alectinib in the treatment of ALK-positive non-small cell lung cancer: an update on its properties, efficacy, safety and place in therapy, Ther. Adv. Med. Oncol. 10 (2018) 1758835918789364.
[87] S.M. Gadgeel, The use of alectinib in the first-line treatment of anaplastic lymphoma kinase-positive non-small-cell lung cancer, Future Oncol. 14 (2018) 1875–1882.
[88] S. Dhillon, M. Clark, Ceritinib: first global approval, Drugs 74 (2014) 1285–1291.
[89] J.C. Soria, D.S.W. Tan, R. Chiari, Y.L. Wu, L. Paz-Ares, J. Wolf, et al., First-line ceritinib versus platinum-based chemotherapy in advanced ALK-rearranged non-small-cell lung cancer (ASCEND-4): a randomised, open-label, phase 3 study, Lancet 389 (2017) 917–929.
[90] T. De Pas, L. Pala, C. Catania, F. Conforti, Molecular and clinical features of second-generation anaplastic lymphoma kinase inhibitors: ceritinib, Future Oncol. 13 (2017) 2629–2644.
[91] A. Mohieldin, A. Rasmy, M. Ashour, M. Al-Nassar, R.H. Ali, F.G. El-Enezi, Efficacy and safety of crizotinib in patients with anaplastic lymphoma kinase-positive advanced-stage non-small-cell lung cancer, Cancer Manag. Res. 10 (2018) 6555–6561.
[92] R.L. Chen, J. Zhao, X.C. Zhang, N.N. Lou, H.J. Chen, X. Yang, J. Su, et al., Crizotinib in advanced non-small-cell lung cancer with concomitant ALK rearrangement and c-Met overexpression, BMC Cancer 18 (2018) 1171.
[93] D.R. Camidge, H.R. Kim, M.J. Ahn, J.C. Yang, J.Y. Han, J.S. Lee, et al., Brigatinib versus crizotinib in ALK-positive non-small-cell lung cancer, N. Engl. J. Med. 379 (2018) 2027–2039.
[94] Y.Y. Syed, Ribociclib: first global approval, Drugs 77 (2017) 799–807.
[95] G.N. Hortobagyi, S.M. Stemmer, H.A. Burris, Y.S. Yap, G.S. Sonke, S. Paluch-Shimon, et al., Ribociclib as first-line therapy for HR-positive, advanced breast cancer, N. Engl. J. Med. 375 (2016) 1738–1748.
[96] G.S. Sonke, L.L. Hart, M. Campone, F. Erdkamp, W. Janni, S. Verma, et al., Ribociclib with letrozole versus letrozole alone in elderly patients with hormone receptor-positive, HER2-negative breast cancer in the randomized MONALEESA-2 trial, Breast Cancer Res. Treat. 167 (2018) 659–669.
[97] J. O'Shaughnessy, K. Petrakova, G.S. Sonke, P. Conte, C.L. Arteaga, D.A. Cameron, et al., Ribociclib plus letrozole versus letrozole alone in patients with de novo HR+, HER2 – advanced breast cancer in the randomized MONALEESA-2 trial, Breast Cancer Res. Treat. 168 (2018) 127–134.
[98] M. Schmidt, M. Sebastian, Palbociclib-the first of a new class of cell cycle inhibitors, Recent Results Cancer Res. 211 (2018) 153–175.
[99] R.S. Finn, M. Martin, H.S. Rugo, S. Jones, S.A. Im, K. Gelmon, et al., Palbociclib and letrozole in advanced breast cancer, N. Engl. J. Med. 375 (2016) 1925–1936.
[100] M. Steins, M. Thomas, M. Geißler, Erlotinib, Recent Results Cancer Res. 211 (2018) 1–17.
[101] V. Hirsh, Turning *EGFR* mutation-positive non-small-cell lung cancer into a chronic disease: optimal sequential therapy with EGFR tyrosine kinase inhibitors, Ther. Adv. Med. Oncol. 10 (2018), https://doi.org/10.1177/1758834017753338 1758834017753338; Erratum in: Ther Adv Med Onco. 2018;10:1758835918769391.
[102] J.H. Park, Y. Liu, M.A. Lemmon, R. Radhakrishnan, Erlotinib binds both inactive and active conformations of the EGFR tyrosine kinase domain, Biochem. J. 448 (2012) 417–423.
[103] M. Voigtlaender, T. Schneider-Merck, M. Trepel, Lapatinib, Recent Results Cancer Res. 211 (2018) 19–44.
[104] R. Madden, S. Kosari, G.M. Peterson, N. Bagheri, J. Thomas, Lapatinib plus capecitabine in patients with HER2-positive metastatic breast cancer: a systematic review, Int. J. Clin. Pharmacol. Ther. 56 (2018) 72–80.
[105] A. Bellesoeur, E. Carton, J. Alexandre, F. Goldwasser, O. Huillard, Axitinib in the treatment of renal cell carcinoma: design, development, and place in therapy, Drug Des. Dev. Ther. 11 (2017) 2801–2811.
[106] T.E. Hutson, S. Al-Shukri, V.P. Stus, O.N. Lipatov, Y. Shparyk, A.H. Bair, et al., Axitinib versus sorafenib in first-line metastatic renal cell carcinoma: overall survival from a randomized phase III trial, Clin. Genitourin Cancer 15 (2017) 72–76.
[107] F. Rossari, F. Minutolo, E. Orciuolo, Past, present, and future of Bcr-Abl inhibitors: from chemical development to clinical efficacy, J. Hematol. Oncol. 11 (2018) 84.
[108] A. Hochhaus, G. Saglio, T.P. Hughes, R.A. Larson, D.W. Kim, S. Issaragrisil, et al., Long-term benefits and risks of frontline nilotinib vs imatinib for chronic myeloid leukemia in chronic phase: 5-year update of the randomized ENESTnd trial, Leukemia 30 (2016) 1044–1054.
[109] X. Tian, H. Zhang, T. Heimbach, H. He, A. Buchbinder, M. Aghoghovbia, et al., Clinical pharmacokinetic and pharmacodynamic overview of nilotinib, a selective tyrosine kinase inhibitor, J. Clin. Pharmacol. 58 (2018) 1533–1540.
[110] M.C. Müller, F. Cervantes, H. Hjorth-Hansen, J.J.W.M. Janssen, D. Milojkovic, D. Rea, et al., Ponatinib in chronic myeloid leukemia (CML): consensus on patient treatment and management from a European expert panel, Crit. Rev. Oncol. Hematol. 120 (2017) 52–59.
[111] J.E. Cortes, D.W. Kim, J. Pinilla-Ibarz, P.D. le Coutre, R. Paquette, C. Chuah, et al., Ponatinib efficacy and safety in Philadelphia chromosome-positive leukemia: final 5-year results of the phase 2 PACE trial, Blood 132 (2018) 393–404.
[112] H.T. Wang, M. Xia, A meta-analysis of efficacy and safety of sorafenib versus other targeted agents for metastatic renal cell carcinoma, Medicine (Baltimore) 98 (2019) e13779.
[113] T. Wen, H. Xiao, C. Luo, L. Huang, M. Xiong, Efficacy of sequential therapies with sorafenib-sunitinib versus sunitinib-sorafenib in metastatic renal cell carcinoma: a systematic review and meta-analysis, Oncotarget 8 (2017) 20441–20451.
[114] R. Iacovelli, E. Verri, M. Cossu Rocca, G. Aurilio, D. Cullurà, et al., Is there still a role for sorafenib in metastatic renal cell carcinoma?. A systematic review and meta-analysis of the effectiveness of sorafenib over other targeted agents, Crit. Rev. Oncol. Hematol. 99 (2016) 324–331.
[115] G.M. Keating, Sorafenib: a review in hepatocellular carcinoma, Target Oncol. 12 (2017) 243–253.
[116] K.P. Garnock-Jones, Cobimetinib: first global approval, Drugs 75 (2015) 1823–1830.
[117] J. Signorelli, A. Shah Gandhi, Cobimetinib, Ann. Pharmacother. 51 (2017) 146–153.
[118] G.M. Keating, Cobimetinib plus vemurafenib: a review in $BRAF^{V600}$ mutation-positive unresectable or metastatic melanoma, Drugs 76 (2016) 605–615.
[119] R.T. Dungo, G.M. Keating, Afatinib: first global approval, Drugs 73 (2013) 1503–1515.
[120] S. Wind, D. Schnell, T. Ebner, M. Freiwald, P. Stopfer, Clinical pharmacokinetics and pharmacodynamics of afatinib, Clin. Pharmacokinet. 56 (2017) 235–250.
[121] H. Wecker, C.F. Waller, Afatinib, Recent Results Cancer Res. 211 (2018) 199–215.
[122] S.M. Abdallah, V. Hirsh, Irreversible tyrosine kinase inhibition of epidermal growth factor receptor with afatinib in *EGFR* activating mutation-positive advanced non-small-cell lung cancer, Curr. Oncol. 25 (Suppl. 1) (2018) S9–S17.
[123] D. Miklos, C.S. Cutler, M. Arora, E.K. Waller, M. Jagasia, I. Pusic, et al., Ibrutinib for chronic graft-versus-host disease after failure of prior therapy, Blood 130

(2017) 2243–2250.
[124] M.A. Spinner, G. Varma, R.H. Advani, Novel approaches in Waldenström macroglobulinemia, Hematol. Oncol. Clin. North Am. 32 (2018) 875–890.
[125] P. Strati, N. Jain, S. O'Brien, Chronic lymphocytic leukemia: diagnosis and treatment, Mayo Clin. Proc. 93 (2018) 651–664.
[126] S. Pal Singh, F. Dammeijer, R.W. Hendriks, Role of Bruton's tyrosine kinase in B cells and malignancies, Mol. Cancer 17 (2018) 57.
[127] J.B. Smaill, A.J. Gonzales, J.A. Spicer, H. Lee, J.E. Reed, K. Sexton, et al., Tyrosine kinase inhibitors. 20. Optimization of substituted quinazoline and pyrido[3,4-*d*] pyrimidine derivatives as orally active, irreversible inhibitors of the epidermal growth factor receptor family, J. Med. Chem. 59 (2016) 8103–8124.
[128] Y.L. Wu, Y. Cheng, X. Zhou, K.H. Lee, K. Nakagawa, S. Niho, et al., Dacomitinib versus gefitinib as first-line treatment for patients with EGFR-mutation-positive non-small-cell lung cancer (ARCHER 1050): a randomised, open-label, phase 3 trial, Lancet Oncol. 18 (2017) 1454–1466.
[129] T.S. Mok, Y. Cheng, X. Zhou, K.H. Lee, K. Nakagawa, S. Niho, et al., Improvement in overall survival in a randomized study that compared dacomitinib with gefitinib in patients with advanced non-small-cell lung cancer and *EGFR*-activating mutations, J. Clin. Oncol. 36 (2018) 2244–2250.
[130] Y. Kobayashi, T. Fujino, M. Nishino, T. Koga, M. Chiba, Y. Sesumi, S. Ohara, et al., *EGFR* T790M and C797S mutations as mechanisms of acquired resistance to dacomitinib, J. Thorac. Oncol. 13 (2018) 727–731.
[131] S.L. Greig, Osimertinib: first global approval, Drugs 76 (2016) 263–273.
[132] U. Malapelle, B. Ricciuti, S. Baglivo, F. Pepe, P. Pisapia, P. Anastasi, et al., Osimertinib, Recent Results Cancer Res. 211 (2018) 257–276.
[133] S.S. Ramalingam, J.C. Yang, C.K. Lee, T. Kurata, D.W. Kim, T. John, N. Nogami, et al., Osimertinib as first-line treatment of *EGFR* mutation-positive advanced non-small-cell lung cancer, J. Clin. Oncol. 36 (2018) 841–849.
[134] T. Mok, J.J. Yang, K.C. Lam, Treating patients with EGFR-sensitizing mutations: first line or second line–is there a difference? J. Clin. Oncol. 31 (2013) 1081–1088.
[135] E.D. Deeks, Neratinib: first global approval, Drugs 77 (2017) 1695–1704.
[136] H.R. Tsou, E.G. Overbeek-Klumpers, W.A. Hallett, M.F. Reich, M.B. Floyd, B.D. Johnson, et al., Optimization of 6,7-disubstituted-4-(arylamino) quinoline-3-carbonitriles as orally active, irreversible inhibitors of human epidermal growth factor receptor-2 kinase activity, J. Med. Chem. 48 (2005) 1107–1131.
[137] N. Jiang, J.J. Lin, J. Wang, B.N. Zhang, A. Li, Z.Y. Chen, et al., Novel treatment strategies for patients with HER2-positive breast cancer who do not benefit from current targeted therapy drugs, Exp. Ther. Med. 16 (2018) 2183–2192.
[138] H. Singh, A.J. Walker, L. Amiri-Kordestani, J. Cheng, S. Tang, P. Balcazar, et al., U.S. Food and Drug administration approval: neratinib for the extended adjuvant treatment of early-stage HER2-positive breast cancer, Clin. Cancer Res. 24 (2018) 3486–3491.
[139] D. Cella, J.L. Beaumont, Pazopanib in the treatment of advanced renal cell carcinoma, Ther. Adv. Urol. 8 (2016) 61–69 Erratum in: Ther Adv Urol 2016;8:291.
[140] P.A. Harris, A. Boloor, M. Cheung, R. Kumar, R.M. Crosby, R.G. Davis-Ward, et al., Discovery of 5-[[4-[(2,3-dimethyl-2H-indazol-6-yl)methylamino]-2-pyrimidinyl] amino]-2-methyl-benzenesulfonamide (pazopanib), a novel and potent vascular endothelial growth factor receptor inhibitor, J. Med. Chem. 51 (2008) 4632–4640.
[141] S. Miwa, N. Yamamoto, K. Hayashi, A. Takeuchi, K. Igarashi, et al., Therapeutic targets for bone and soft-tissue sarcomas, Int. J. Mol. Sci. (2019) 20 pii: E170.
[142] F.A. Schutz, T.K. Choueiri, C.N. Sternberg, Pazopanib: clinical development of a potent anti-angiogenic drug, Crit. Rev. Oncol. Hematol. 77 (2011) 163–171.
[143] C.N. Sternberg, I.D. Davis, J. Mardiak, C. Szczylik, E. Lee, J. Wagstaff, et al., Pazopanib in locally advanced or metastatic renal cell carcinoma: results of a randomized phase III trial, J. Clin. Oncol. 28 (2010) 1061–1068.
[144] R.J. Motzer, T.E. Hutson, D. Cella, J. Reeves, R. Hawkins, J. Guo, et al., Pazopanib versus sunitinib in metastatic renal-cell carcinoma, N. Engl. J. Med. 369 (2013) 722–731.
[145] W.T. van der Graaf, J.Y. Blay, S.P. Chawla, D.W. Kim, B. Bui-Nguyen, P.G. Casali, et al., Pazopanib for metastatic soft-tissue sarcoma (PALETTE): a randomised, double-blind, placebo-controlled phase 3 trial, Lancet 379 (2012) 1879–1886.
[146] T.J. Ettrich, T. Seufferlein, Regorafenib, Recent Results Cancer Res. 211 (2018) 45–56.
[147] M. Røed Skårderud, A. Polk, K. Kjeldgaard Vistisen, F.O. Larsen, D.L. Nielsen, Efficacy and safety of regorafenib in the treatment of metastatic colorectal cancer: a systematic review, Cancer Treat. Rev. 62 (2018) 61–73.
[148] A. Poveda, X. García Del Muro, J.A. López-Guerrero, R. Cubedo, V. Martínez, I. Romero, et al., GEIS guidelines for gastrointestinal sarcomas (GIST), Cancer Treat. Rev. 55 (2017) 107–119.
[149] J. Bruix, S. Qin, P. Merle, A. Granito, Y.H. Huang, G. Bodoky, et al., Regorafenib for patients with hepatocellular carcinoma who progressed on sorafenib treatment (RESORCE): a randomised, double-blind, placebo-controlled, phase 3 trial, Lancet 389 (2017) 56–66.
[150] S.M. Wilhelm, J. Dumas, L. Adnane, M. Lynch, C.A. Carter, G. Schütz, et al., Regorafenib (BAY 73-4506): a new oral multikinase inhibitor of angiogenic, stromal and oncogenic receptor tyrosine kinases with potent preclinical antitumor activity, Int. J. Cancer 129 (2011) 245–255.
[151] R. Zeiser, H. Andrlová, F. Meiss, Trametinib (GSK1120212), Recent Results Cancer Res. 211 (2018) 91–100.
[152] K.T. Flaherty, J.R. Infante, A. Daud, R. Gonzalez, R.F. Kefford, J. Sosman, et al., Combined BRAF and MEK inhibition in melanoma with BRAF V600 mutations, N. Engl. J. Med. 367 (2012) 1694–1703.
[153] R. Dummer, P.A. Ascierto, H.J. Gogas, A. Arance, M. Mandala, G. Liszkay, et al., Encorafenib plus binimetinib versus vemurafenib or encorafenib in patients with *BRAF*-mutant melanoma (COLUMBUS): a multicentre, open-label, randomised phase 3 trial, Lancet Oncol. 19 (2018) 603–615.
[154] J. Sun, J.S. Zager, Z. Eroglu, Encorafenib/binimetinib for the treatment of BRAF-mutant advanced, unresectable, or metastatic melanoma: design, development, and potential place in therapy, Onco Targets Ther. 11 (2018) 9081–9089.
[155] C. Talati, K. Sweet, Recently approved therapies in acute myeloid leukemia: a complex treatment landscape, Leuk. Res. 73 (2018) 58–66.
[156] P.W. Manley, G. Caravatti, P. Furet, J. Roesel, P. Tran, T. Wagner, et al., Comparison of the kinase profile of midostaurin (Rydapt) with that of its predominant metabolites and the potential relevance of some newly identified targets to leukemia therapy, Biochemistry 57 (2018) 5576–5590.
[157] M. Kim, S. Williams, Midostaurin in combination with standard chemotherapy for treatment of newly diagnosed FMS-like tyrosine kinase 3 (FLT3) mutation-positive acute myeloid leukemia, Ann. Pharmacother. 52 (2018) 364–369.
[158] K. Döhner, G. Marcucci, F. Lo-Coco, R.B. Klisovic, A. Wei, J. Sierra, et al., Midostaurin plus chemotherapy for acute myeloid leukemia with a *FLT3* Mutation, N. Engl. J. Med. 377 (2017) 454–464.
[159] A.S. Mims, W. Blum, Progress in the problem of relapsed or refractory acute myeloid leukemia, Curr. Opin. Hematol. 26 (2019) 88–95.
[160] A.E. Perl, J.K. Altman, J. Cortes, C. Smith, M. Litzow, M.R. Baer, et al., Selective inhibition of FLT3 by gilteritinib in relapsed or refractory acute myeloid leukaemia: a multicentre, first-in-human, open-label, phase 1-2 study, Lancet Oncol. 18 (2017) 1061–1075.
[161] A. Markham, S. Dhillon, Acalabrutinib: first global approval, Drugs 78 (2018) 139–145.
[162] R. Roskoski Jr., Ibrutinib inhibition of Bruton protein-tyrosine kinase (BTK) in the treatment of B cell neoplasms, Pharmacol. Res. 113 (2016) 395–408.
[163] T. Barf, T. Covey, R. Izumi, B. van de Kar, M. Gulrajani, B. van Lith, et al., Acalabrutinib (ACP-196): a covalent Bruton tyrosine kinase inhibitor with a differentiated selectivity and in vivo potency profile, J. Pharmacol. Exp. Ther. 363 (2017) 240–252.
[164] M. Wang, S. Rule, P.L. Zinzani, A. Goy, O. Casasnovas, S.D. Smith, G. Damaj, et al., Acalabrutinib in relapsed or refractory mantle cell lymphoma (ACE-LY-004): a single-arm, multicentre, phase 2 trial, Lancet 391 (2018) 659–667.
[165] Y.Y. Syed, Lorlatinib: first global approval, Drugs 79 (2019) 93–98.
[166] S. Basit, Z. Ashraf, K. Lee, M. Latif, First macrocyclic 3rd-generation ALK inhibitor for treatment of ALK/ROS1 cancer: clinical and designing strategy update of lorlatinib, Eur. J. Med. Chem. 134 (2017) 348–356.
[167] A.T. Shaw, E. Felip, T.M. Bauer, B. Besse, A. Navarro, S. Postel-Vinay, et al., Lorlatinib in non-small-cell lung cancer with ALK or ROS1 rearrangement: an international, multicentre, open-label, single-arm first-in-man phase 1 trial, Lancet Oncol. 18 (2017) 1590–1599.
[168] B.J. Solomon, B. Besse, T.M. Bauer, E. Felip, R.A. Soo, D.R. Camidge, et al., Lorlatinib in patients with ALK-positive non-small-cell lung cancer: results from a global phase 2 study, Lancet Oncol. 19 (2018) 1654–1667 Erratum in: Lancet Oncol 2019;20:e10.
[169] J.N. Markowitz, K.M. Fancher, Cabozantinib: a multitargeted oral tyrosine kinase inhibitor, Pharmacotherapy 38 (2018) 357–369.
[170] N.M. Tannir, G. Schwab, V. Grünwald, Cabozantinib: an active novel multikinase inhibitor in renal cell carcinoma, Curr. Oncol. Rep. 19 (2017) 14.
[171] H. Singh, M. Brave, J.A. Beaver, J. Cheng, S. Tang, E. Zahalka, et al., U.S. food and drug administration approval: cabozantinib for the treatment of advanced renal cell carcinoma, Clin. Cancer Res. 23 (2017) 330–335.
[172] S. Medavaram, Y. Zhang, Emerging therapies in advanced hepatocellular carcinoma, Exp. Hematol. Oncol. 7 (2018) 17.
[173] L.J. Scott, Larotrectinib: first global approval, Drugs (2019), https://doi.org/10.1007/s40265-018-1044-x.
[174] A. Drilon, T.W. Laetsch, S. Kummar, S.G. DuBois, U.N. Lassen, G.D. Demetri, et al., Efficacy of larotrectinib in TRK fusion-positive cancers in adults and children, N. Engl. J. Med. 378 (2018) 731–739.
[175] R.J. Dowling, I. Topisirovic, B.D. Fonseca, N. Sonenberg, Dissecting the role of mTOR: lessons from mTOR inhibitors, Biochim. Biophys. Acta 1804 (2010) 433–439.
[176] J. Monod, J.P. Changeux, F. Jacob, Allosteric proteins and cellular control systems, J. Mol. Biol. 6 (1963) 306–329.
[177] J.J. Augustine, K.A. Bodziak, D.E. Hricik, Use of sirolimus in solid organ transplantation, Drugs 67 (2007) 369–391.
[178] G. Doros, J.M. Massaro, D.E. Kandzari, R. Waksman, J.J. Koolen, D.E. Cutlip, et al., Rationale of a novel study design for the BIOFLOW V study, a prospective, randomized multicenter study to assess the safety and efficacy of the Orsiro sirolimus-eluting coronary stent system using a Bayesian approach, Am. Heart J. 193 (2017) 35–45.
[179] S.R. Johnson, A.M. Taveira-DaSilva, J. Moss, Lymphangioleiomyomatosis, Clin. Chest Med. 37 (2016) 389–403.
[180] J.J. Bissler, F.X. McCormack, L.R. Young, J.M. Elwing, G. Chuck, J.M. Leonard, et al., Sirolimus for angiomyolipoma in tuberous sclerosis complex or lymphangioleiomyomatosis, N. Engl. J. Med. 358 (2008) 140–151.
[181] F.X. McCormack, Y. Inoue, J. Moss, L.G. Singer, C. Strange, K. Nakata, et al., Efficacy and safety of sirolimus in lymphangioleiomyomatosis, N. Engl. J. Med. 364 (2011) 1595–1606.
[182] J. O'Shaughnessy, J. Thaddeus Beck, M. Royce, Everolimus-based combination therapies for HR+, HER2- metastatic breast cancer, Cancer Treat. Rev. 69 (2018) 204–214.
[183] R.J. Motzer, B. Escudier, S. Oudard, T.E. Hutson, C. Porta, S. Bracarda, et al., Efficacy of everolimus in advanced renal cell carcinoma: a double-blind, randomised, placebo-controlled phase III trial, Lancet 372 (2008) 449–456.
[184] S. Buti, A. Leonetti, A. Dallatomasina, M. Bersanelli, Everolimus in the management of metastatic renal cell carcinoma: an evidence-based review of its place in

therapy, Core Evid. 11 (2016) 23–36.
[185] P. Gajate, O. Martínez-Sáez, T. Alonso-Gordoa, E. Grande, Emerging use of everolimus in the treatment of neuroendocrine tumors, Cancer Manag. Res. 9 (2017) 215–224.
[186] F.J. DiMario Jr., M. Sahin, D. Ebrahimi-Fakhari, Tuberous sclerosis complex, Pediatr. Clin. North Am. 62 (2015) 633–648.
[187] D. Lebwohl, O. Anak, T. Sahmoud, J. Klimovsky, I. Elmroth, T. Haas, et al., Development of everolimus, a novel oral mTOR inhibitor, across a spectrum of diseases, Ann. N. Y. Acad. Sci. 1291 (2013) 14–32.
[188] L. Bergmann, L. Maute, M. Guschmann, Temsirolimus for advanced renal cell carcinoma, Expert Rev. Anticancer Ther. 14 (2014) 9–21.
[189] V.E. Kwitkowski, T.M. Prowell, A. Ibrahim, A.T. Farrell, R. Justice, S.S. Mitchell, et al., FDA approval summary: temsirolimus as treatment for advanced renal cell carcinoma, Oncologist 15 (2010) 428–435.
[190] A. Markham, Baricitinib: first global approval, Drugs 77 (2017) 697–704.
[191] P.C. Taylor, E.C. Keystone, D. van der Heijde, M.E. Weinblatt, L. Del Carmen Morales, J. Reyes Gonzaga, et al., Baricitinib versus placebo or adalimumab in rheumatoid arthritis, N. Engl. J. Med. 376 (2017) 652–662.
[192] S. Ajayi, H. Becker, H. Reinhardt, M. Engelhardt, R. Zeiser, N. von Bubnoff, et al., Ruxolitinib, Recent Results Cancer Res. 212 (2018) 119–132.
[193] G.L. Plosker, Ruxolitinib: a review of its use in patients with myelofibrosis, Drugs 75 (2015) 297–308.
[194] C. Harrison, J.J. Kiladjian, H.K. Al-Ali, H. Gisslinger, R. Waltzman, V. Stalbovskaya, et al., JAK inhibition with ruxolitinib versus best available therapy for myelofibrosis, N. Engl. J. Med. 366 (2012) 787–798.
[195] J.A. Rodríguez-Portal, Efficacy and safety of nintedanib for the treatment of idiopathic pulmonary fibrosis: an update, Drugs R. D. 18 (2018) 19–25.
[196] L. Richeldi, R.M. du Bois, G. Raghu, A. Azuma, K.K. Brown, U. Costabel, et al., Efficacy and safety of nintedanib in idiopathic pulmonary fibrosis, N. Engl. J. Med. 370 (2014) 2071–2082.
[197] G. Sathiyamoorthy, S. Sehgal, R.W. Ashton, Pirfenidone and nintedanib for treatment of idiopathic pulmonary fibrosis, South Med. J. 110 (2017) 393–398.
[198] S.M. Hoy, Netarsudil ophthalmic solution 0.02%: first global approval, Drugs 78 (2018) 389–396.
[199] R.K. Donegan, R.L. Lieberman, Discovery of molecular therapeutics for glaucoma: challenges, successes, and promising directions, J. Med. Chem. 59 (2016) 788–809.
[200] C.W. Lin, B. Sherman, L.A. Moore, C.L. Laethem, D.W. Lu, P.P. Pattabiraman, et al., Discovery and preclinical development of netarsudil, a novel ocular hypotensive agent for the treatment of glaucoma, J. Ocul. Pharmacol. Ther. 34 (2018) 40–51.
[201] C.A. Lipinski, F. Lombardo, B.W. Dominy, P.J. Feeney, Experimental and computational approaches to estimate solubility and permeability in drug discovery and development settings, Adv. Drug Deliv. Rev. 23 (1997) 3–25.
[202] A.L. Hopkins, C.R. Groom, A. Alex, Ligand efficiency: a useful metric for lead selection, Drug Discov. Today 9 (2004) 430–431.
[203] G.F. Smith, Medicinal chemistry by the numbers: the physicochemistry, thermodynamics and kinetics of modern drug design, Prog. Med. Chem. 48 (2009) 1–29.
[204] P.D. Leeson, B. Springthorpe, The influence of drug-like concepts on decision-making in medicinal chemistry, Nat. Rev. Drug Discov. 6 (2007) 881–890.
[205] C.A. Lipinski, Rule of five in 2015 and beyond: target and ligand structural limitations, ligand chemistry structure and drug discovery project decisions, Adv. Drug Deliv. Rev. 101 (2016) 34–41.
[206] S. Ekins, N.K. Litterman, C.A. Lipinski, B.A. Bunin, Thermodynamic proxies to compensate for biases in drug discovery methods, Pharm. Res. 33 (2016) 194–205.
[207] A.L. Hopkins, G.M. Keserü, P.D. Leeson, D.C. Rees, C.H. Reynolds, The role of ligand efficiency metrics in drug discovery, Nat. Rev. Drug Discov. 13 (2014) 105–121.
[208] P.D. Leeson, Molecular inflation, attrition, and the rule of five, Adv. Drug Deliv. Rev. 101 (2016) 22–33.
[209] D.F. Veber, S.R. Johnson, H.Y. Cheng, B.R. Smith, K.W. Ward, K.D. Kopple, Molecular properties that influence the oral bioavailability of drug candidates, J. Med. Chem. 45 (2002) 2615–2623.
[210] T.I. Oprea, Property distribution of drug-related chemical databases, J. Comput. Aided Mol. Des. 14 (2000) 251–264.
[211] S.H. Bertz, The first general index of molecular complexity, J. Am. Chem. Soc. 1103 (1981) 3559–3601.
[212] J.B. Hendrickson, P. Huang, A.G. Toczko, Molecular complexity: a simplified formula adapted to individual atoms, J. Chem. Inf. Compout. Sci. 27 (1987) 63–67.
[213] P. Cohen, D.R. Alessi, Kinase drug discovery–what's next in the field? ACS Chem. Biol. 8 (2013) 96–104.
[214] K. Budzyn, P.D. Marley, C.G. Sobey, Targeting Rho and Rho-kinase in the treatment of cardiovascular disease, Trends Pharmacol. Sci. 27 (2006) 97–104.
[215] D.M. Goldstein, A. Kuglstatter, Y. Lou, M.J. Soth, Selective p38alpha inhibitors clinically evaluated for the treatment of chronic inflammatory disorders, J. Med. Chem. 53 (2010) 2345–2353.
[216] C.C. Mok, The jakinibs in systemic lupus erythematosus: progress and prospects, Expert Opin. Investig. Drugs 28 (2019) 85–92.
[217] M. Golpich, E. Amini, F. Hemmati, N.M. Ibrahim, B. Rahmani, Z. Mohamed, et al., Glycogen synthase kinase-3 beta (GSK-3β) signaling: Implications for Parkinson's disease, Pharmacol. Res. 97 (2015) 16–26.
[218] V. Nozal, A. Martinez, Tau Tubulin Kinase 1 (TTBK1), a new player in the fight against neurodegenerative diseases, Eur. J. Med. Chem. 161 (2019) 39–47.
[219] H.M. Kantarjian, T. Fojo, M. Mathisen, L.A. Zwelling, Cancer drugs in the United States: *justum pretium* – the just price, J. Clin. Oncol. 31 (2013) 3600–3604.
[220] T. Yezefski, A. Schwemm, M. Lentz, K. Hone, V. Shankaran, Patient assistance programs: a valuable, yet imperfect, way to ease the financial toxicity of cancer care, Semin. Hematol. 55 (2018) 185–188.
[221] S.Y. Zafar, J.M. Peppercorn, D. Schrag, D.H. Taylor, A.M. Goetzinger, X. Zhong, et al., The financial toxicity of cancer treatment: a pilot study assessing out-of-pocket expenses and the insured cancer patient's experience, Oncologist 18 (2013) 381–390.
[222] S.B. Dusetzina, A.N. Winn, G.A. Abel, H.A. Huskamp, N.L. Keating, Cost sharing and adherence to tyrosine kinase inhibitors for patients with chronic myeloid leukemia, J. Clin. Oncol. 32 (2014) 306–311.
[223] R. Roskoski Jr., Guidelines for preparing color figures for everyone including the colorblind, Pharmacol. Res. 119 (2017) 240–241 Erratum in: Pharmacol Res 2019;139:569.